NASA Technical Memorandum 85918

(NASA-TM-85918) COMPARISON OF MEASURED AND CALCULATED TEMPERATURES FOR A MACH 8 HYPERSONIC WING TEST STRUCTURE (NASA) 140 p HC A07/MF A01 CSCL 01C

N86-22563

Unclas G3/05 05902

Comparison of Measured and Calculated Temperatures for a Mach 8 Hypersonic Wing Test Structure

Robert D. Quinn and Roger A. Fields

March 1986

National Aeronautics and
Space Administration

NASA Technical Memorandum 85918

Comparison of Measured and Calculated Temperatures for a Mach 8 Hypersonic Wing Test Structure

Robert D. Quinn
Roger A. Fields, Ames Research Center, Dryden Flight Research Facility, Edwards, California

March 1986

National Aeronautics and
Space Administration

Ames Research Center
Dryden Flight Research Facility
Edwards, California 93523

SUMMARY

Structural temperatures were measured on a hypersonic wing test structure during a heating test that simulated a Mach 8 thermal environment. Measured data are compared to design calculations and to temperature predictions obtained from a finite-difference thermal analysis.

INTRODUCTION

During the past decade, numerous structural concepts have been studied for a wide spectrum of military and civil applications in the hypersonic speed domain (ref. 1). One investigation (ref. 2) to select the best structural concept for the specific design case of a Mach 8 hypersonic cruise vehicle revealed a ranking of several promising hot structure concepts. The concepts were evaluated on the basis of minimum-total-system cost. A full-scale test structure was designed and fabricated (ref. 3) using the highest ranking structural concept. The test structure was a 7.9-m^2 planform area of a NASA-specified Mach 8 hypersonic research plane wing. The structure was constructed of single-sheet, spanwise-stiffened, beaded panels made of René 41 with heat shields on the external surfaces made of corrugated René 41 and TD NiCr.

The hypersonic wing test structure (HWTS) was extensively tested in the NASA Ames Dryden Flight Loads Research Facility (FLRF) (ref. 4) to evaluate 1) the structural concept itself and the final structural design, and 2) the flight loads instrumentation, high-temperature calibration methods, and temperature simulation techniques. Testing of the HWTS was divided into 1) individual panel tests (ref. 5), 2) room-temperature loading tests of the entire structure (ref. 6), and 3) combined heating and loading tests of the entire structure.

This report covers the latter series of tests which includes the application to the structure of the design loads and thermal environment of a Mach 8 flight profile. Structural temperatures measured during testing are presented and compared to both design calculations and to calculated data from a finite-difference thermal analysis.

TEST ARTICLE

The design of the HWTS was based on the mission loads and temperatures calculated for the wing portion of a hypersonic research airplane concept as shown by the shaded area in figure 1.

A nominal research mission profile for the hypersonic research airplane, shown in figure 2, consists of horizontal takeoff at 103 m/sec, subsonic climb to a 7.32-km altitude, and acceleration at a dynamic pressure of 47.88 kN/m^2 to Mach 8 at an altitude of 30.8 km. A 5-min cruise flight is performed at Mach 8 and altitudes

between 30.8 and 35.8 km. Descent follows a constant 23.94-kN/m^2 dynamic pressure profile.

A major design consideration was the pushover-pullup loads maneuver shown by the dashed line profile in figure 2. This maneuver is initiated at Mach 8 at an altitude of 27.4 km, and consists of a -0.5-g pushover, a 2.5-g pullup, and a return to the nominal research mission descent profile. A more specific time history for this loads maneuver is shown in figure 3. Preload and postload maneuvers precede and follow the actual loads maneuver, providing transitions to and from the nominal flight profile. The entire loads maneuver took 42 sec, with a maximum dynamic pressure of 83.78 kN/m^2 obtained during this time.

Figure 4 shows the general dimensions and shape of the HWTS with a transition section. The wing is cantilevered from wing station (W.S.) 1.067. The wing was tested inverted, so the compressively loaded surface of the actual vehicle would be on the lower surface of the test structure. (In the remainder of this report, "upper surface" refers to that nearest the sky and "lower surface" to that nearest the ground in the test setup.) Although not part of the aircraft design, the transition section was included to provide a buffer between the support structure and the test portion of the wing. The five most critically compression-loaded panels are the lower root panels, shaded in figure 4 and numbered 1 through 5 from fore to aft.

Skin panels (fig. 5) of the HWTS are the primary load-carrying members. They were formed from a single sheet of René 41 with seven alternating up-and-down circular arc beads parallel to the wing spars. Doublers were spot-welded to the ends of the panel to prevent local end failure and to reduce excessive deformation caused by shear. Overall panel dimensions are 48.8 cm by 109.0 cm; beads are 0.066 cm thick having a radius of 2.654 cm with an included angle of 155°. The flat sections between the beads are 1.113 cm wide and 0.091 cm thick. Figure 5 shows four channel sections which are spot-welded to the beaded panel to provide attachment points for metallic heat shields. The beaded panels are attached to the caps of orthogonal spars and ribs by screws.

Figure 6 shows the HWTS mounted in a support fixture with the heat shields removed. Z-shaped clips are used to connect the heat shields to the structure. The HWTS has six spars perpendicular to the aircraft centerline, producing five chordwise bays. The outboard portion of the structure between the leading edge rib and the 30% rib is covered by an insulation packet; the insulation is intended to keep maximum structural temperatures below 1005 K and to keep spanwise temperature gradients constant.

Both the spar and rib webs have sine wave corrugations (figs. 6(a) and 6(b)) allowing for thermal expansion. Figure 6(b) shows the HWTS with heat shields installed. The heat shields are slightly corrugated in the chordwise direction. In general, two heat shields cover each full-size beaded panel. Heat shield extensions were provided around the boundaries of the test structure to improve the heating simulation of the outer spars and rib webs.

Figure 7 shows the attachment of the wing to the support structure. Twelve horizontal links provide spanwise horizontal load reaction and reaction for bending moment about an axis parallel to the ground and along the wing root. Each link has a spherical ball at each end so that thermal growth of the wing is not restricted by the support structure. Water-cooled fittings were placed between the links and the

wing to maintain the support structure at room temperature during tests. Also shown in figure 7 is an insulation packet that extends along the wing root to prevent heat losses. Vertical and chordwise (fore and aft) load and torsion reactions are provided by the eight ball-ended links shown in figure 8. The torsion occurs about an axis horizontal to the ground and perpendicular to the root.

To apply pressure loads normal to the beaded panel surfaces, pressure pans were constructed and added to the HTWS. Figure 9 shows the top view of a pressure pan exposed by removing an upper beaded panel. Two lines are attached to the pan; the larger one is a pressure feedline and the other is a pressure monitor line. Each of the lower surface root panels (panels 1 through 5 in fig. 4) is backed by a pressure pan so an internal pressure of 5.2 kN/m^2 can be applied to the panels during testing. The pans were constructed from 0.0076-cm-thick stainless steel. Doublers were spot-welded to the center of the pans to facilitate pressure feedline and pressure monitor line attachment. The total thickness at the center of the pans is 0.1600 cm.

Additional details about the test article and design missions are given in references 3 and 6.

TEST EQUIPMENT AND INSTRUMENTATION

Thermocouple Instrumentation

A total of 296 thermocouples were installed on the HWTS as shown in figure 10. One hundred thirty-one were located on spars and ribs (fig. 10(a)), 76 on beaded skin panels (fig. 10(a)), and 89 on the heat shields (figs. 10(b) and 10(c)). The shaded area in figure 10(a) indicates the location of the thermal insulation between the heat shields and the beaded skin panels.

Hydraulic Loading System

Twenty channels of closed-loop, electrohydraulic equipment (ref. 4) were used in applying loads to the test structure at locations shown in figure 11. Ten hydraulic jacks applied vertical loads to the structure (fig. 12), with eight of these jacks applying loads through two-point whiffletrees. Load-point pairs connected to the whiffletrees were 4/7, 5/8, 6/9, 10/13, 11/14, 16/22, 17/24, and 18/25. Horizontal (fore and aft) loads were applied by the remaining 10 hydraulic jacks at single points.

Heating System

The heating system was designed to heat the entire upper and lower surfaces of the HWTS to temperatures of the Mach 8 design flight profile. Infrared quartz lamps used to provide radiant heat flux for aerodynamic heating simulation were mounted on polished aluminum reflectors as shown in figure 13. The reflectors were water-cooled, enabling them to withstand the high temperatures of the heating tests. Both lower and upper heater systems (figs. 14 and 15) were slightly contoured to match the shape of the HWTS and were mounted on rollers and tracks so they could be easily removed for access to the structure and then precisely repositioned. The heaters

were positioned with the reflector surfaces approximately 15.2 cm from the heat shields of the HWTS. Lamps in the upper heater were uniformly distributed (2.54 cm apart) over the surface, inboard of the 30% rib. Lamps were spaced 1.27 cm apart, from the leading edge to and including the 30% rib. Lamps in the lower heater were uniformly distributed (2.54 cm apart) from the leading edge to and including the 30% rib except along the spar caps. Lamps were spaced 3.81 cm apart inboard of the 30% rib in the lower heater. Because the test structure has load attachment points on the lower surface, gaps in the heater were provided along the spar caps enabling connections with the hydraulic vertical-loading system (see fig. 12). To fill in those gaps, a double row of quartz lamps mounted on long, narrow, water-cooled, aluminum reflectors were installed parallel to the spar caps between load points as shown in figure 13. A total of 1206 lamps were used on the upper heater and 842 lamps were used on the lower heater.

Figure 16 shows an overall view of the test setup with the upper and lower heaters in place around the HWTS. Figure 17 shows a closer view of the heaters above and below the test structure. Load attachments can be seen passing through the lower heater. The plumbing for reflector water includes a pressure gage for each feed line to ascertain cooling provisions. Prior to a heating test, insulating curtains were draped around the wing structure and heater system, as shown in figure 18, to reduce radiation and convection heat losses.

TEST PROCEDURE

Two series of tests were conducted on the HWTS. During the first series of tests, the temperature of the heat shields was raised to 561 K at an approximate rate of 1 K/sec and holding. After quasi-equilibrium was obtained (approximately 40 min at 561 K), the structural loads that would be experienced by this wing section during a 2.5-g load maneuver at Mach 8 were applied. Figure 19 illustrates the applied load distribution. Vectors in the figure indicate the direction and magnitude of the applied loads. In addition to the loads, an internal pressure of 5.2 kN/m^2 was concurrently applied to the lower root beaded panels using the pressure pans described in the TEST ARTICLE section. Throughout this first series of tests, the FLRF analog thermal control system (ref. 4) was used to control the infrared heating system. Because of a 24 power control channel limit, the quartz lamps were divided into 24 control zones as shown in figure 20. The lower heater (fig. 20(a)) was divided into 10 zones and the upper heater (fig. 20(b)) was divided into 14 zones. The locations of the heat shield thermocouples which provided feedback temperature for each control zone are also shown.

The second series of tests consisted of heating the heat shields to the temperature time histories that simulated the thermal environment produced by the Mach 8 flight profile of figure 2. During this test series, the FLRF digital thermal control system was used. The quartz lamps were divided into 89 control zones (fig. 21), 42 on the lower heater (fig. 21(a)) and 47 on the upper heater (fig. 21(b)). Typical temperature time histories are shown in figure 22. Figures 22(a) through 22(g) show temperature profiles for the lower heater from the leading edge chordwise to the wing root. Figures 22(h) through 22(n) show corresponding profiles for the upper heater. Temperatures at other wing chords vary little from those shown in figure 22. The dashed lines show data calculated during design of the HWTS (ref. 3) for the Mach 8 flight profile, including the 2.5-g load maneuver. Solid lines show how the control zones were actually programmed for the

heating tests. As can be seen, variations were made in the profiles to accommodate the capabilities of the heating system. The symbols show measured test temperatures from control thermocouples in the corresponding zones. The rapid rise in temperature at 1264 sec in figure 22 corresponds to the 2.5-g load maneuver. Loads were applied to the HWTS at the appropriate time (21.07 min or 1264 sec) using a load-versus-time profile simulating the maneuver (see normal load factor in fig. 3). The application and removal of the load took 24 sec.

RESULTS AND DISCUSSION

Measured Temperatures

Measured spar and rib temperatures for the Mach 8 flight profile test are shown (figs. 23-30) for profile times of 400, 600, 800, 1000, and 1200 sec, and at 1250 sec (start of pull-up maneuver), and at 1270 sec (end of pull-up maneuver). Heat shield temperatures are also shown in these figures. Note that the leading edge spar web temperatures (fig. 23) and all rib web temperatures (figs. 23, 24, 26, and 29) are equal to or higher than the cap temperatures. Whereas, data for the spars inboard of the leading edge (figs. 24, 25, 27, and 28) show a more normal temperature distribution where web temperatures are less than cap temperatures. The relatively higher web temperatures obtained in the leading edge area were the result of insulation that was installed between the heat shield and structural panels in this part of the HWTS (figs. 6(a) and 10(a)). Although the insulation reduced both cap and web temperatures, it proved more effective on cap temperatures because the web of the 30% rib (which separates the leading edge from the rest of the HWTS structure) received additional heat by radiation from the hot inboard structure which was not insulated from the heat shields. The web of the 30% rib in turn radiated to the other webs in the leading edge. These hotter surfaces also radiated to the spar caps; however, because the radiation view factors to the webs are larger than the view factors to the caps, radiation to the webs was much more effective. The reason why the rib webs are hotter than the rib caps at the inboard wing locations is not so obvious. It is believed that the reason is due to the difference between the radiation view factor from the beaded skin panels to the ribs and from the beaded skin panels to the spars. The beads of the skin panels run parallel to the spars, with a large part of the panel being shaded from the spar webs, whereas almost all of the skin panel can see the rib web. Consequently, the radiation view factor from the skin panel to the rib is larger than the view factor from the skin panel to the spar, and therefore, the rib web is heated at a faster rate than the spar web.

Temperatures of the beaded skin panels were also measured during the heating test and these temperatures are presented in table 1.

Thermal Analyses

Design Temperatures- The manufacturer of the HWTS used a finite-difference thermal analyzer computer program to calculate design temperatures at W.S. 1.93, W.S. 3.03, and W.S. 4.11 (fig. 31). Further information on the design analysis can be found in reference 3. Selected design temperature profiles are shown in figures 32, 33, and 34. Also shown for comparison are measured temperatures. Temperature profiles for skin panels and spars at W.S. 1.93 are shown in figures 32(a)

and 32(b). Agreement between the measured and design temperatures is in general poor. However, it may be noted that the largest discrepancies occur during the high heating part of the profile and agreement improves near the end of the profile. It should be noted here that the pressure pan shown in figure 32 was not used in the design calculations. To determine how much effect the pressure pan has on the structural temperatures, calculations were made with and without the pressure pan. Results for the upper and lower skins and the spar web are shown in figure 35. The addition of the pressure pan results in lower structural temperatures, indicating that if data were obtained without the pressure pan, agreement with the design temperatures would be somewhat improved. However, the overall agreement would still be considered poor. Comparison between measured and design temperatures of W.S. 3.03 are presented in figure 33. The agreement is poor during the high heating part of the profile, but becomes much better during the last 200 sec of the profile. Measured and calculated temperatures for the leading edge at W.S. 4.11 and fuselage station 24.13 are shown in figure 34. As can be seen, the design temperatures are much higher than the measured data.

Calculated Structural Temperatures- In an attempt to determine whether the measured temperatures could be predicted theoretically, selected locations on the wing were modeled for a two-dimensional solution using a finite-difference (lumped parameter) thermal analyzer computer program (ref. 7). Heating inputs used in this analysis were the heat shield temperature/time histories used in the laboratory heating test. Thermal models were made at locations shown in figure 36. Models were made of bay 3 (model 1) at W.S. 1.93 and bay 8 (model 2) at W.S. 3.02. Thermal models were also made of the leading edge at bay 18 (model 3), and of the 30% rib (model 4), which includes parts of bays 13 and 18. Since bays 1, 2, 3, 4, and 5 are all structurally identical, thermal model 1 may be used to analyze any of these bays.

Drawings of typical HWTS structure are shown in figures 37 and 38. Figure 37 shows a cross section of the structure that is typical for all of the HWTS, except the leading edge area. Figure 38 shows a cross section of the leading edge. The only difference between the leading edge and other locations, except for actual dimensions, is the addition of insulation between the beaded skin panels and the heat shield.

When making the thermal models, the beaded skin panels and corrugated spar webs were represented by equivalent flat plates that had thermal capacitance and thermal resistance equal to the values of the actual structure. The primary mode of heat transfer in the HWTS is by radiation. Therefore, the calculation of view factors and net emissivities for the thermal model is very important. It quickly became apparent that view factors could not be adequately computed by assuming that the beaded skin panels were flat plates because portions of the panels were shaded from the heat shields and the internal structure. For example, the view factor calculated between the heat shield and the beaded panel assuming flat surfaces was 0.97, whereas the value computed when shading was accounted for was 0.75. View factors calculated between the beaded panels and the spar caps and webs varied from model to model depending on location. However, these view factors were also significantly lower than values computed for flat surfaces. The emissivity of the heat shield and the wing structure was 0.8 (ref. 3). The net emissivity was calculated to be 0.667 (ref. 8).

Models 1, 2, 3, and 4 are shown in figures 39, 40, 41, and 42, respectively. For model 1, it was only necessary to model half of the bay because of symmetry and

because the chordwise temperatures of the bay did not change significantly. Figure 39(a) shows how the structure was divided into "lumps" (elements) and identifies the various structural components. Figure 39(b) shows the number and location of the conduction resistors and temperature inputs, and figures 39(c) through 39(j) show the radiation resistors. Figures 40, 41, and 42 show the same information for the other thermal models. Some additional comments about how the leading edge insulation was modeled (figs. 41 and 42) are appropriate since it has a great effect on the calculated internal temperatures. In figure 41(a) it can be seen that the insulation was divided into three lumps. One lump was the Inconel foil, the next lump was the micro-quartz, and the third lump was the Inconel foil. It should also be noted (fig. 41(c)) that only radiation was allowed between the outer layer of Inconel foil and the micro-quartz and the inner layer of Inconel foil and the beaded skin panels. The mode of heat transfer through the micro-quartz and the inner layer of Inconel was conduction (fig. 41(b)). The view factors between the Inconel foil and the micro-quartz and the beaded panels were calculated to be 1.0. The emissivity of the Inconel foil and the micro-quartz was assumed to be 0.5. Effective emissivities between the beaded panel and the Inconel foil, the micro-quartz and the Inconel foil, and the Inconel foil and the heat shields were 0.44, 0.33, and 0.44, respectively. Model 1 was analyzed with and without the pressure pan to determine the effect of the pressure pan on the structural temperatures. The results are shown in figure 35, and were discussed in the previous section. Model 1 was divided into small lumps to obtain the temperature gradient of the skin panel. Since measured skin data were available only at the center of each skin panel, comparisons between measured and calculated skin panel temperature gradients could not be made. Consequently, subsequent thermal models were divided into larger lumps that were more consistent with available measured data, and also required less setup and computing time.

The results from the theoretical analysis are shown in figures 43, 44, 45, 46, and 47. Also shown for comparison are the measured data from the laboratory heating test. Temperatures of the upper and lower skin at W.S. 1.93 are shown in figure 43(a). The measured and calculated data are in good agreement during the first 800 sec of the profile. After 800 sec, calculations tend to overpredict the measured data with a maximum difference of 30 K occurring at 1000 sec on the upper skin. The measured and calculated spar temperatures shown in figure 43(b) are in good agreement during the first 600 sec of the profile. After 600 sec, the calculated spar cap temperatures are approximately 30 K higher than the measured data. The calculated web temperatures show a marked departure from the measured values after 800 sec and overpredict the measured data by as much as 65 K at 1000 sec. Differences between the predictions and the measured data are most probably due to the two-dimensional nature of the thermal model and inaccuracies in the computed view factors and emissivities.

Measured and calculated skin and spar temperatures at W.S. 3.03 are presented in figures 44(a) and 44(b). Calculated temperatures for both upper and lower skins and upper spar cap tend to overpredict the measured data during the later part of the profile. However, the overall agreement is considered fair. The calculated temperatures for the lower spar cap are in good agreement with the measured data. Calculated web temperatures are in better agreement with the measured data than were the computed web temperatures for W.S. 1.93, indicating that the addition of the pressure pans makes computing accurate temperatures more difficult. However, as can be seen in figure 44(b), the calculated data are still 30 to 40 K higher than measured data between 900 sec and 1200 sec.

Figure 45 shows comparisons between measured and calculated temperatures for the upper and lower skins and the spar at the leading edge of the wing structure. Insulation was located between the heat shield and the skin panels. As shown in figure 45(a), the measured and calculated temperatures of the skin panels are in good agreement. The calculated lower spar cap and web temperatures, shown in figure 45(b), agree fairly well with the measured data. However, the predicted upper spar cap temperatures are 30 to 35 K higher than the measured temperatures during the last half of the profile.

Calculated temperatures for the 30% leading edge rib and the skin panels inboard and outboard of the 30% rib are plotted in figure 46. Also shown for comparison are the measured temperatures. The outboard or leading edge skin panel temperatures are shown in figure 46(a). As shown, agreement between the measured and calculated data is good. The upper and lower rib cap temperatures and the rib web temperatures are shown in figure 46(b). As can be seen, calculated temperatures are in good agreement with the measured data. The inboard skin panel temperatures are presented in figure 46(c). Measured data were available only for the lower skin. Agreement between the calculated and measured temperatures is good from 0 to 600 sec and from 1000 to 1300 sec. For profile times 700 to 900 sec, calculated values overestimate the measured data by 40 to 70 K.

The distribution of temperatures in bays 1 through 5, which contain the most critically loaded panels (fig. 4), at W.S. 1.93 is shown in figure 47 for 800 sec. Shown in this figure are measured temperatures, the design calculated temperatures, and temperatures calculated during the present investigation. In the present investigation, temperatures were computed for bays 2, 3, and 4 only. Calculations were not made for bays 1 and 5 because of the difficulty in defining the boundary conditions for the outside bays. As shown in figure 47, the level and gradients of the design temperatures are in poor agreement with the measured data. The temperatures and temperature gradients computed in this investigation are in fair to good agreement with the experimental data. Since the design and measured temperatures were obtained only at the center of each skin panel and at the spar caps, one might assume that the temperature distribution would follow a sawtooth pattern as indicated by the dashed lines in figure 47. However, results of this analysis show that the actual temperature distribution is quite different. The temperature of the skin panel is almost constant until the skin comes in contact with the spar caps, at which time the temperature of the skin drops to the temperature of the spar cap. As shown, the skin temperature decreases approximately 75 K in a distance of 0.064 m.

CONCLUDING REMARKS

The hypersonic wing test structure (HWTS) is a unique structure because radiation serves as the primary mode of heat transfer. Heat transferred by conduction for this type of structure is almost negligible compared to conventional aircraft structures (e.g., Space Shuttle), in which conduction is the primary mode of heat transfer. This makes thermal analysis of the HWTS more challenging than analysis of a conventional structure because of the difficulty in calculating large numbers of accurate view factors. Also, conduction thermal properties are generally known more accurately than radiation thermal properties.

Results of a thermal analysis of the HWTS made for the present investigation and results from the design thermal analysis are compared with measured structural

tempertures obtained during a laboratory heating test that simulated a Mach 8 thermal environment. These comparisons led to the following conclusions:

1. The design temperatures were significantly higher and in poor agreement with the measured data.

2. The measured temperature gradients were much larger than the design predicted temperature gradients.

3. The temperature and temperature distributions calculated in the present investigation were in fair to good agreement with the measured data. The largest discrepancies occurred at the spar webs, and it is believed that these differences would be significantly reduced with a three-dimensional thermal analysis.

4. When making a thermal analysis of a structure where internal radiation is an important factor, view factors must be accurately determined, and the effects of shading must be considered.

REFERENCES

1. Hearth, Donald P.; and Preyes, Albert E.: Hypersonic Approach to an Expanded Program. J. Astron. Aeron., 1976.

2. Plank, P. P.; Sakata, I. F.; Davis, G. W.; and Richie, C. C.: Hypersonic Cruise Vehicle Wing Structure Evaluation. NASA CR-1568, 1970.

3. Plank, P. P.; and Penning, F. A.: Hypersonic Wing Test Structure Design, Analysis, and Fabrication. NASA CR-127490, 1973.

4. Sefic, Walter J.: NASA Dryden Flight Loads Facility. NASA TM-81368, 1981.

5. Siegel, William H.: Experimental and Finite Element Investigation of the Buckling Characteristics of a Beaded Skin Panel for a Hypersonic Aircraft. NASA CR-144863, 1978.

6. Fields, Roger A.; Reardon, Lawrence F.; and Siegel, William H.: Loading Tests of a Wing Structure for a Hypersonic Aircraft. NASA TP-1596, 1980.

7. Thermal Analyzer Computer Program for the Solution of General Heat Transfer Problems. LR-18902, Lockheed California Company, July 1965.

8. Jakob, Max: Heat Transfer. Vol. II, John Wiley and Sons, New York, 1957.

TABLE 1.- BEADED SKIN PANEL TEMPERATURES

U = UPPER SURFACE
L = LOWER SURFACE

TIME, sec	TEMPERATURE, K, AT INDICATED THERMOCOUPLE															
	1U	1L	2U	2L	3U	3L	4U	4L	5U	5L	6U	6L	7U	7L	8U	8L
400	345	329	337	330	347	332	339	327	339	331	352	379	348	360	352	379
600	494	432	461	419	495	435	461	419	494	432	527	567	521	516	537	537
800	668	571	641	554	669	571	637	570	633	549	752	761	751	720	756	741
1,000	777	683	753	670	774	677	749	675	734	653	886	881	889	845	889	873
1,200	860	792	844	781	862	786	838	784	819	758	976	973	980	940	982	967
1,250	881	822	868	816	884	820	861	817	841	794	999	1003	1005	973	1006	999
1,270	894	831	879	828	895	829	872	827	852	802	1011	1014	1017	984	1018	1009

TIME, sec	TEMPERATURE, K, AT INDICATED THERMOCOUPLE															
	9U	9L	10U	10L	11U	11L	12U	12L	13U	13L	14U	14L	15U	15L	16U	16L
400	346	357	346	349	353	373	350	378	354	361	–	361	351	366	–	348
600	512	513	508	493	539	542	545	538	544	526	–	519	528	526	–	484
800	742	711	721	691	773	743	782	739	775	739	–	736	755	744	–	676
1,000	878	834	854	818	893	858	906	862	899	863	–	863	886	864	–	807
1,200	969	931	944	916	980	951	990	952	987	953	–	954	971	949	–	914
1,250	994	963	970	950	1006	982	1014	982	1011	983	–	983	996	977	–	949
1,270	1006	972	980	959	1017	992	1027	992	1023	992	–	992	1008	986	–	958

TIME, sec	TEMPERATURE, K, AT INDICATED THERMOCOUPLE												
	17U	17L	18U	18L	19U	19L	20U	20L	21U	21L	22U	22L	23U	23L
400	–	369	–	368	–	312	302	311	303	309	303	311	–	308
600	–	541	–	553	–	367	333	354	337	352	335	359	–	359
800	–	734	–	768	–	521	458	466	454	457	463	471	–	479
1,000	–	847	–	876	–	715	621	698	609	589	628	606	–	649
1,200	–	944	–	965	–	882	775	757	757	742	777	761	–	832
1,250	–	973	–	993	–	929	824	813	803	794	823	813	–	886
1,270	–	982	–	1002	–	942	827	827	816	808	837	827	–	900

THERMOCOUPLE LOCATION

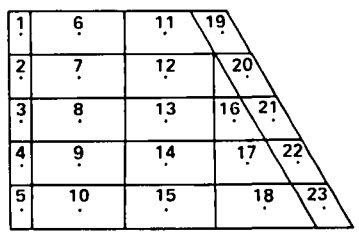

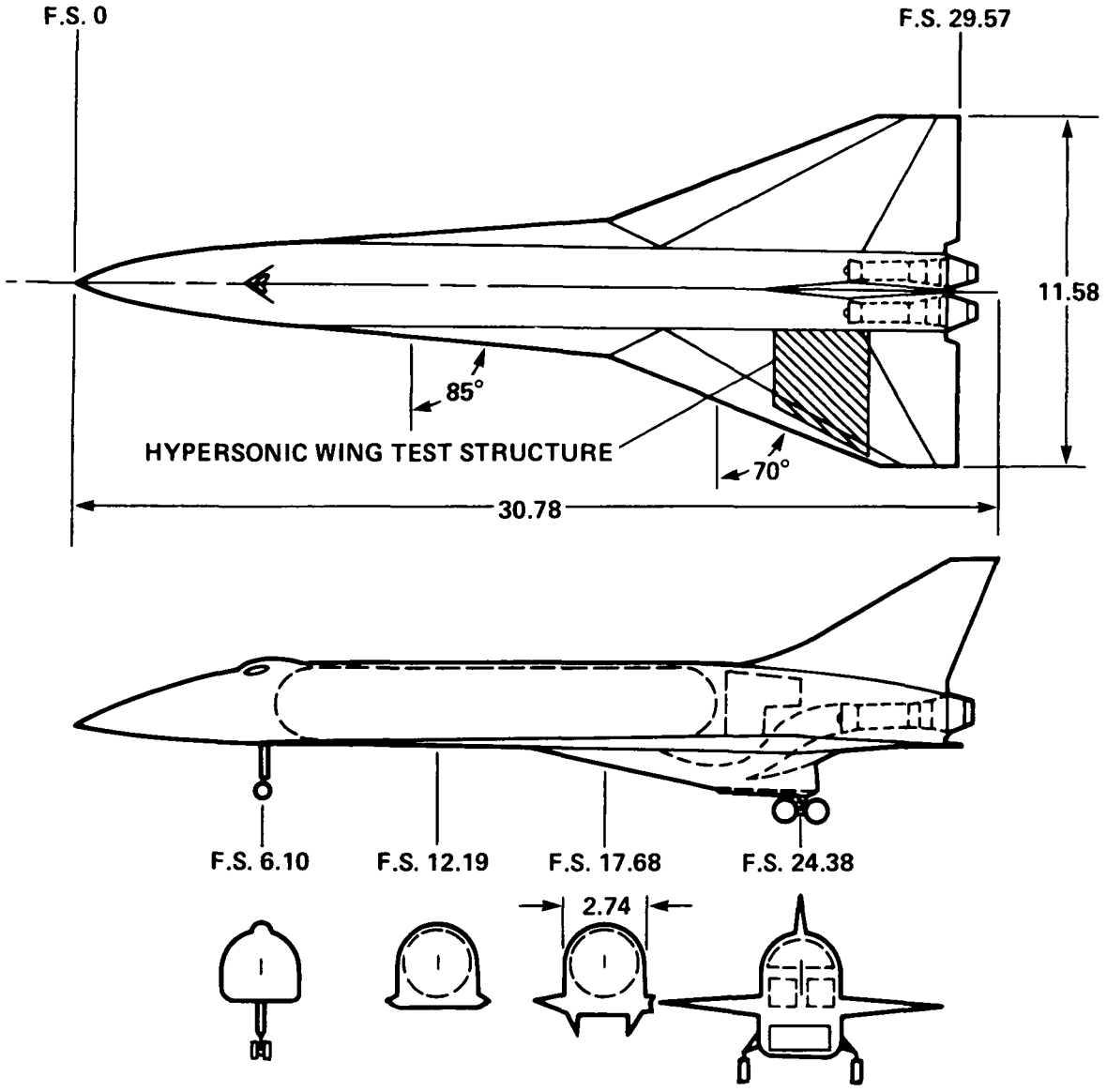

Figure 1.- Hypersonic research airplane configuration. Fuselage stations (F.S.) and dimensions in meters.

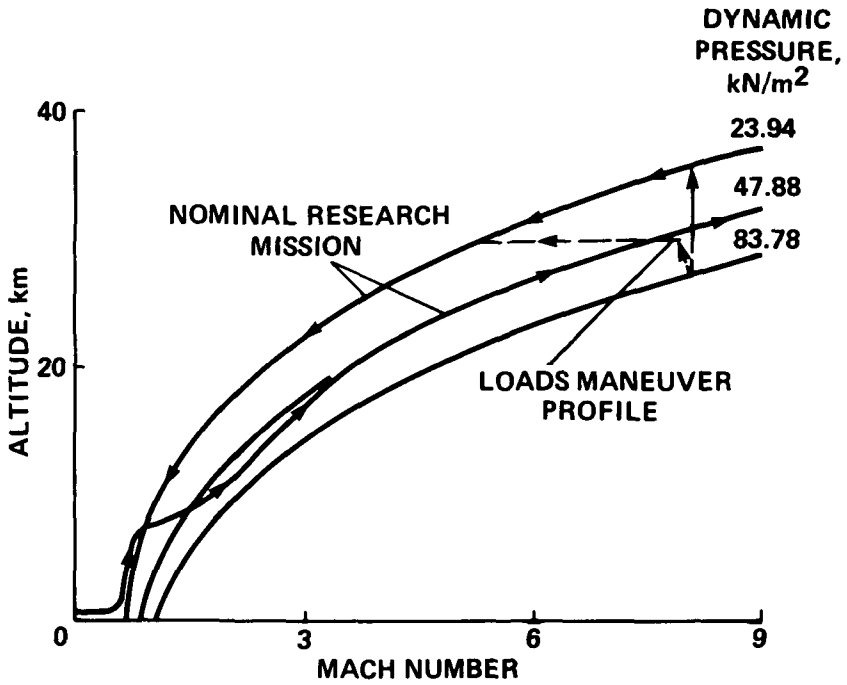

Figure 2.- Hypersonic research airplane research-mission profile.

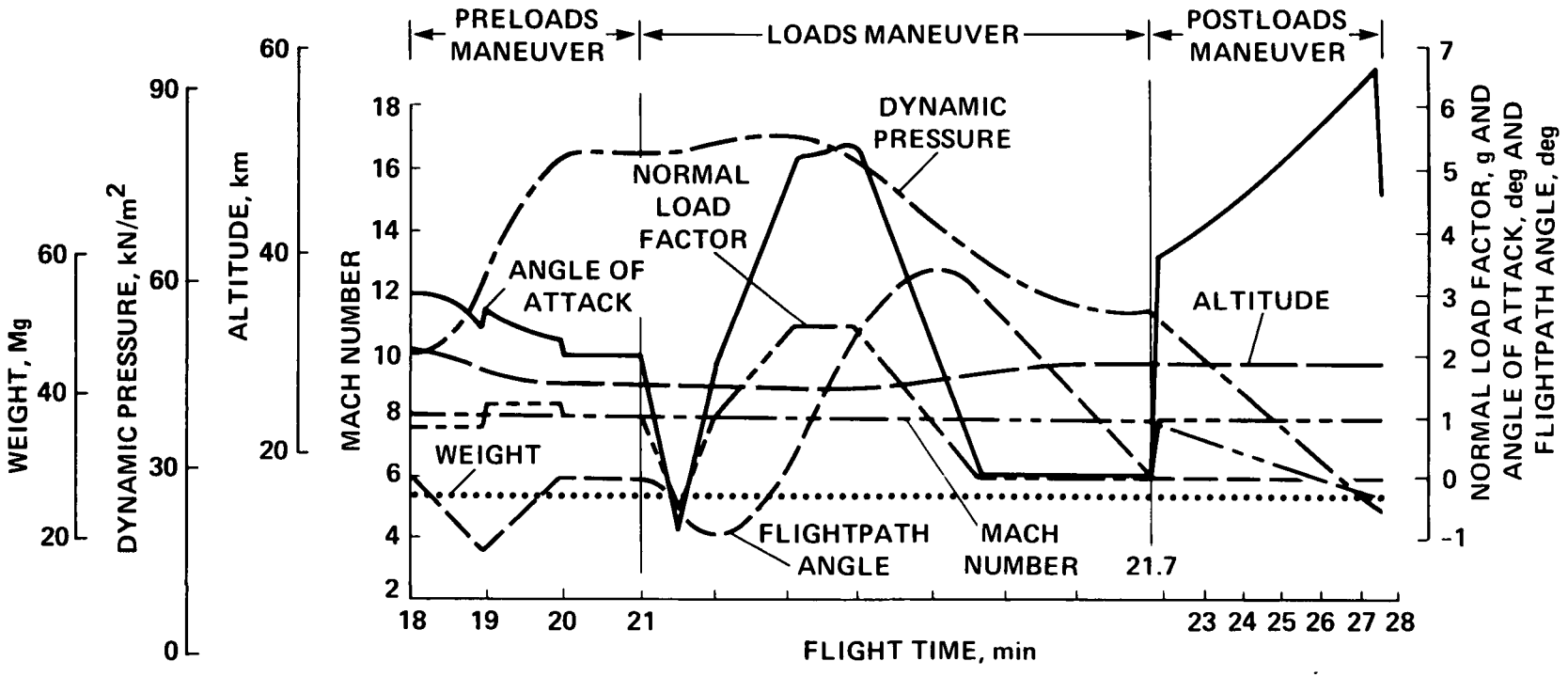

Figure 3.- Time history for a loads maneuver of the hypersonic research airplane.

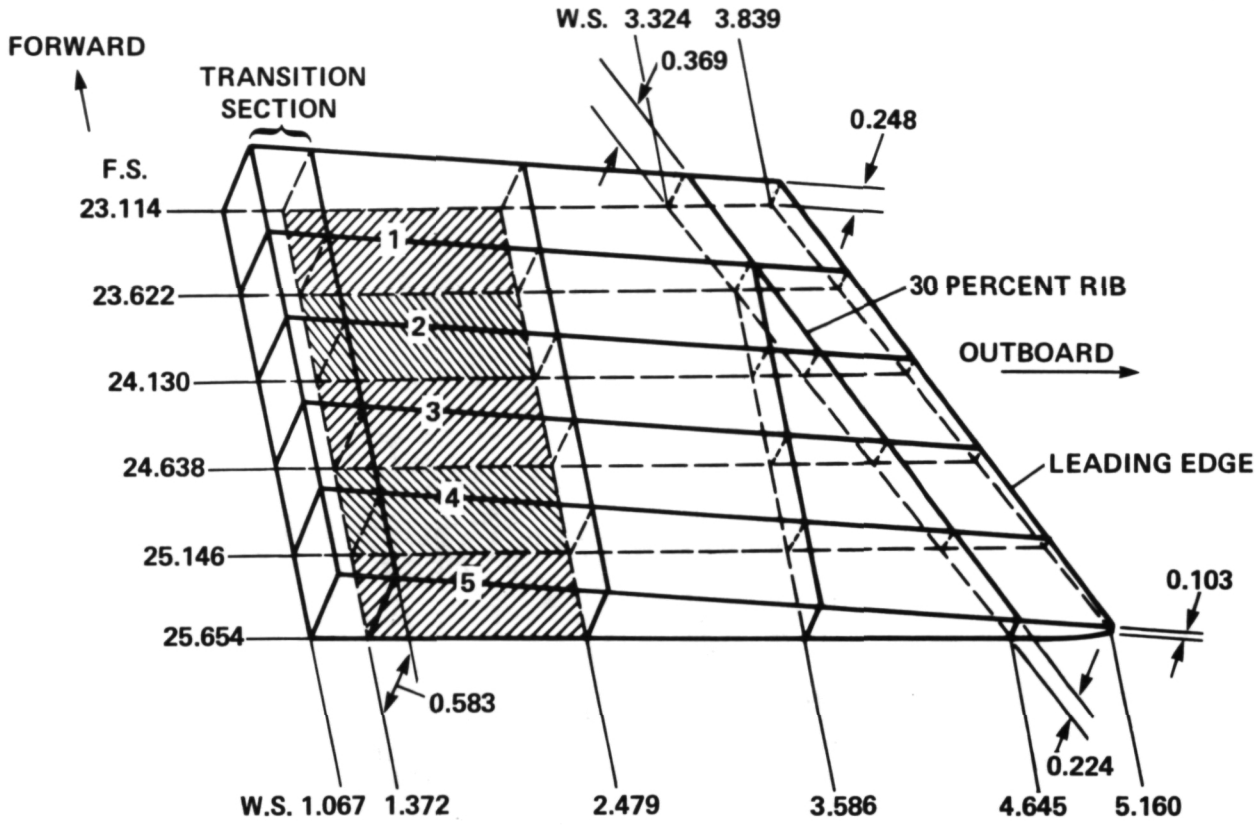

Figure 4.- Hypersonic wing test structure dimensions. The most critically loaded panels are shaded and numbered 1 to 5 going aft. Fuselage stations (F.S.), wing stations (W.S.), and dimensions in meters.

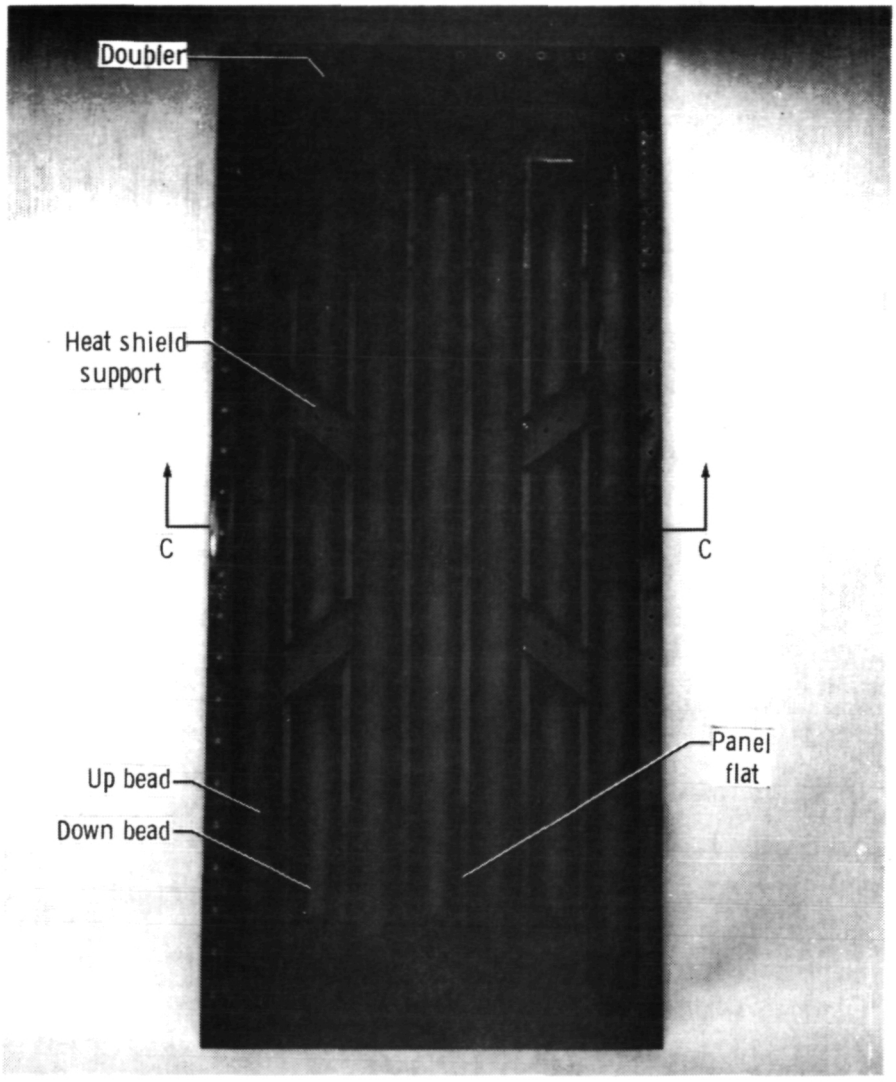

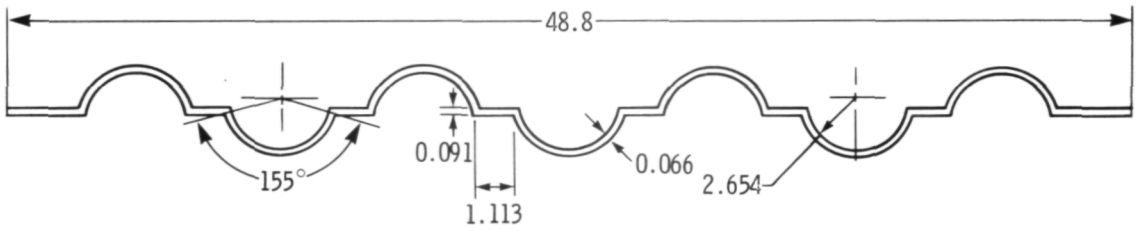

Figure 5.- Beaded panel for HWTS. Dimensions in centimeters.

ORIGINAL PAGE IS
OF POOR QUALITY

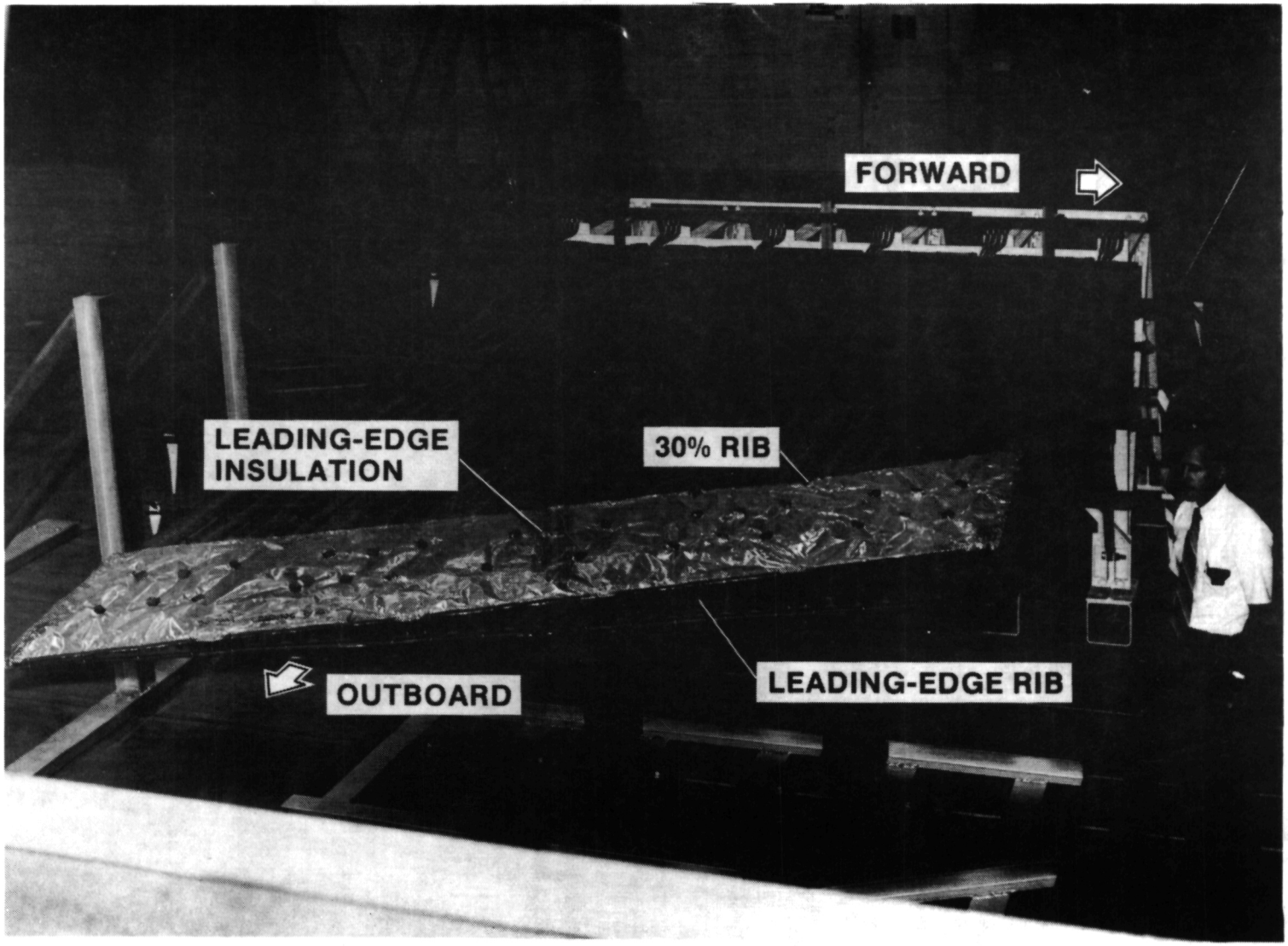

(a) Heat shields removed.

Figure 6.- Hypersonic wing test structure.

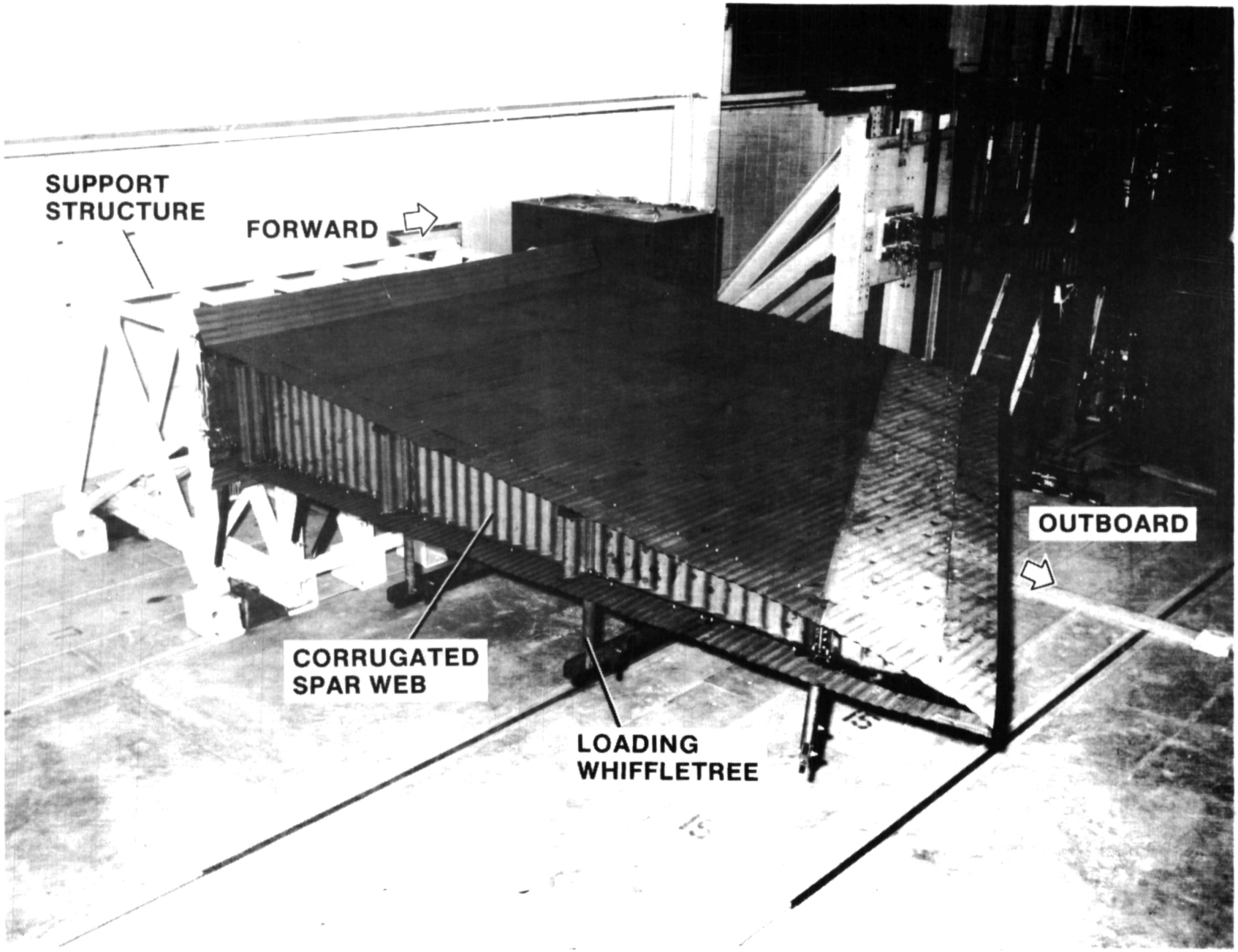

(b) Heat shields installed.

Figure 6.- Concluded.

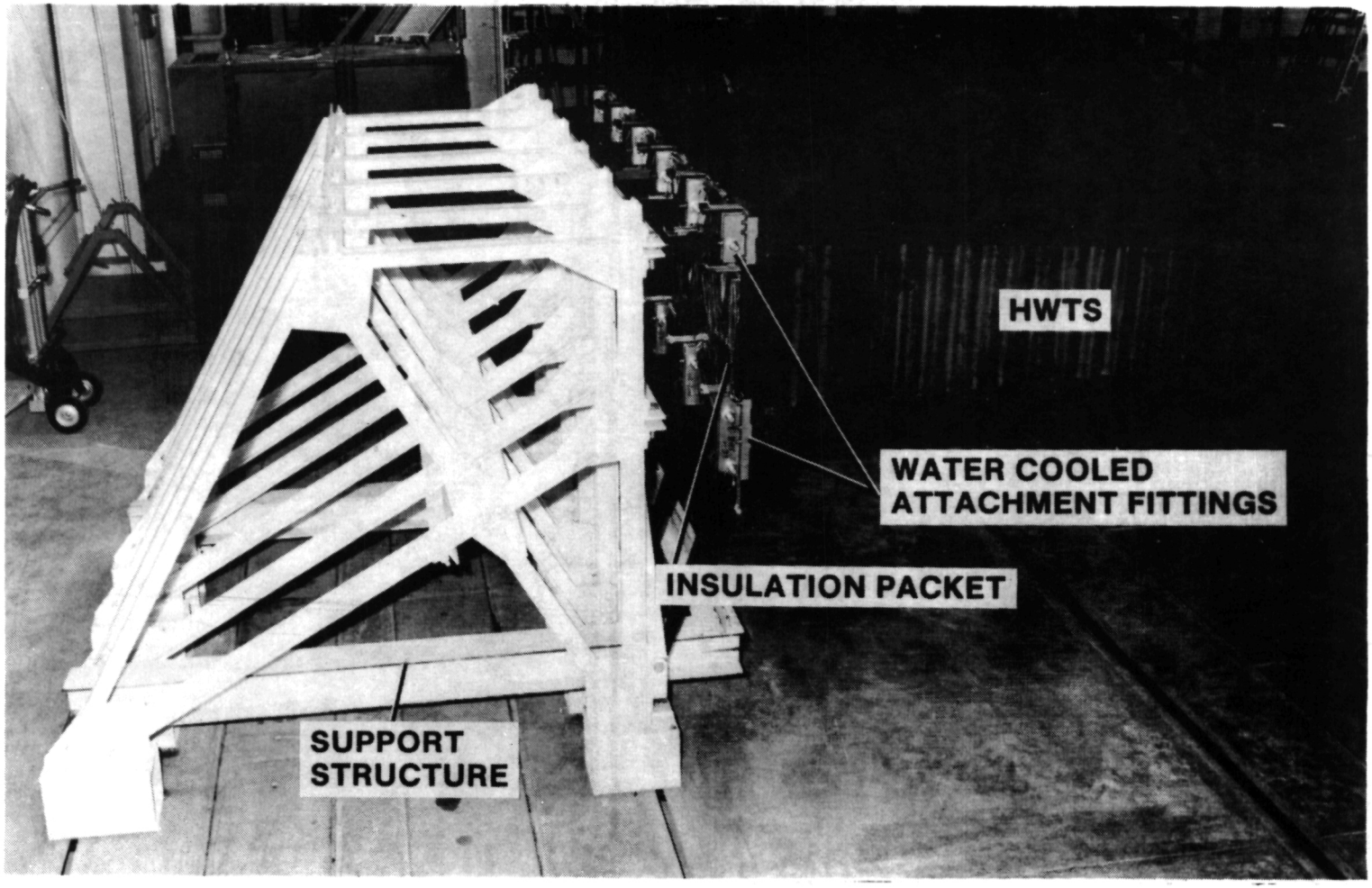

Figure 7.- HWTS support structure.

ORIGINAL PAGE IS
OF POOR QUALITY

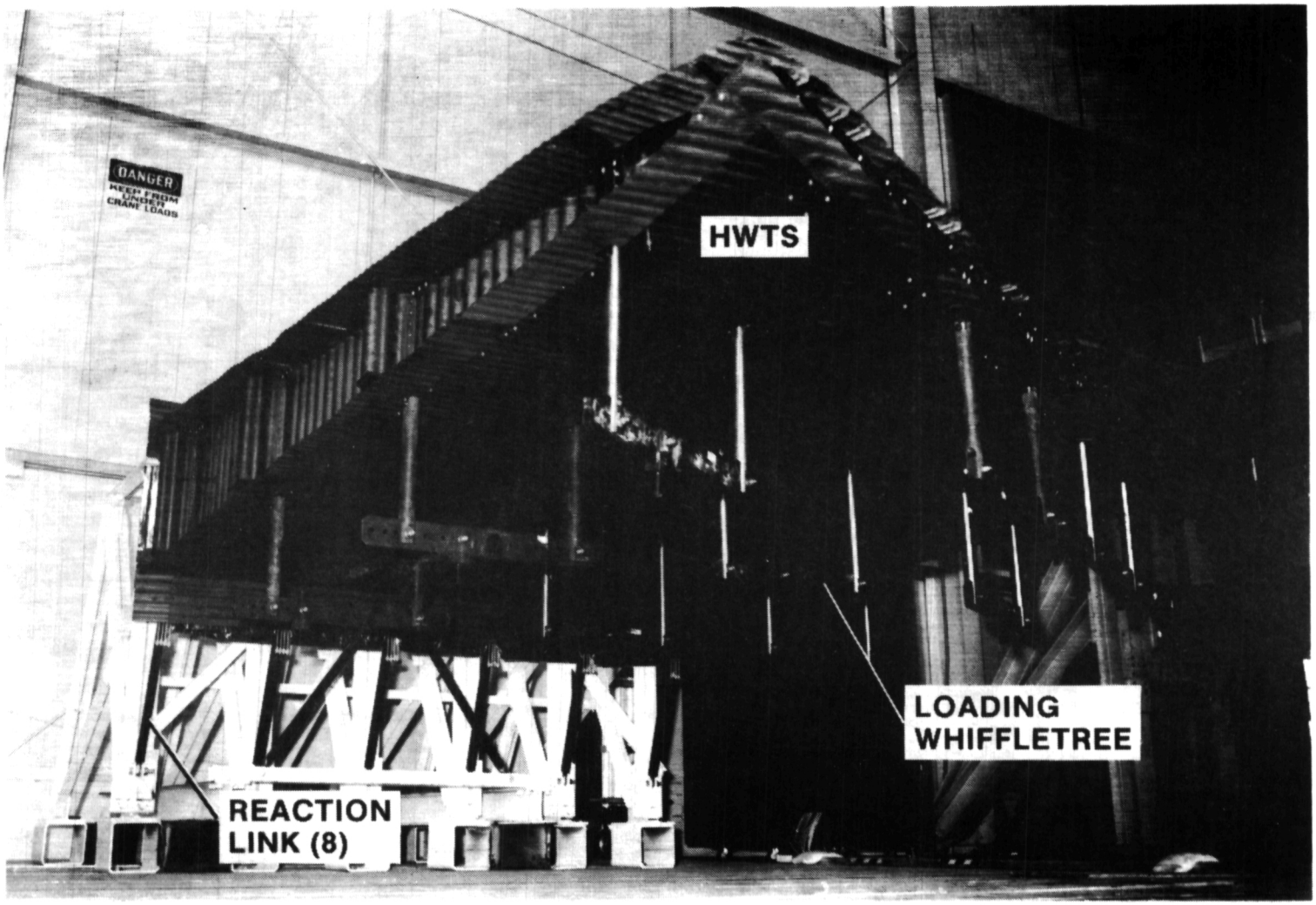

Figure 8.- HWTS load reaction.

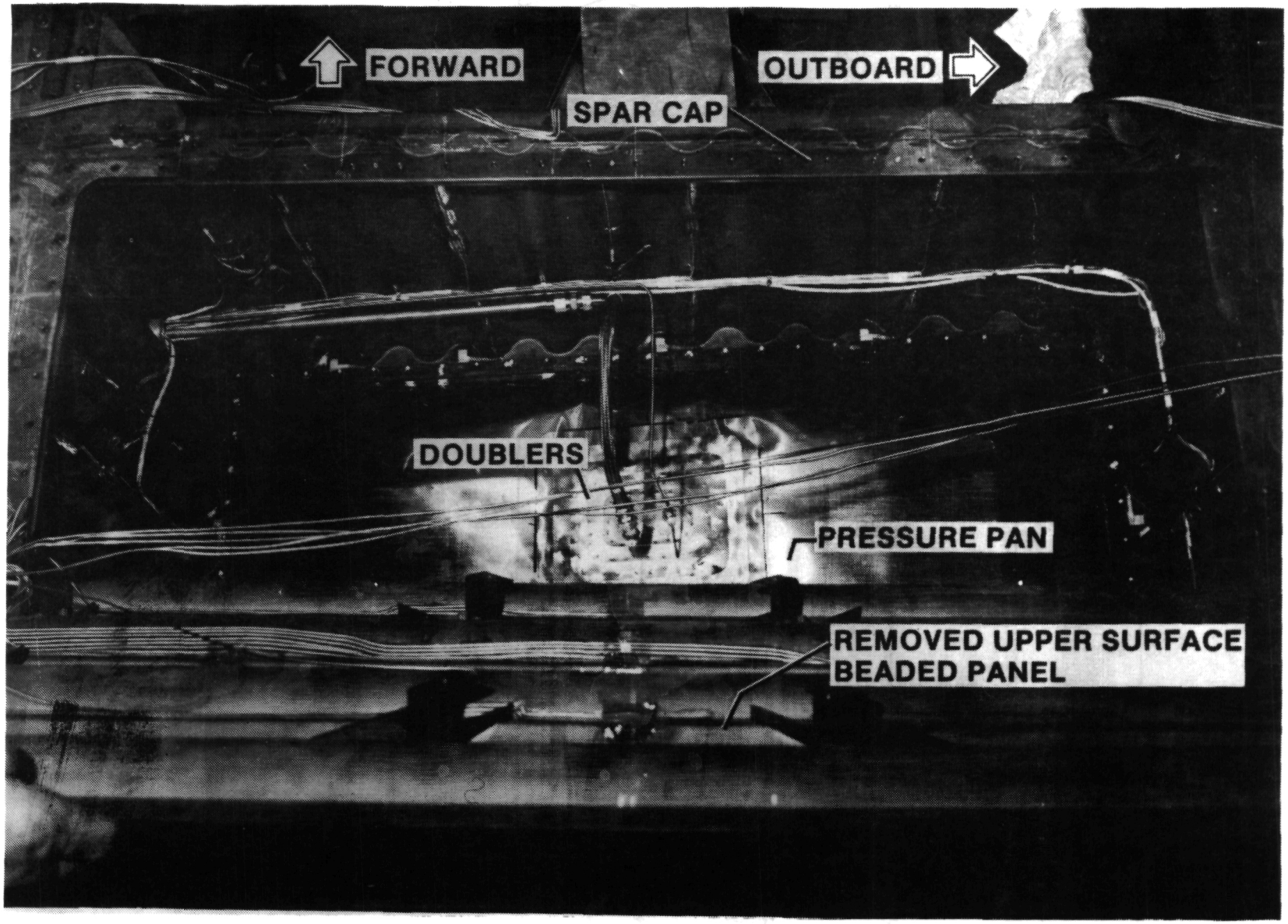

Figure 9.- Interior of HWTS bay showing pressure pan.

ORIGINAL PAGE IS
OF POOR QUALITY

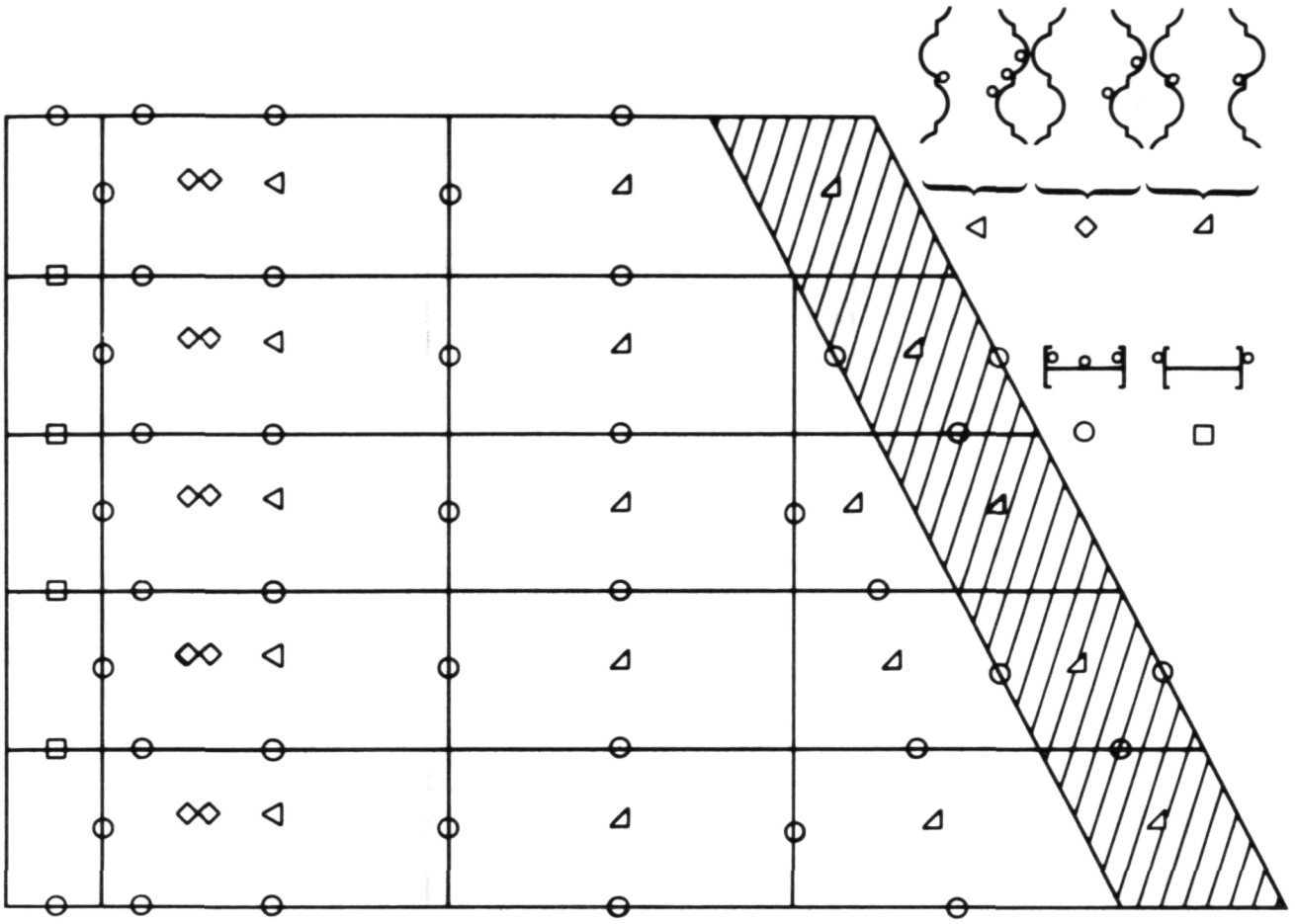

(a) Spars, ribs, and beaded panels.

Figure 10.- Thermocouple locations on the HWTS.

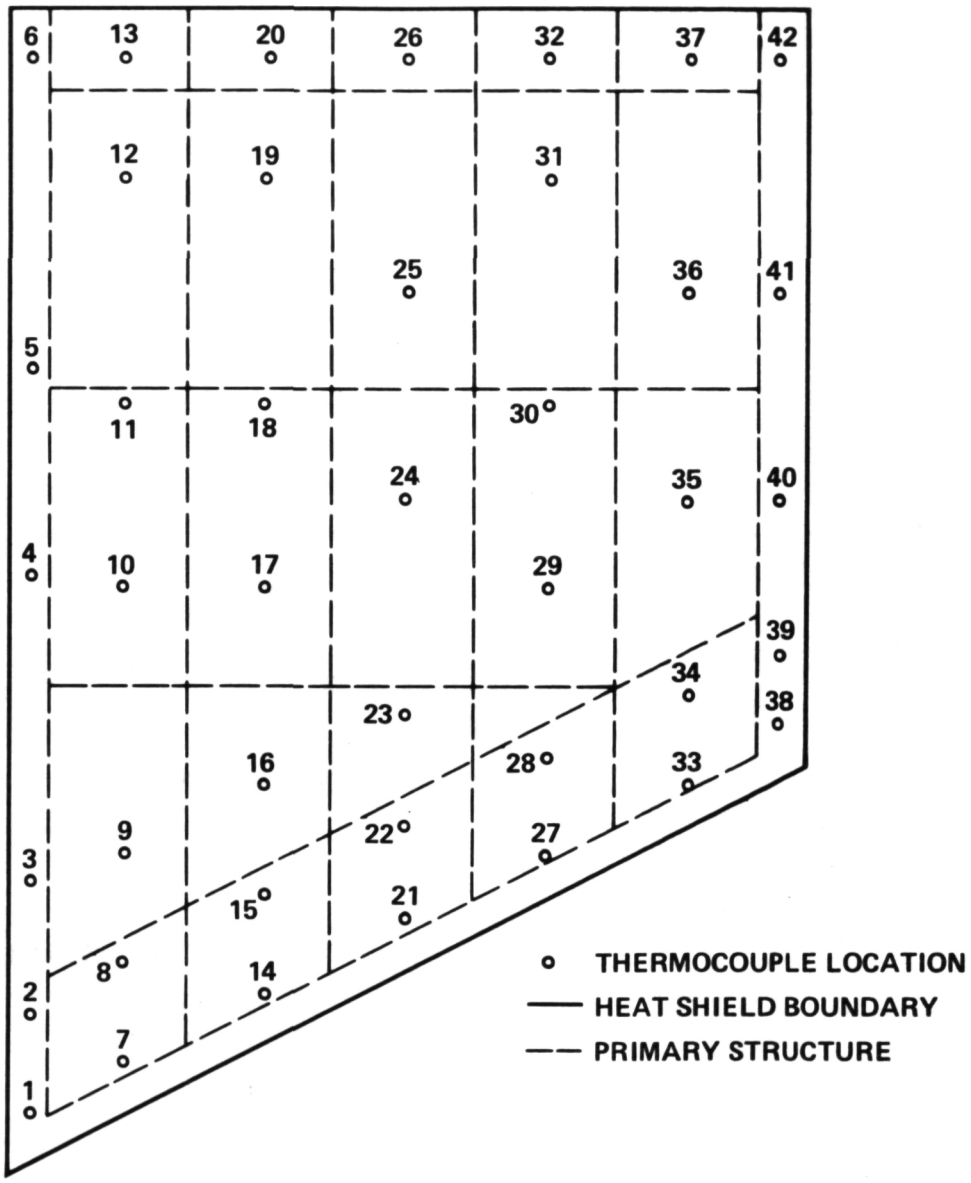

(b) Lower heat shield.

Figure 10.- Continued.

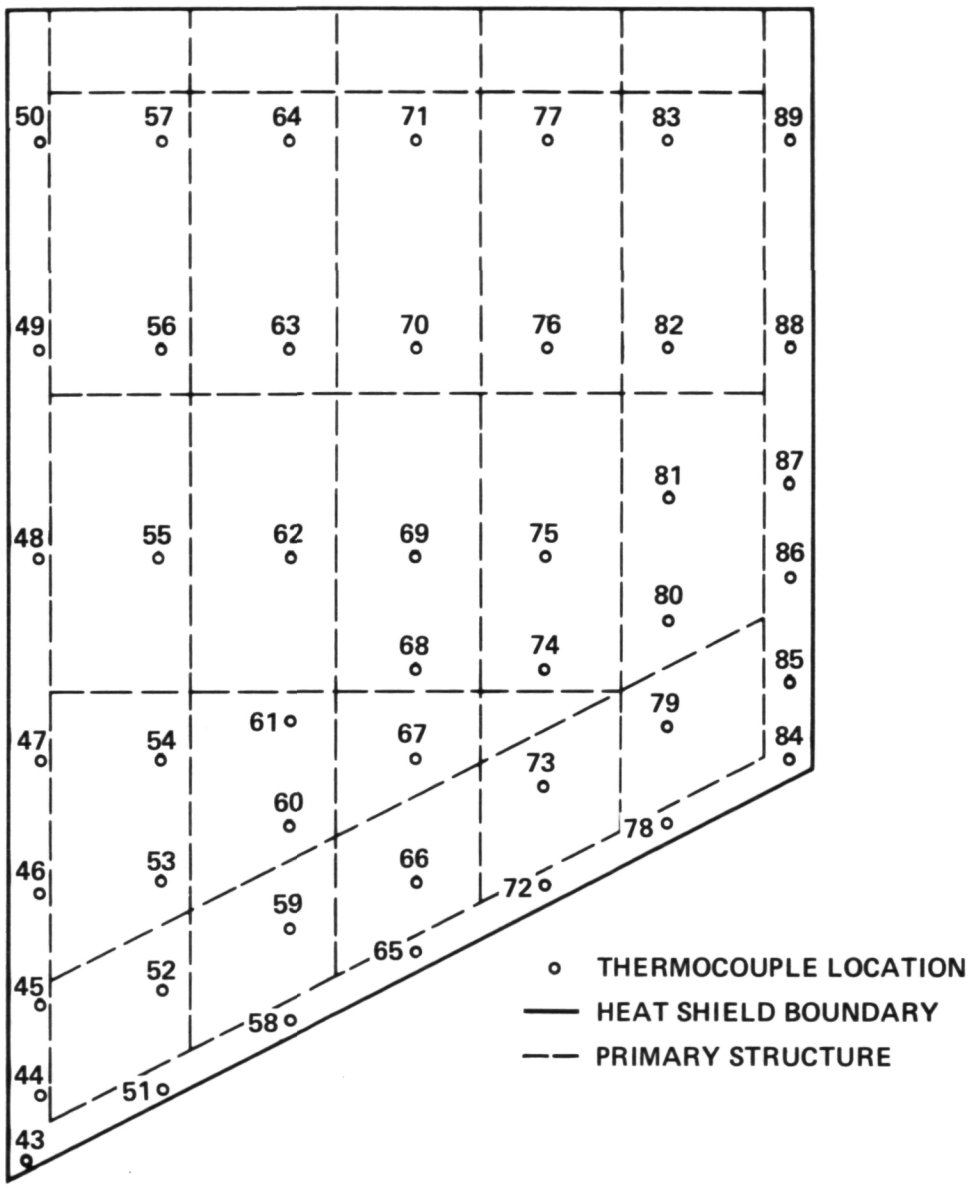

(c) Upper heat shield.

Figure 10.- Concluded.

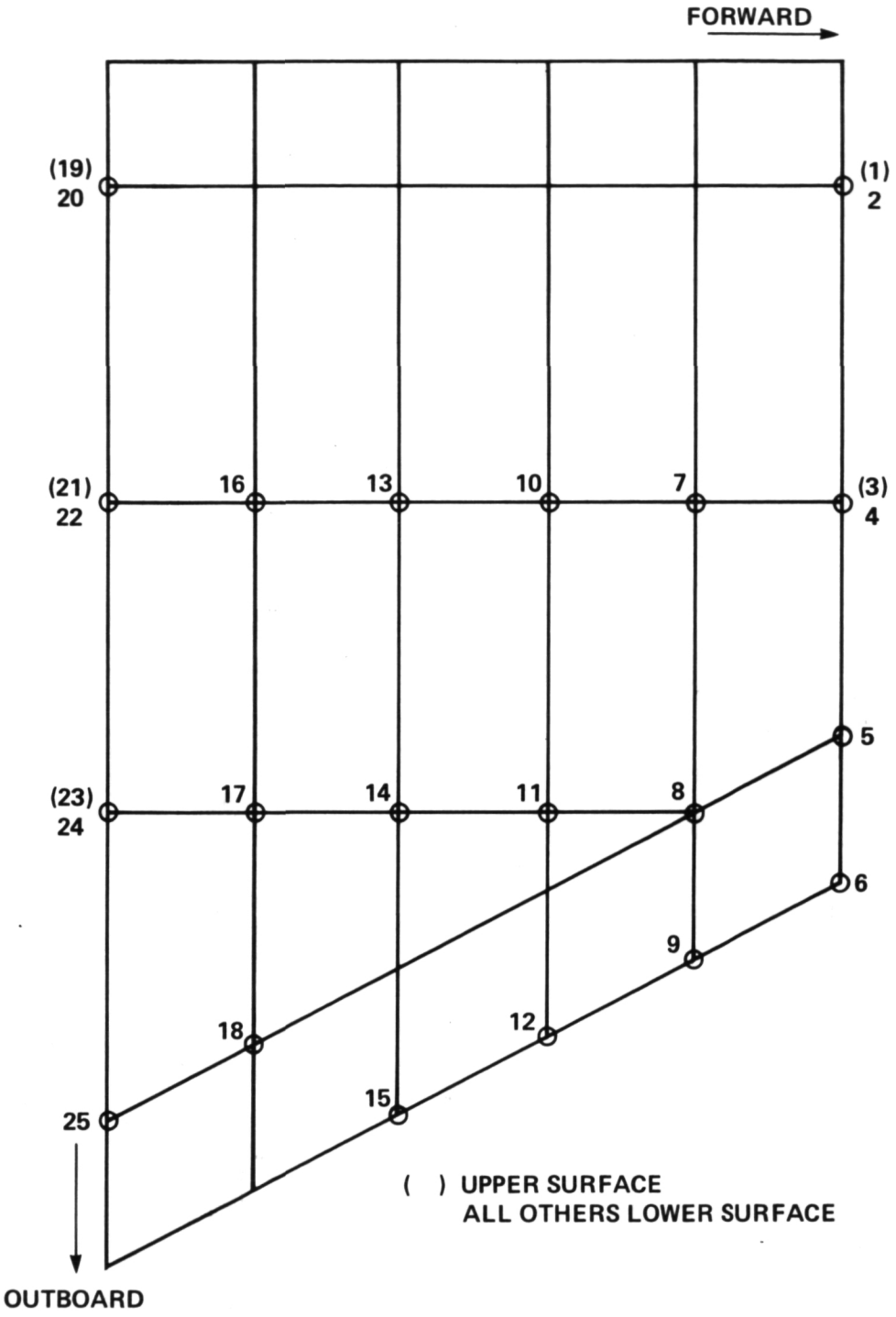

Figure 11.- HWTS load points.

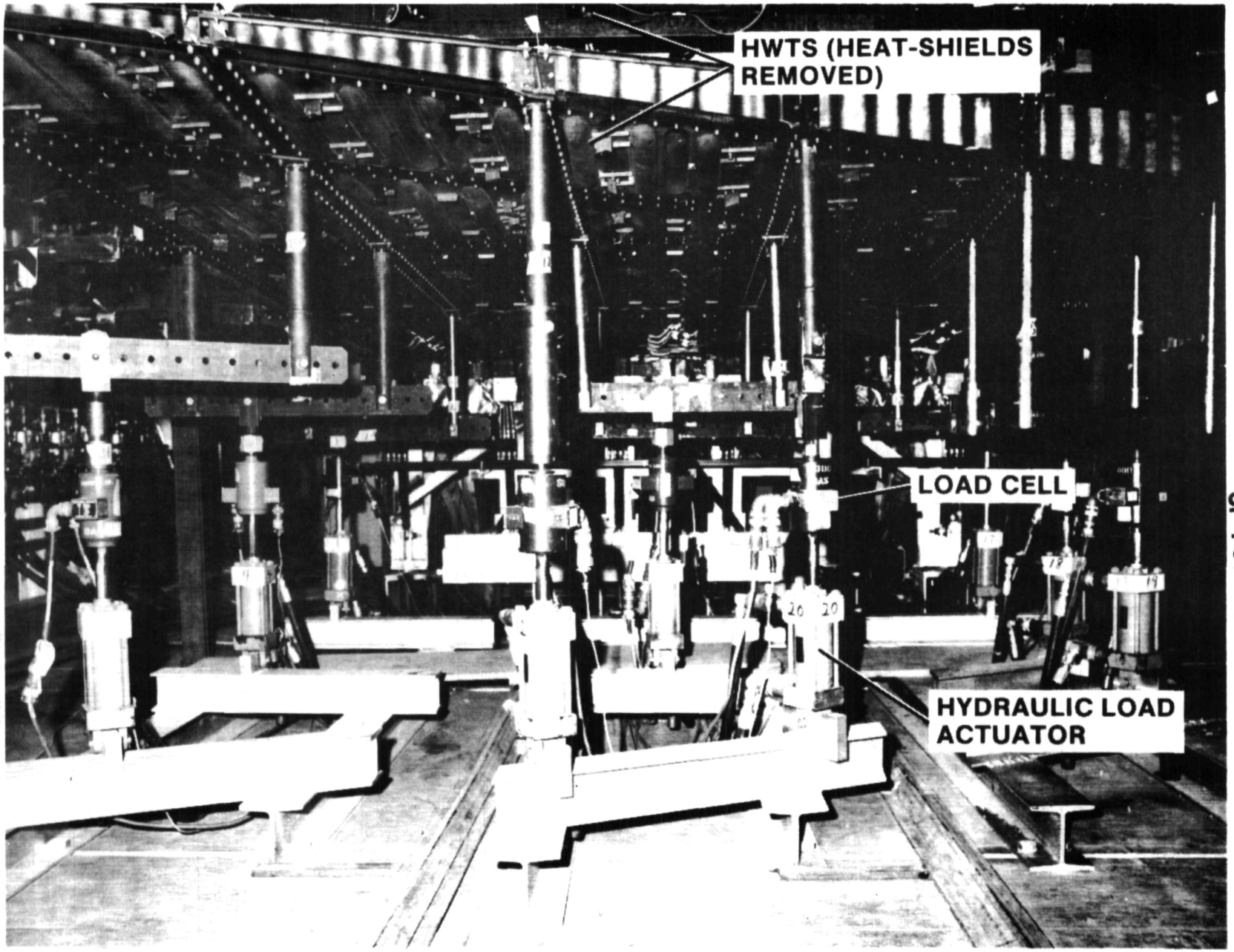

Figure 12.- HWTS vertical loading system.

ORIGINAL PAGE IS OF POOR QUALITY

ORIGINAL PAGE IS
OF POOR QUALITY

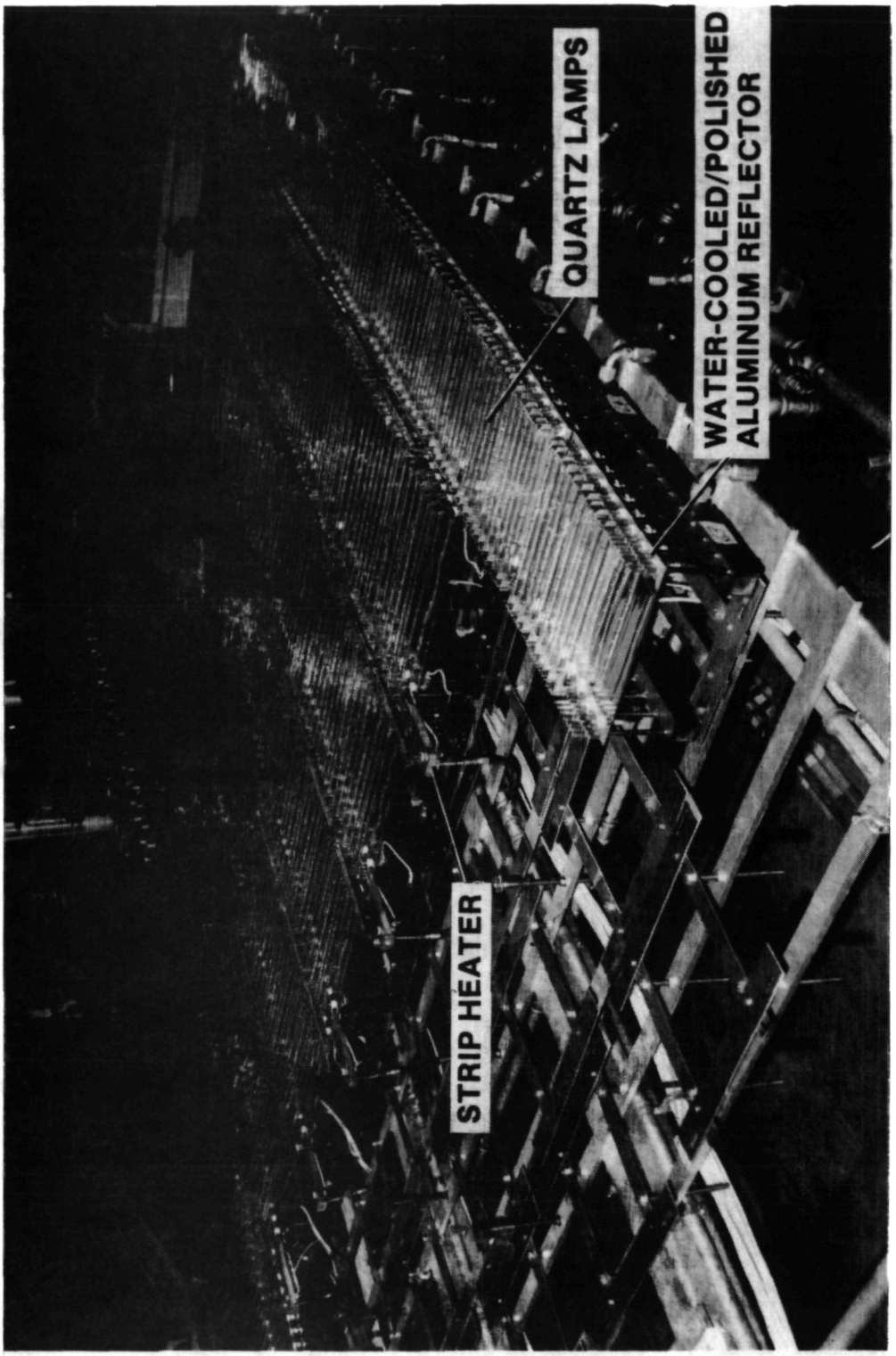

Figure 13.- Radiant heating system for HWTS.

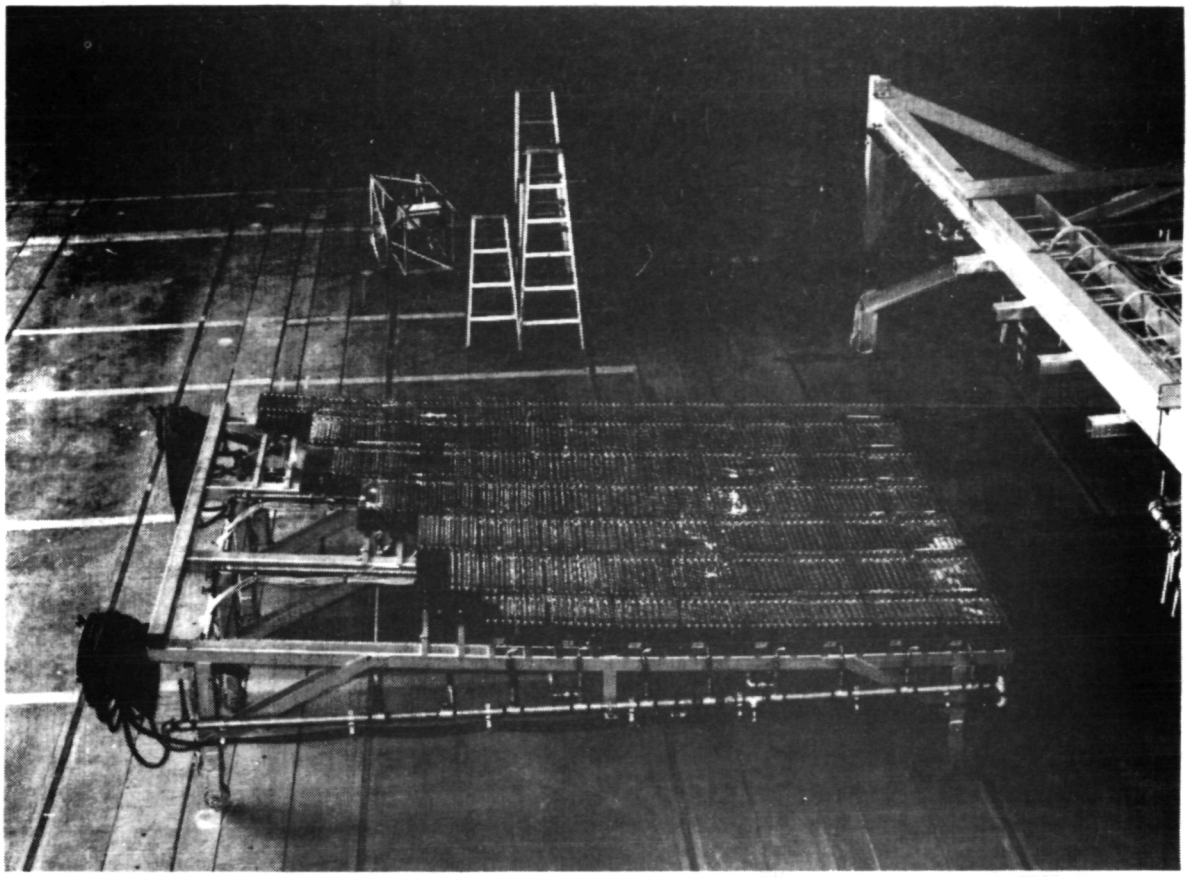

Figure 14.- Radiant heater for HWTS lower surface.

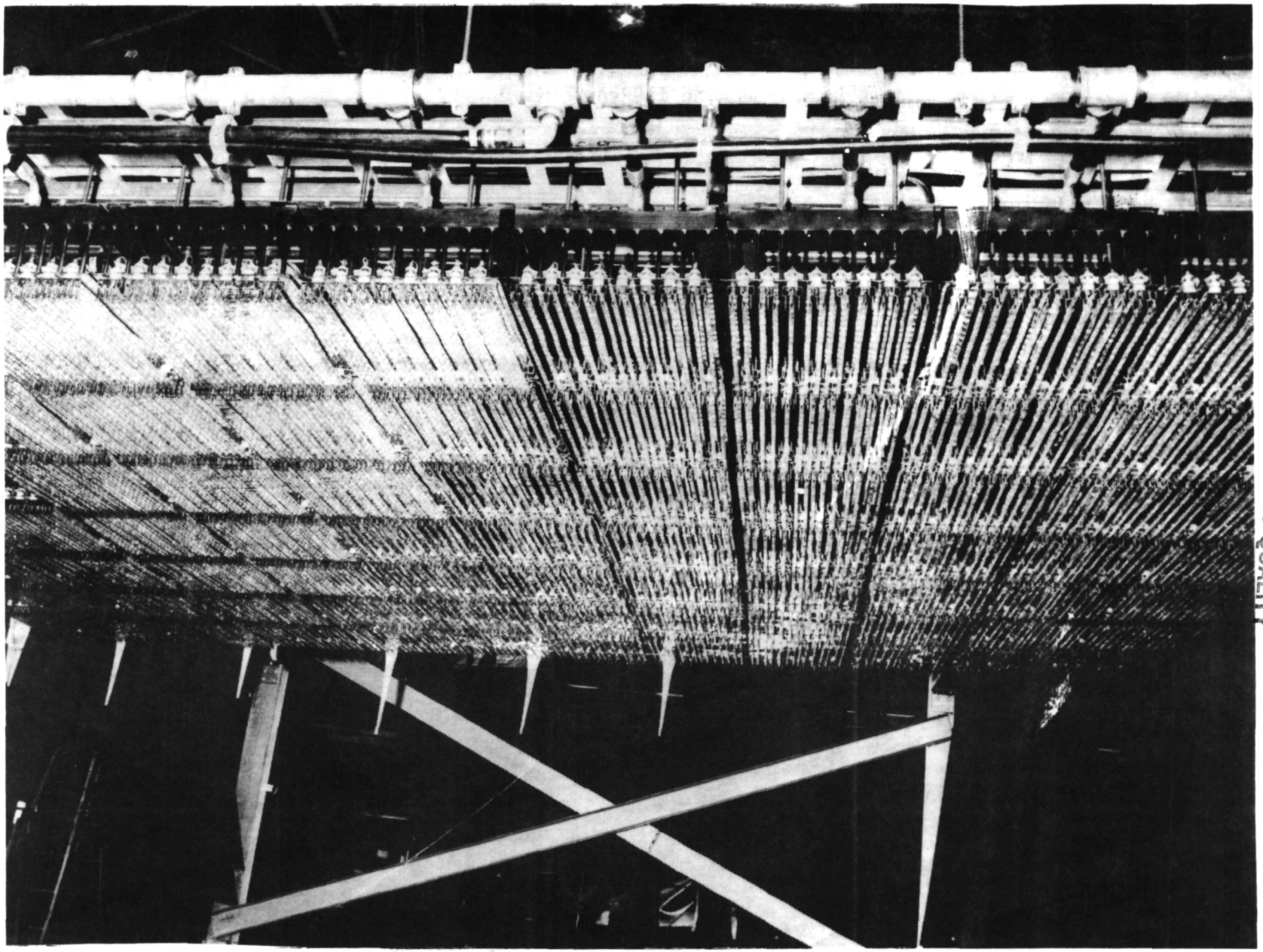

ORIGINAL PAGE IS
OF POOR QUALITY

Figure 15.- Radiant heater for HWTS upper surface.

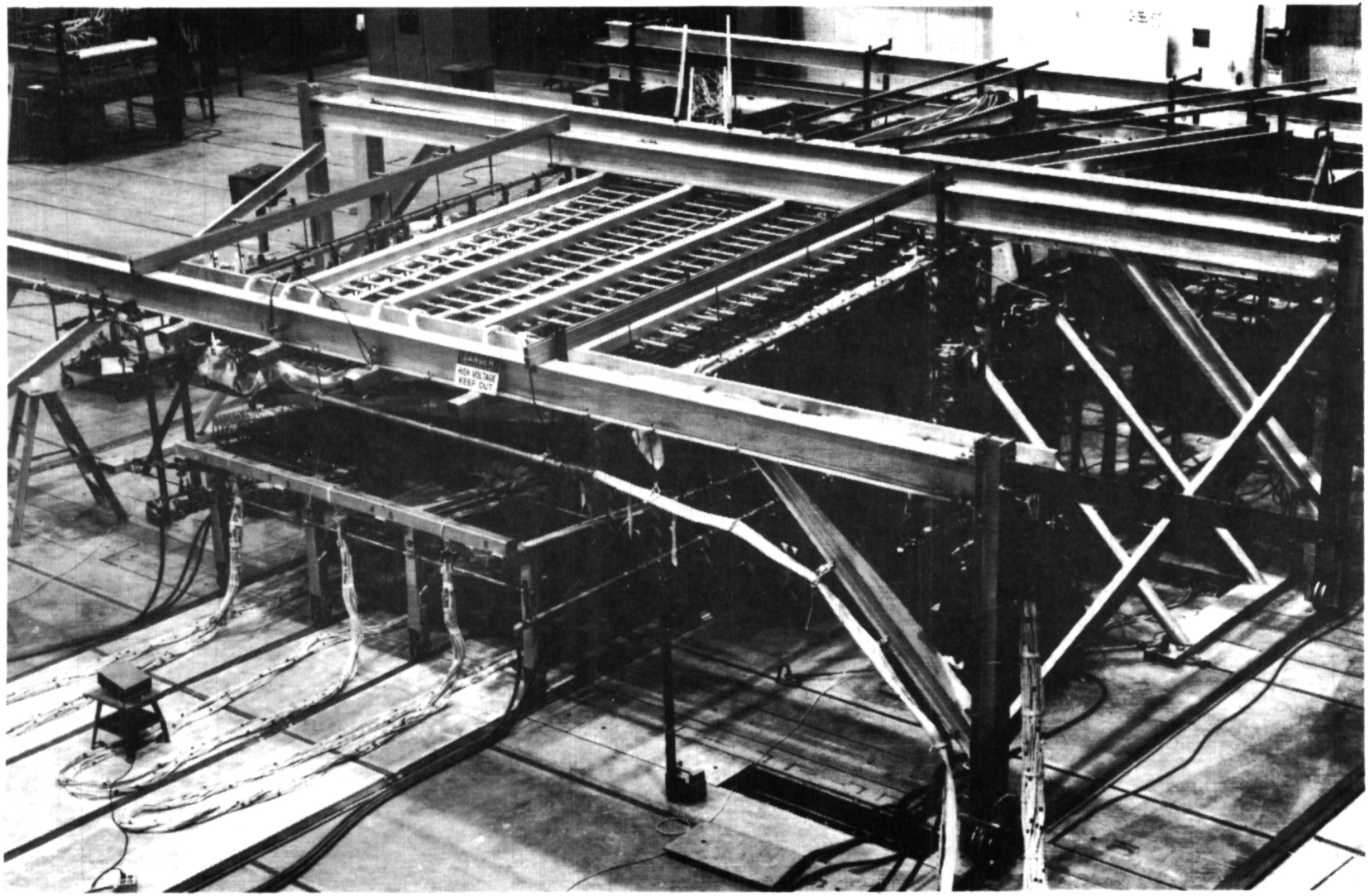

Figure 16.- Overall HWTS test setup.

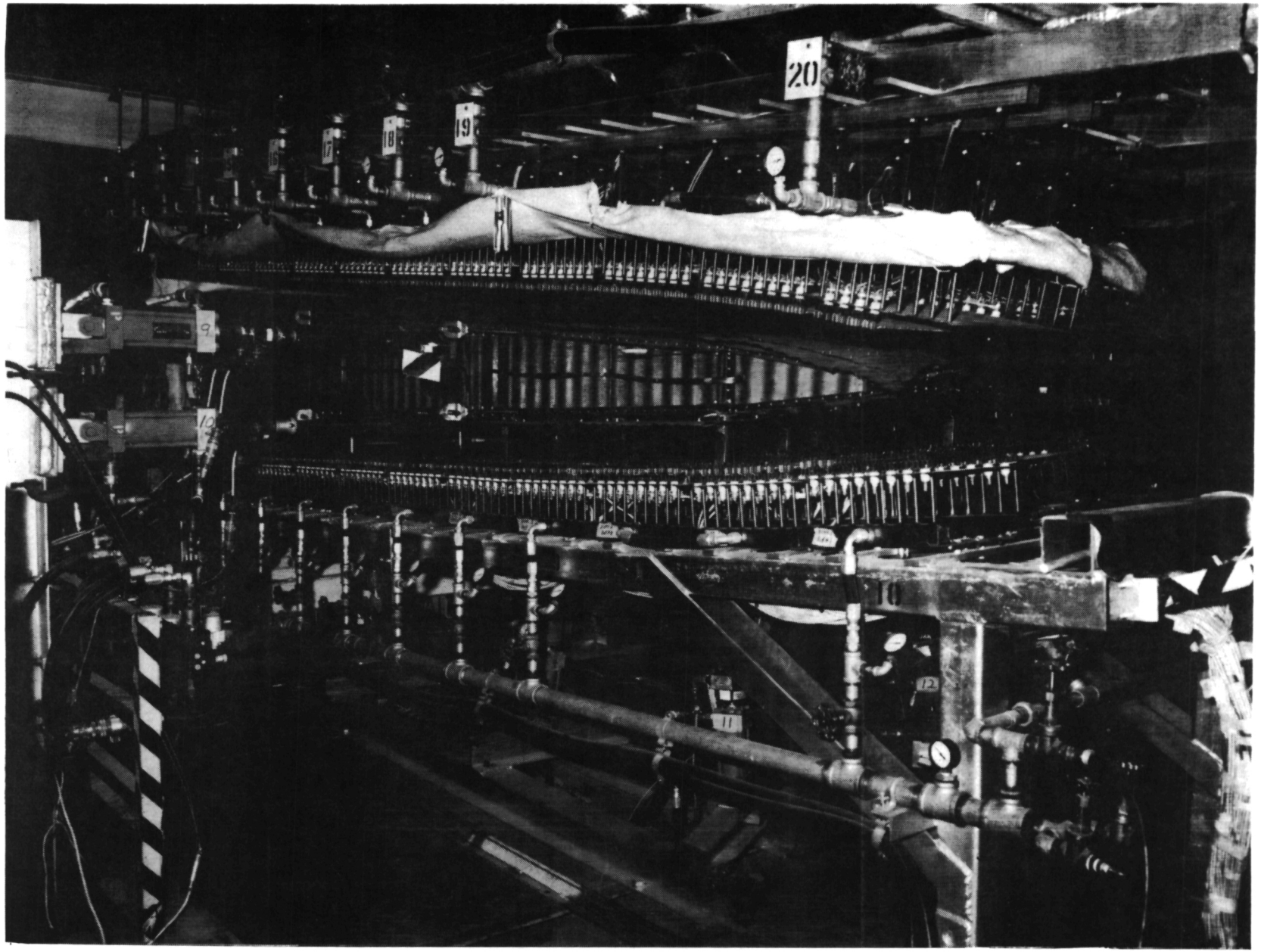

Figure 17.- Closeup of heaters in place around HWTS.

ORIGINAL PAGE IS
OF POOR QUALITY

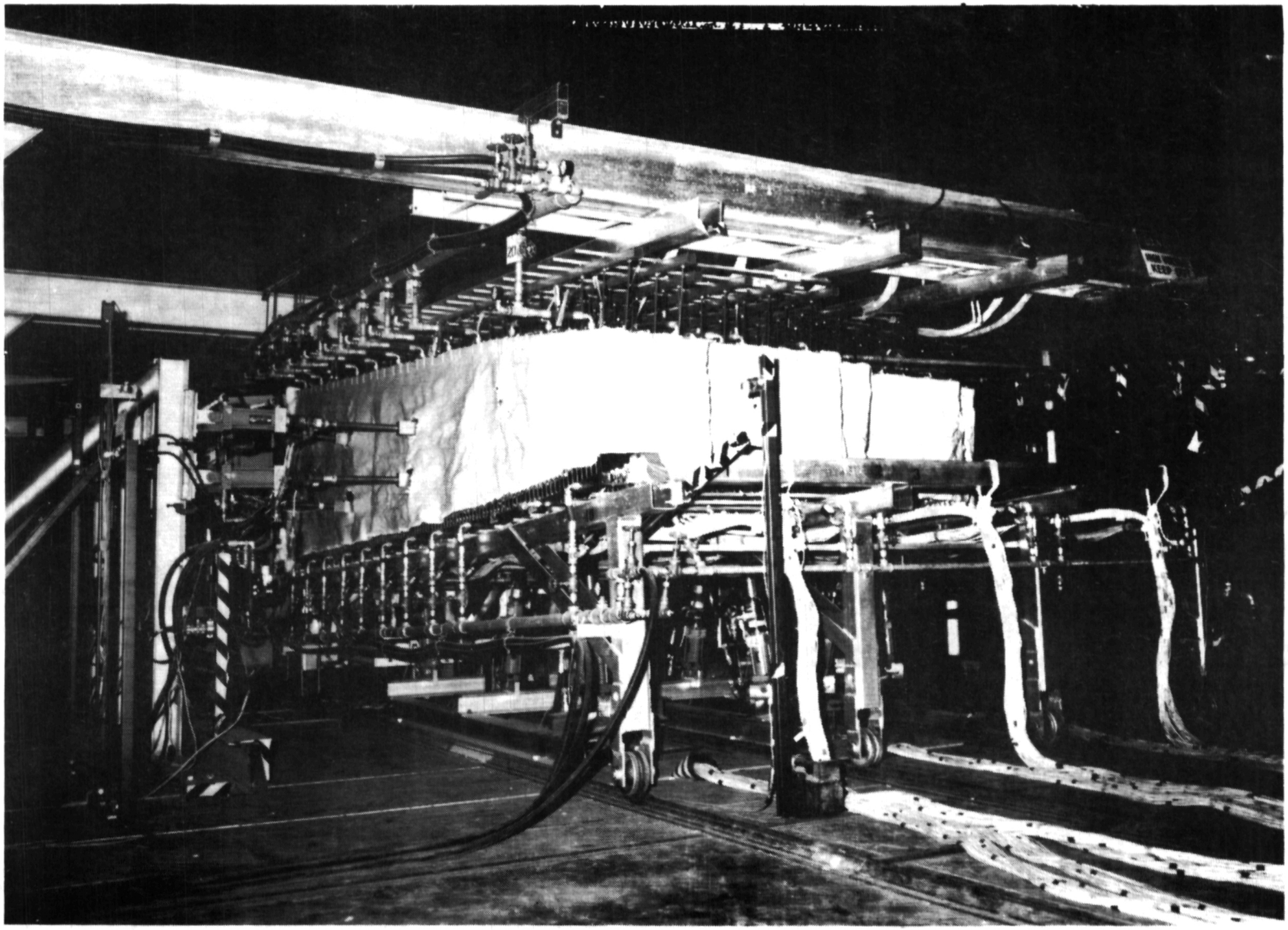

Figure 18.- HWTS heating setup with curtains closed.

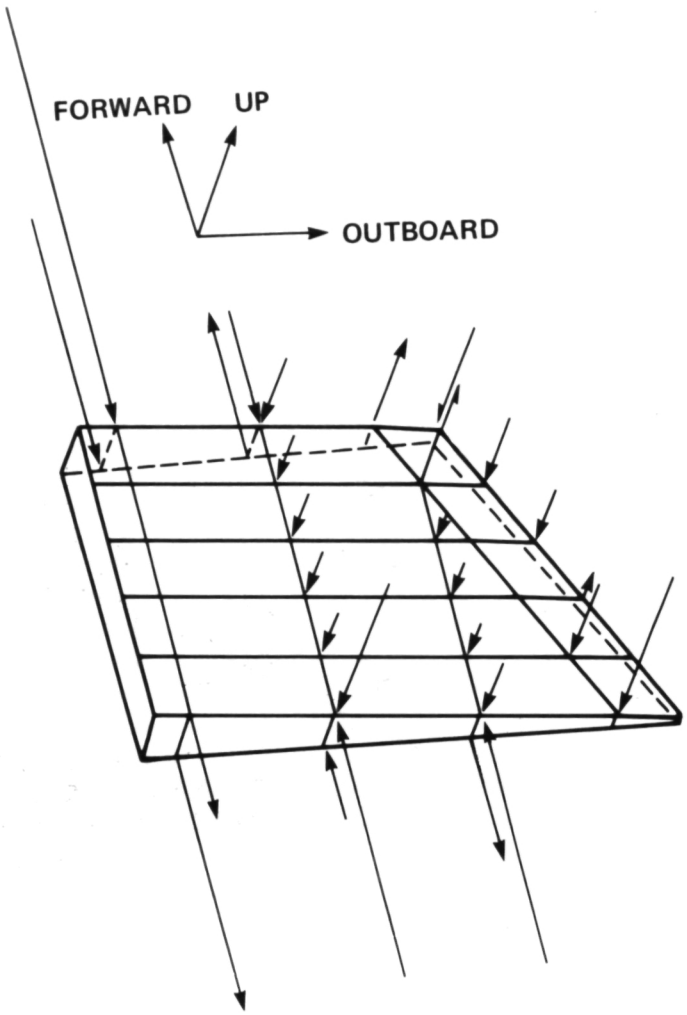

Figure 19.- Applied load distribution on HWTS.

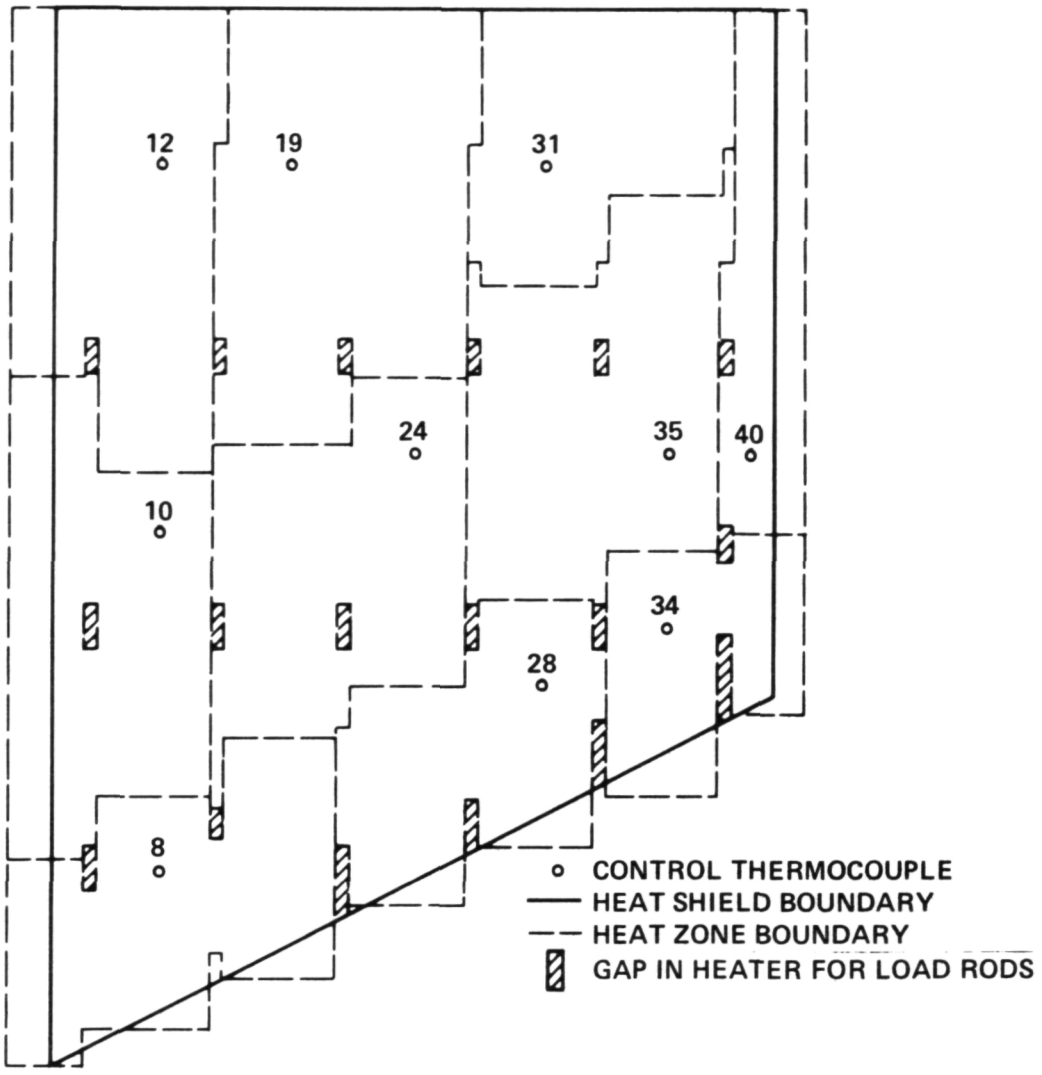

(a) Lower surface heater.

Figure 20.- Analog heating control zones for HWTS.

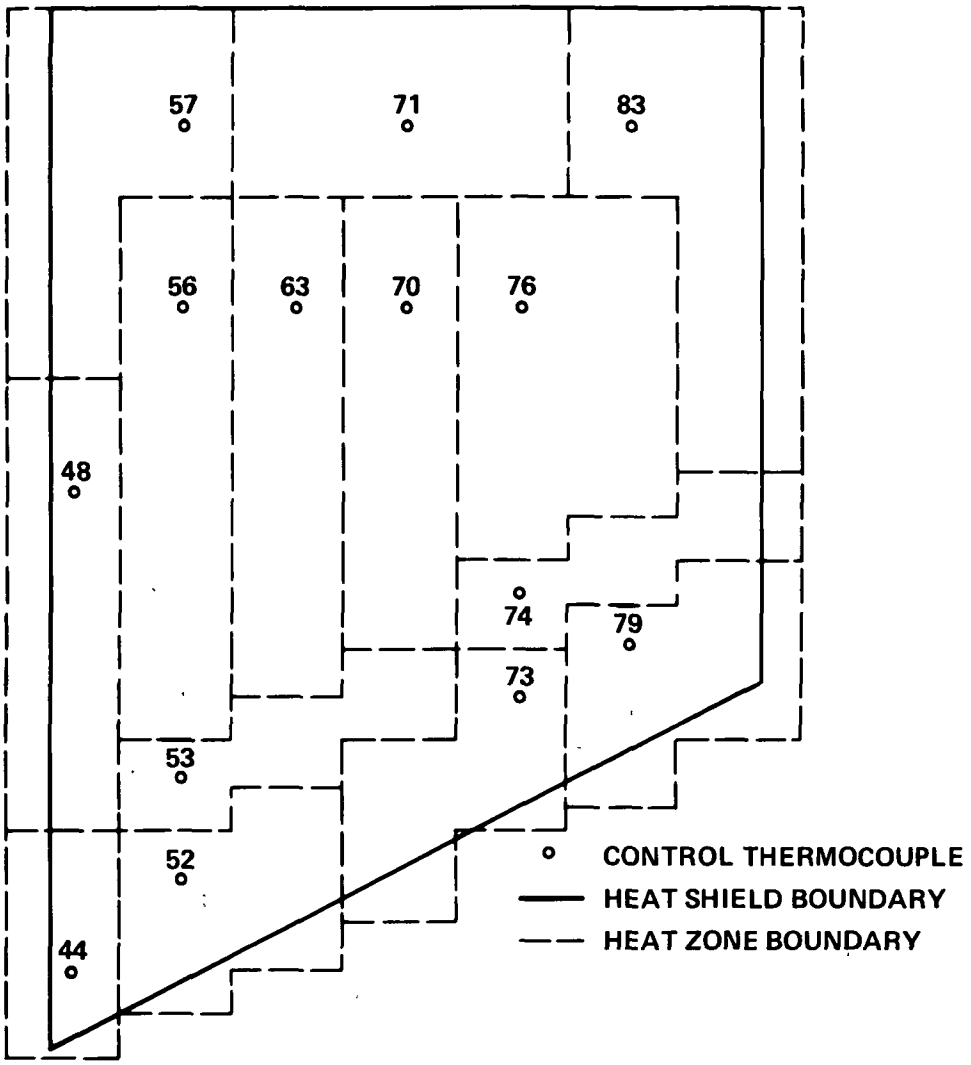

(b) Upper surface heater.

Figure 20.- Concluded.

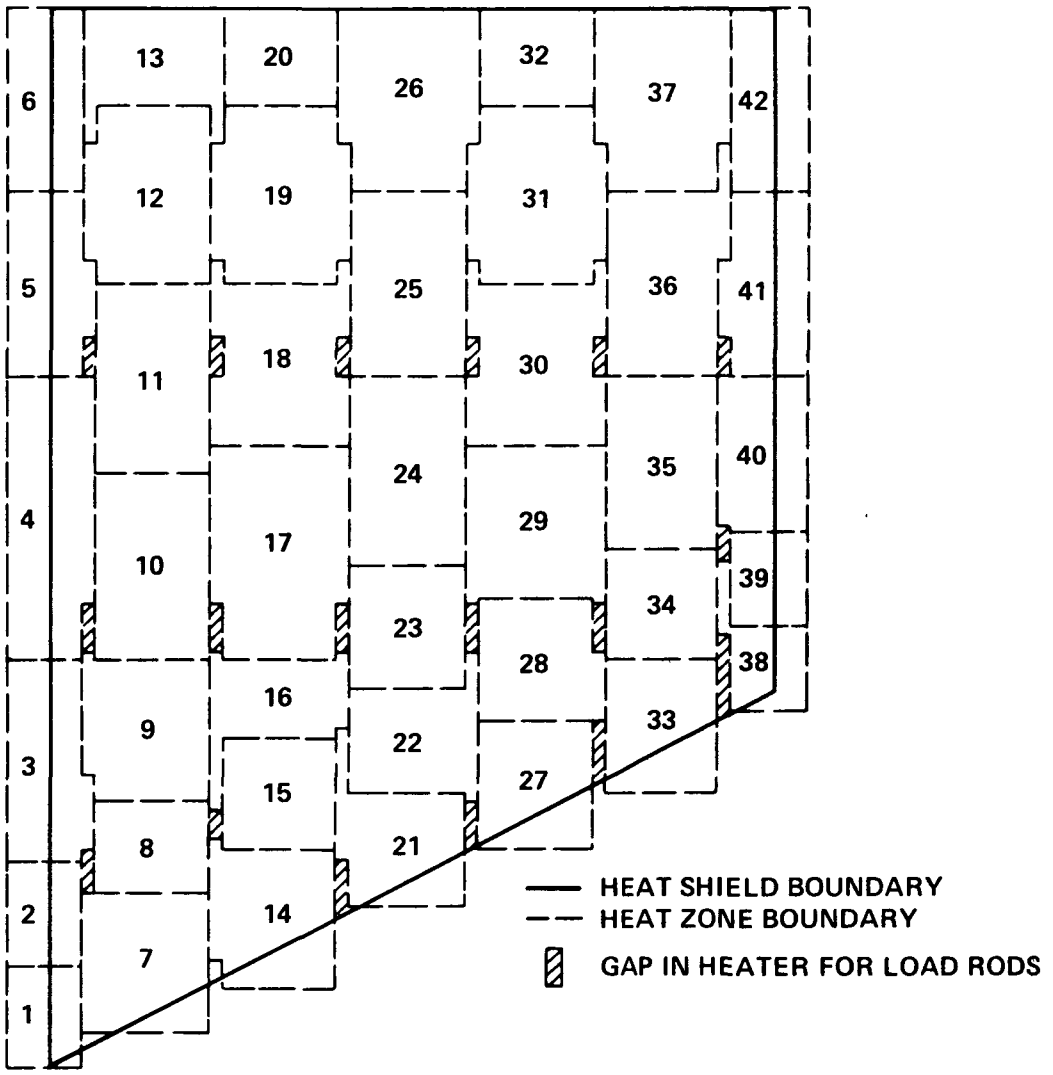

(a) Lower surface heater.

Figure 21.- Digital heating control zones for HWTS.

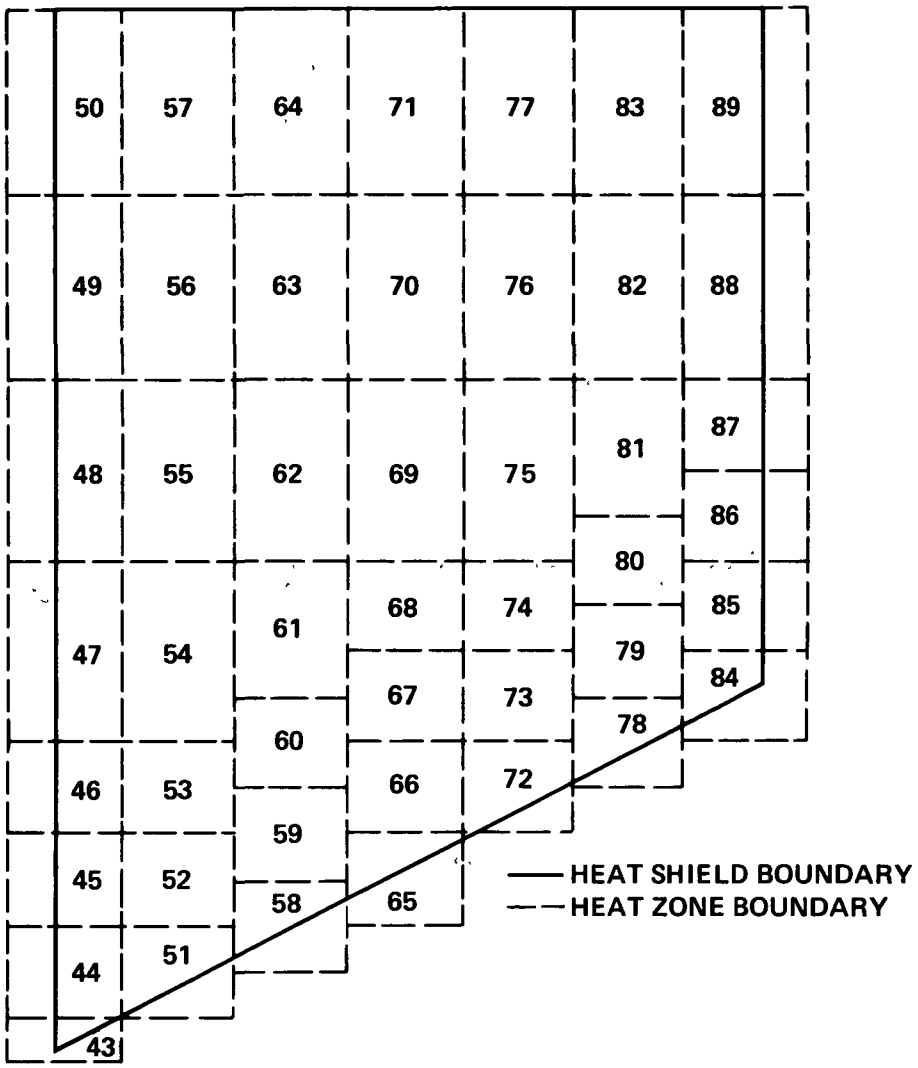

(b) Upper surface heater.

Figure 21.- Concluded.

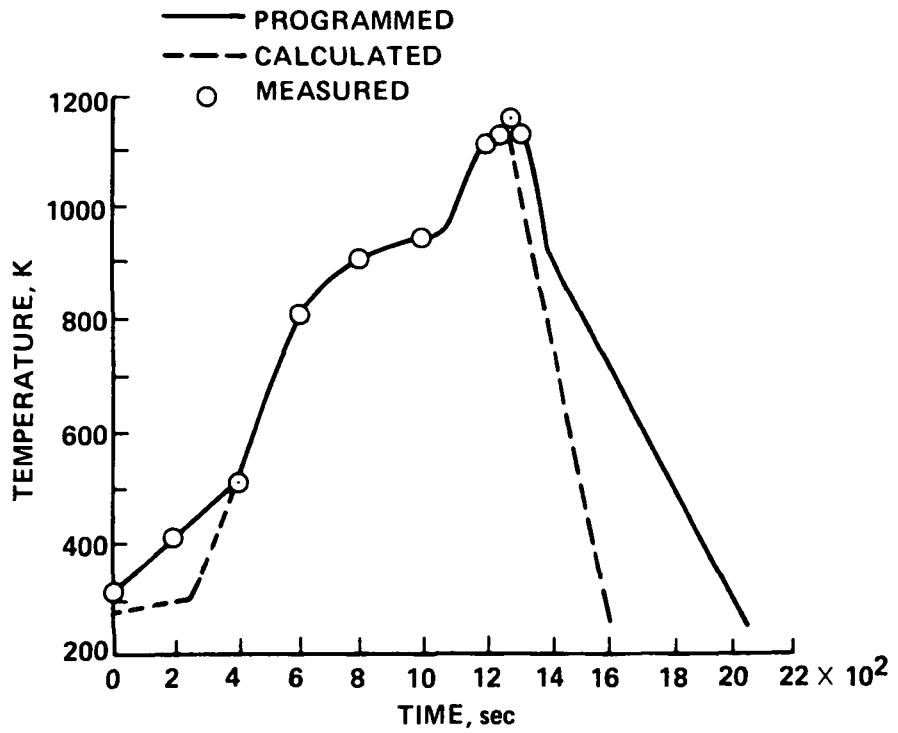

(a) Zone 14.

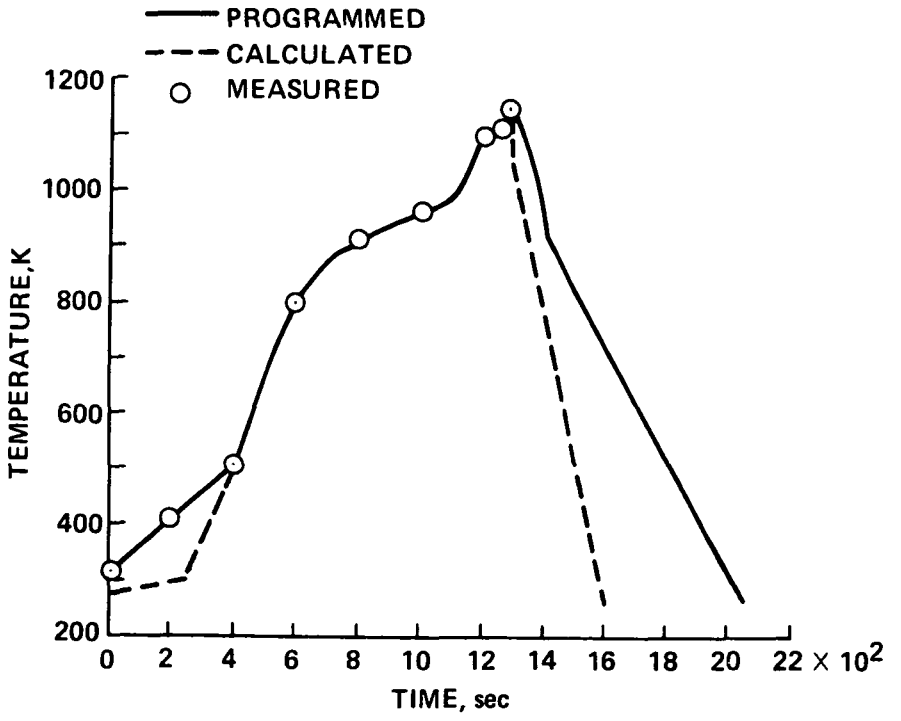

(b) Zone 15.

Figure 22.- Temperature profiles for HWTS.

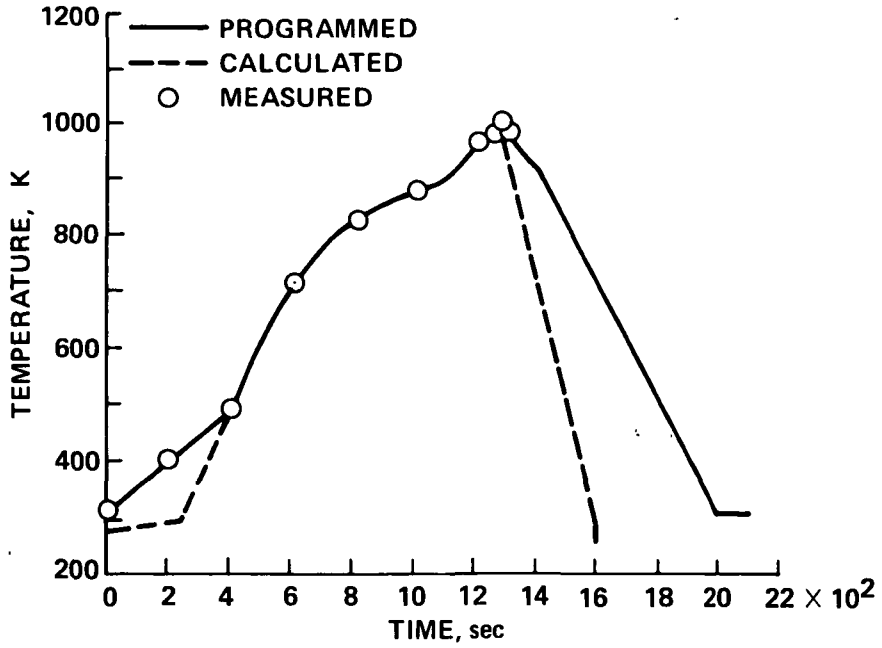

(c) Zone 16.

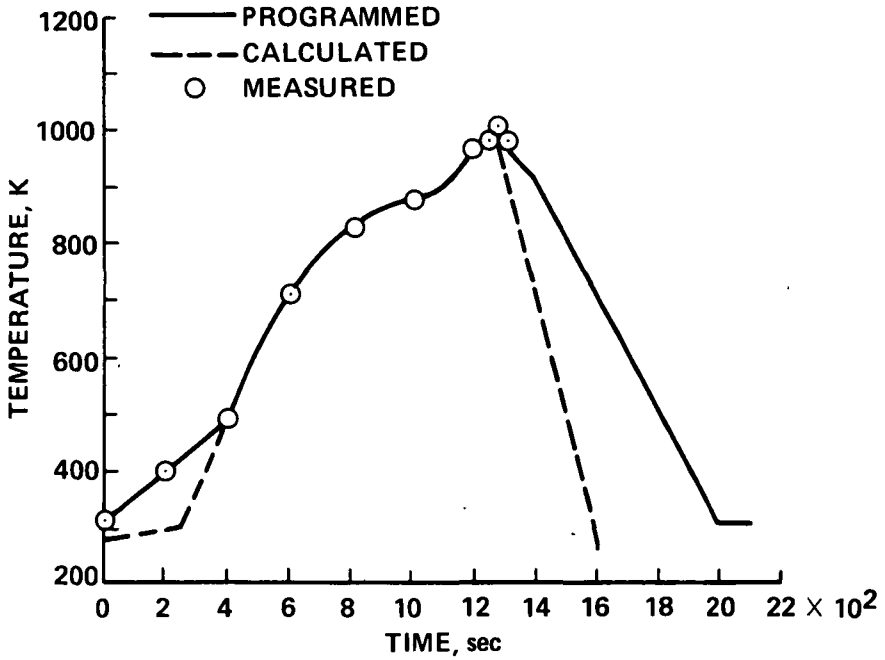

(d) Zone 17.

Figure 22.- Continued.

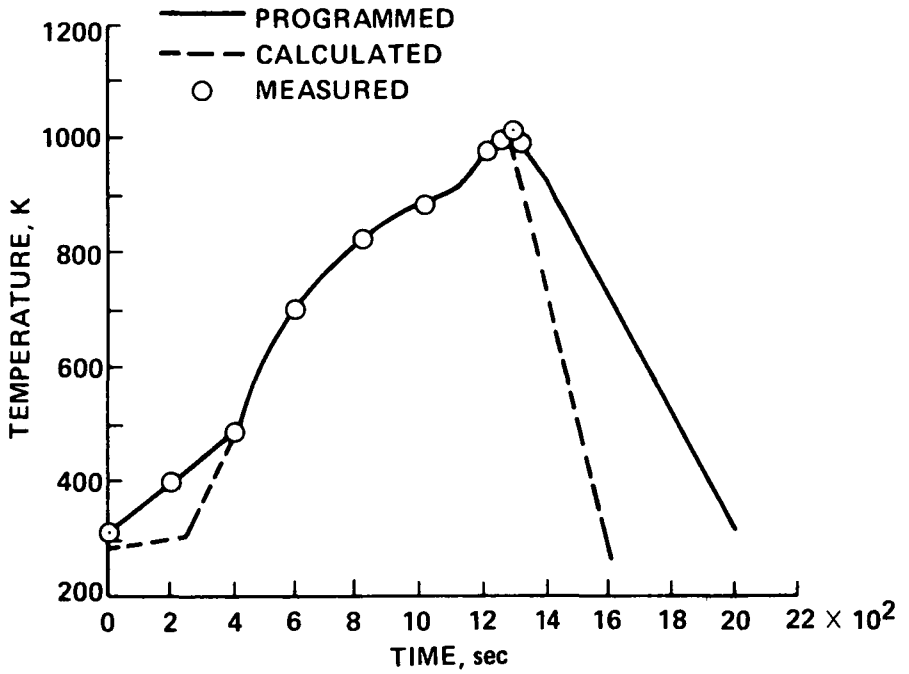

(e) Zone 18.

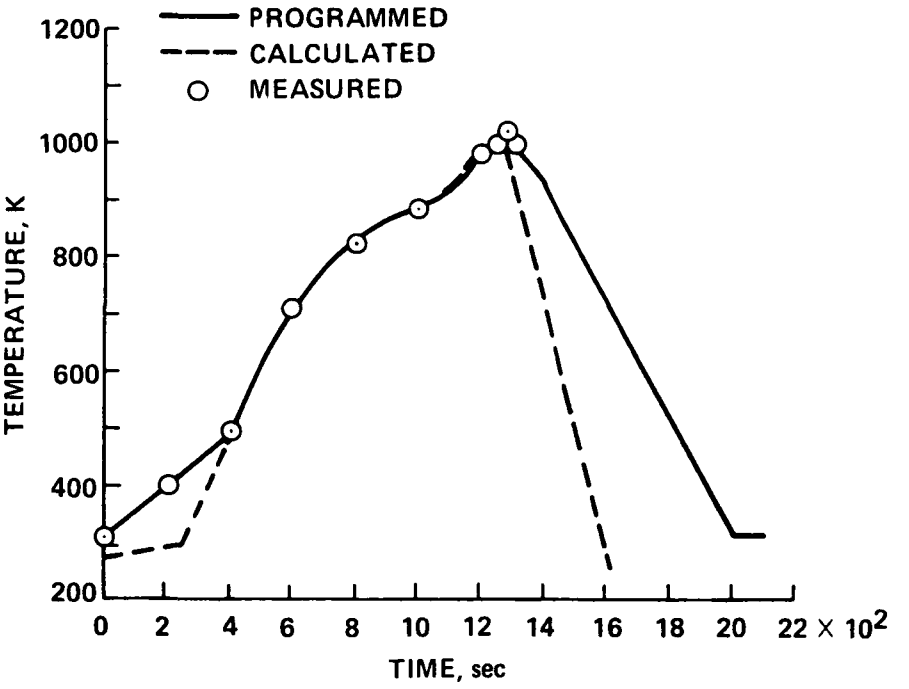

(f) Zone 19.

Figure 22.- Continued.

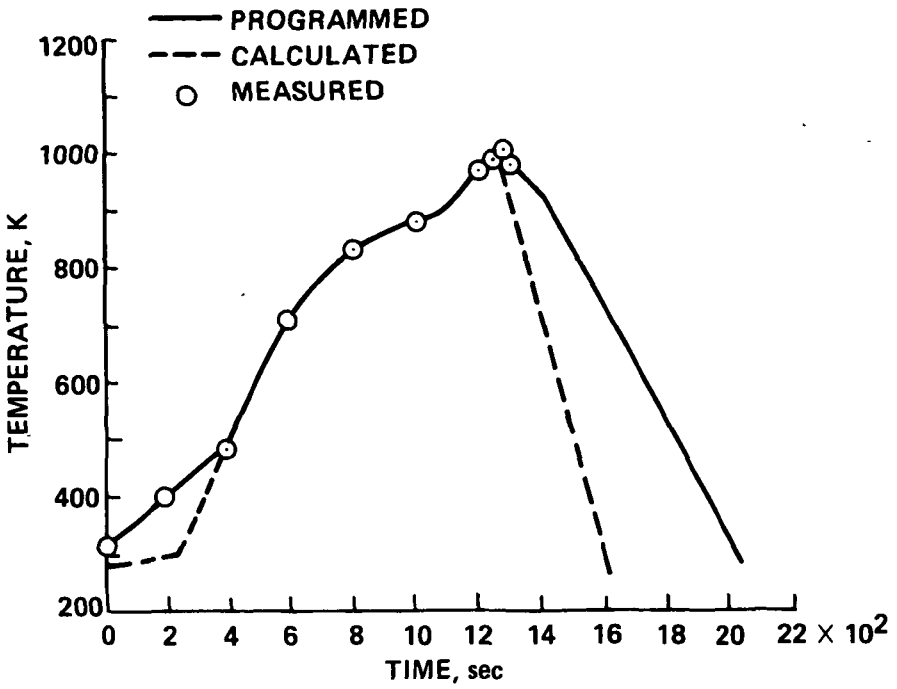

(g) Zone 20.

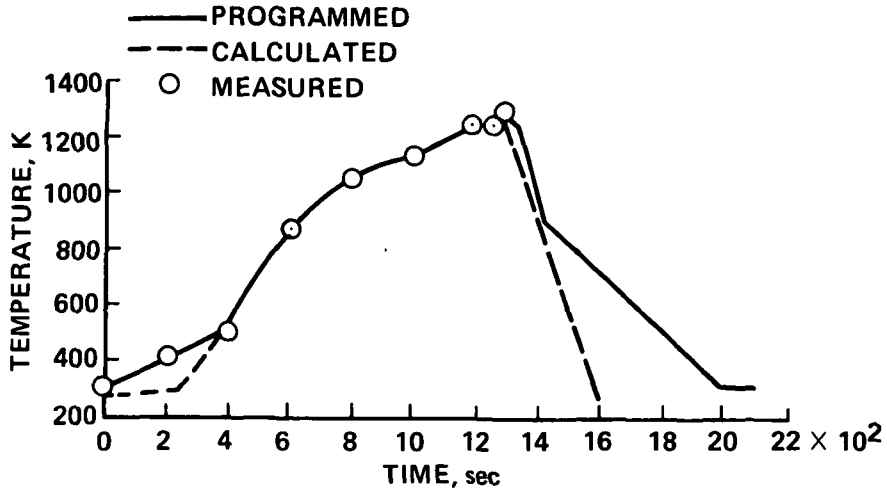

(h) Zone 58.

Figure 22.- Continued.

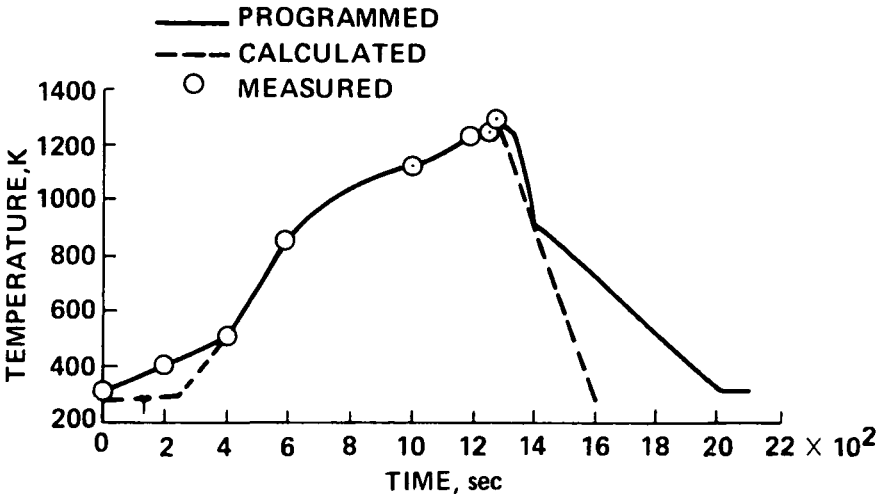

(i) Zone 59.

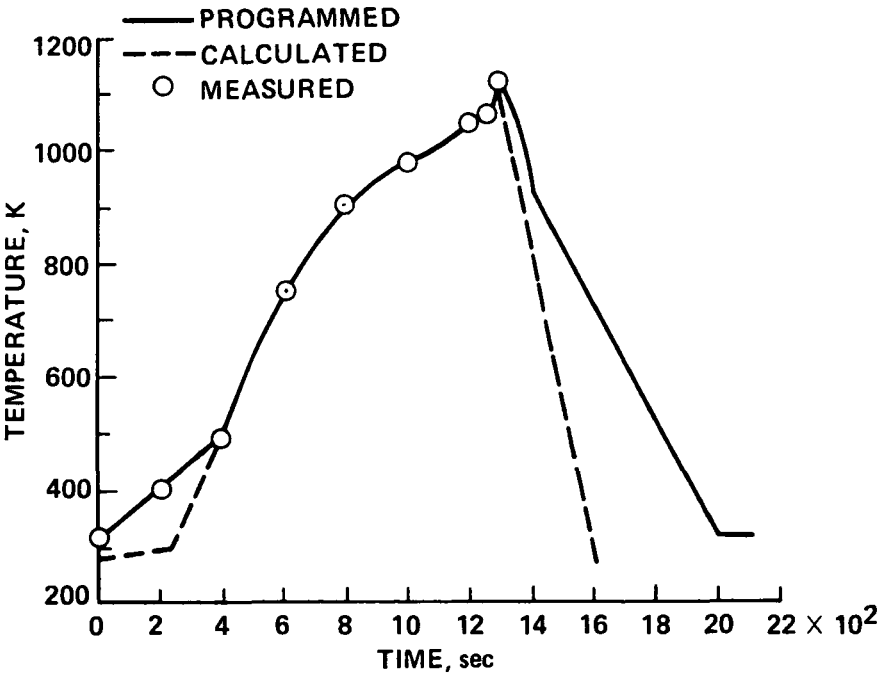

(j) Zone 60.

Figure 22.- Continued.

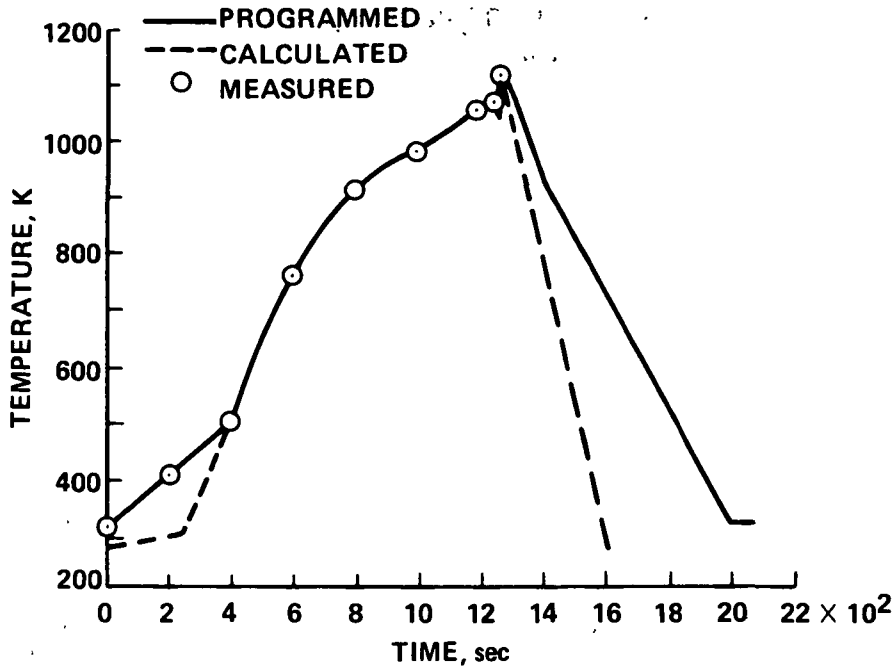

(k) Zone 61.

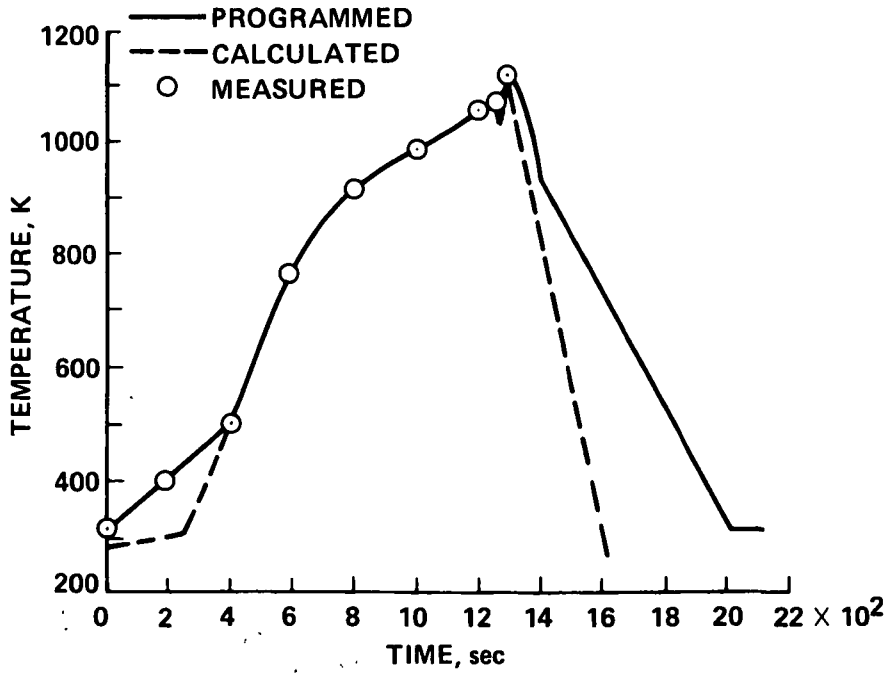

(l) Zone 62.

Figure 22.- Continued.

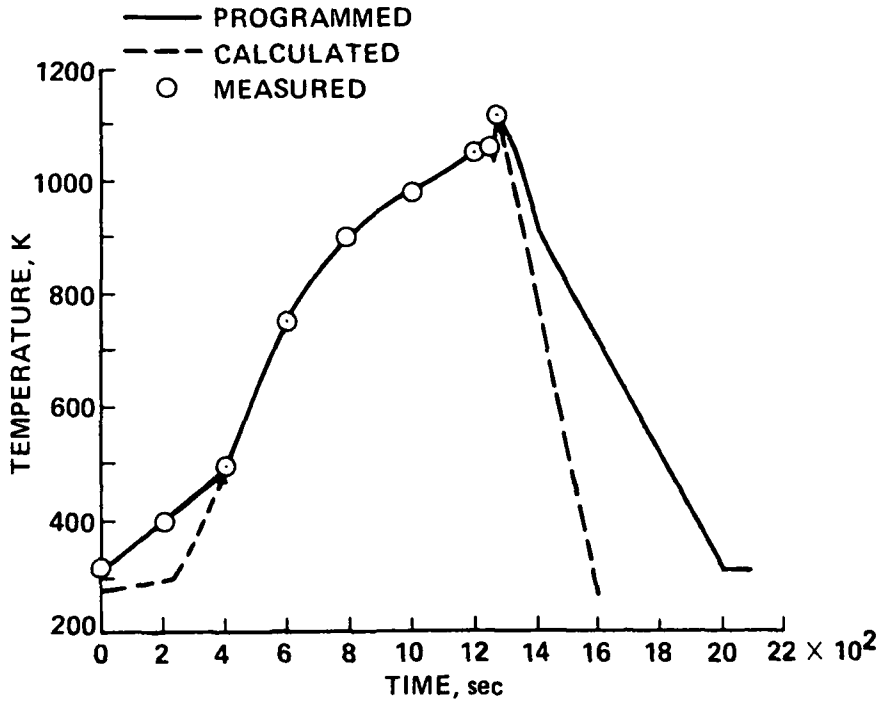

(m) Zone 63.

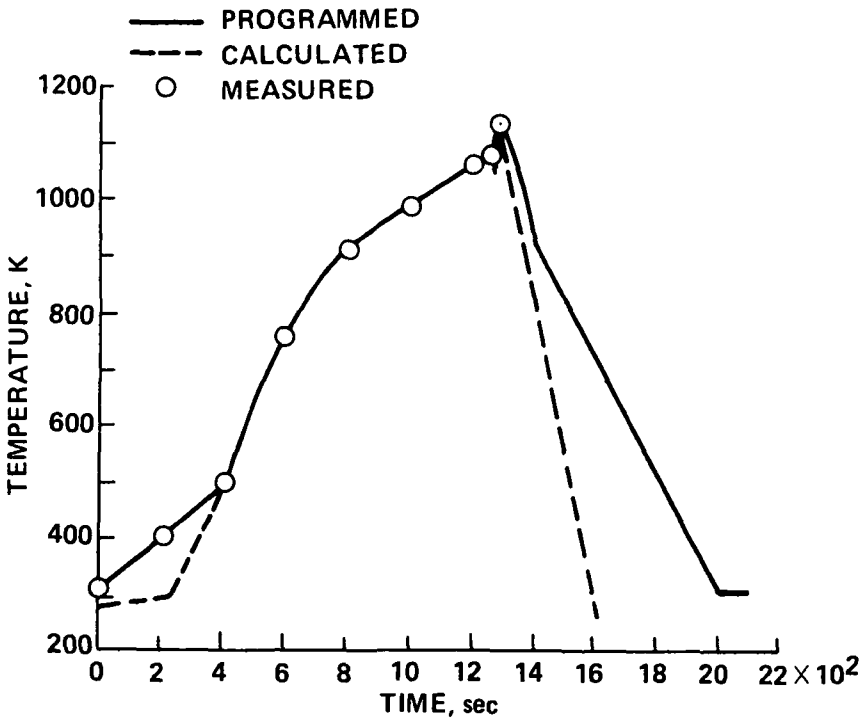

(n) Zone 64.

Figure 22.- Concluded.

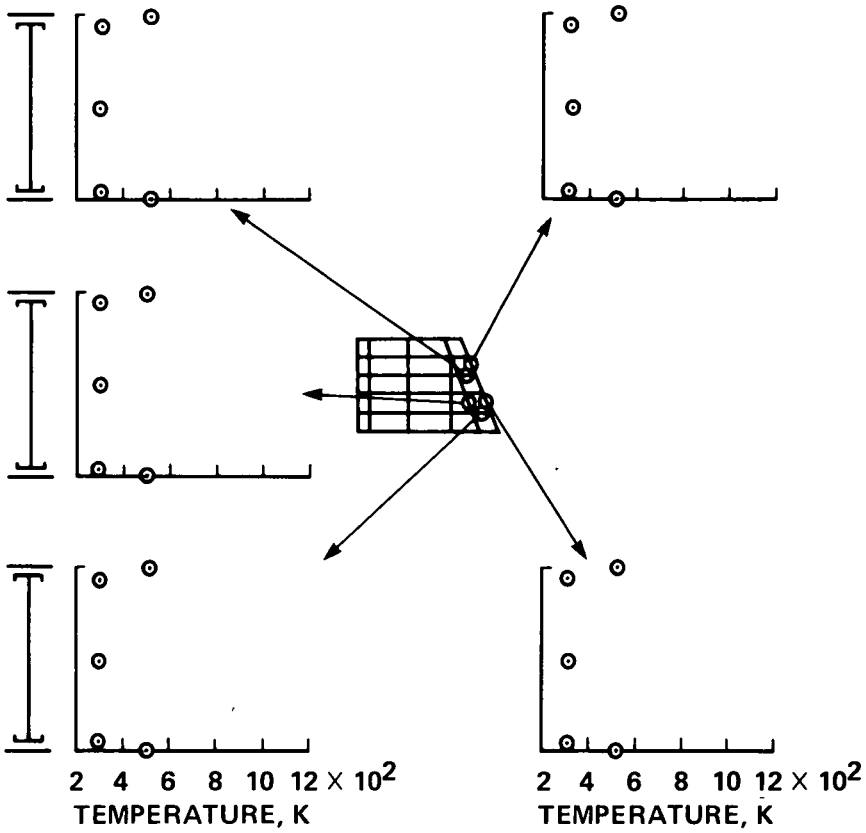

(a) Time = 400 sec.

Figure 23.- Measured spar, rib, and heat shield temperatures.

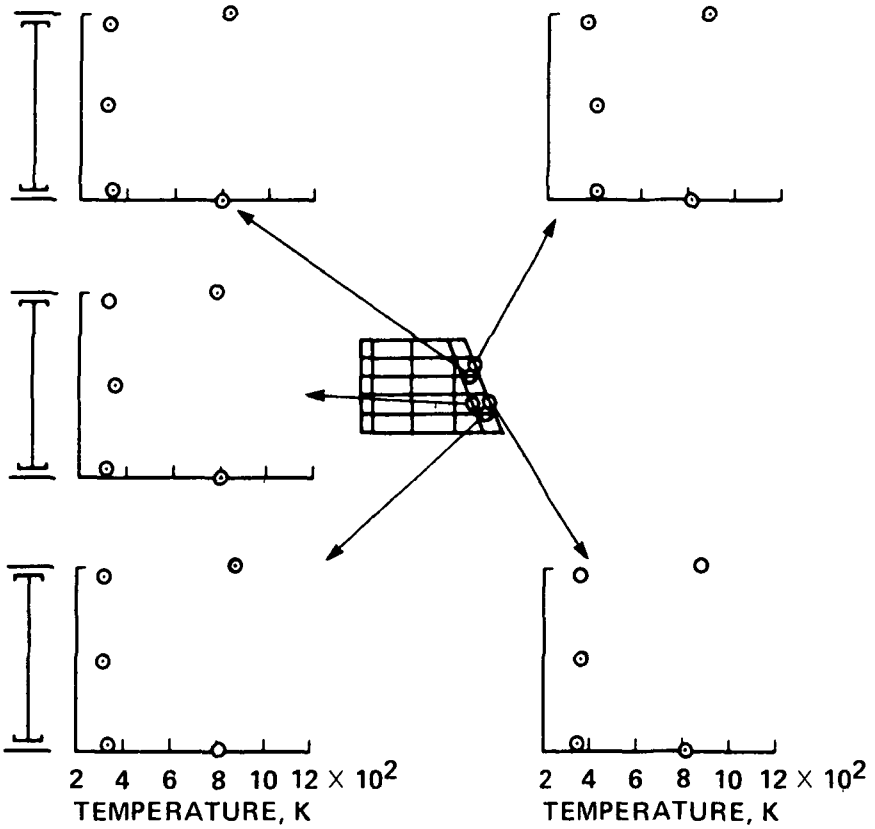

(b) Time = 600 sec.

Figure 23.- Continued.

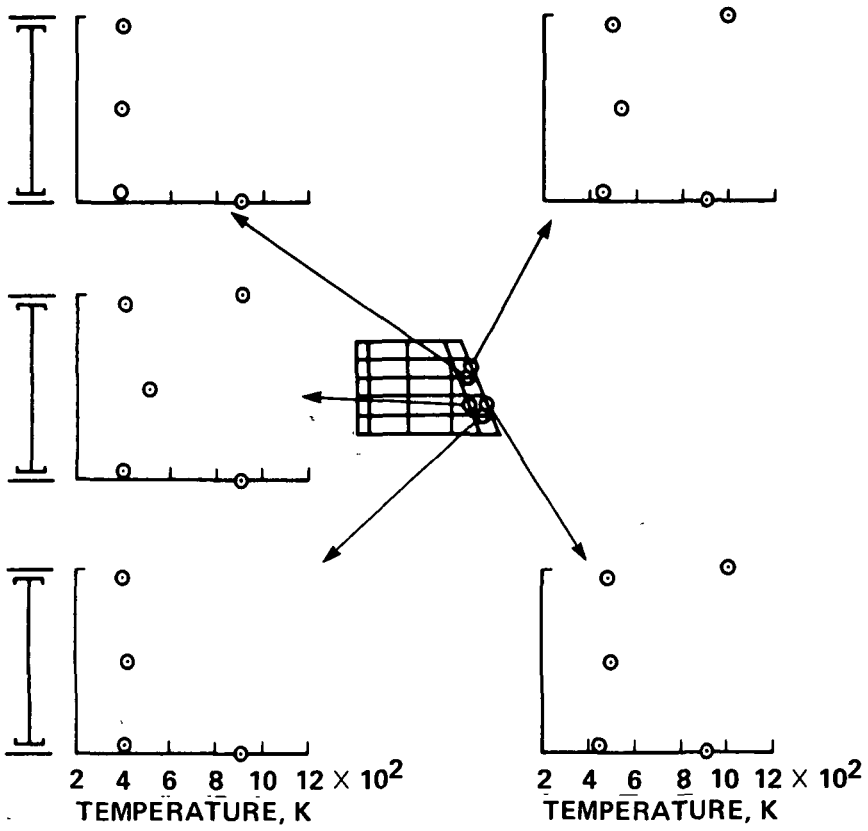

(c) Time = 800 sec.

Figure 23.- Continued.

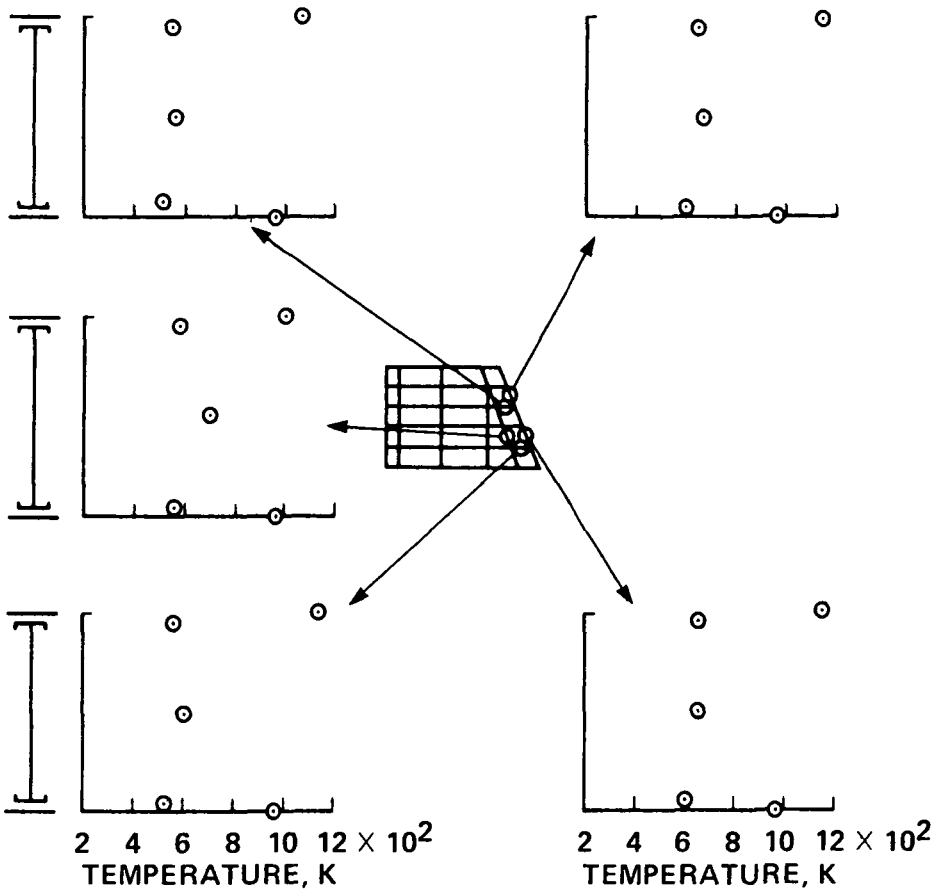

(d) Time = 1000 sec.

Figure 23.- Continued.

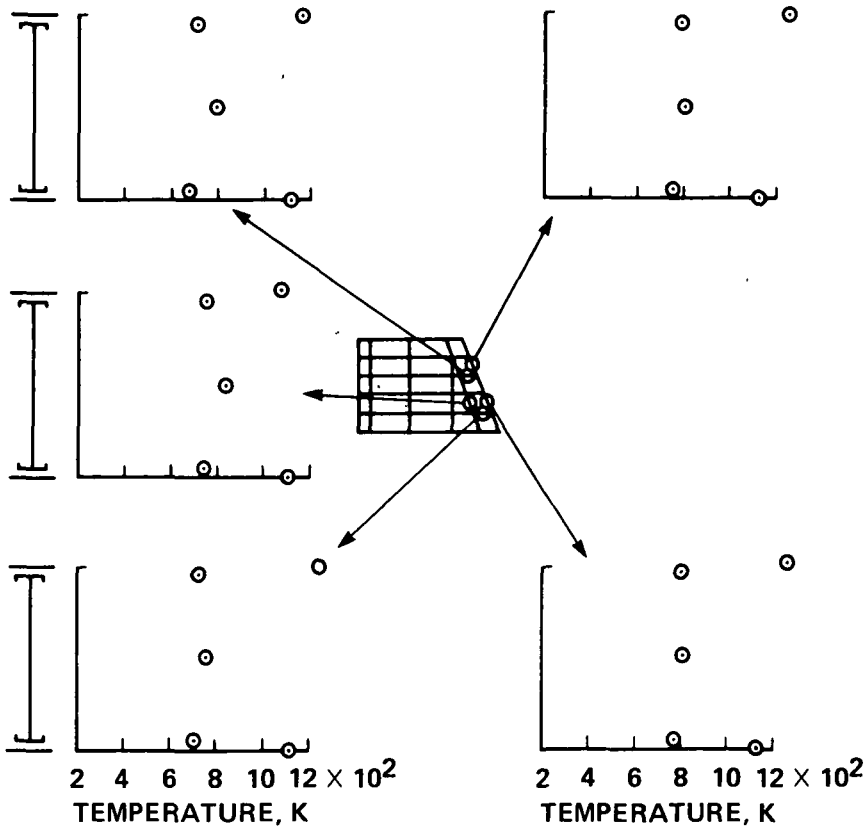

(e) Time = 1200 sec.

Figure 23.- Continued.

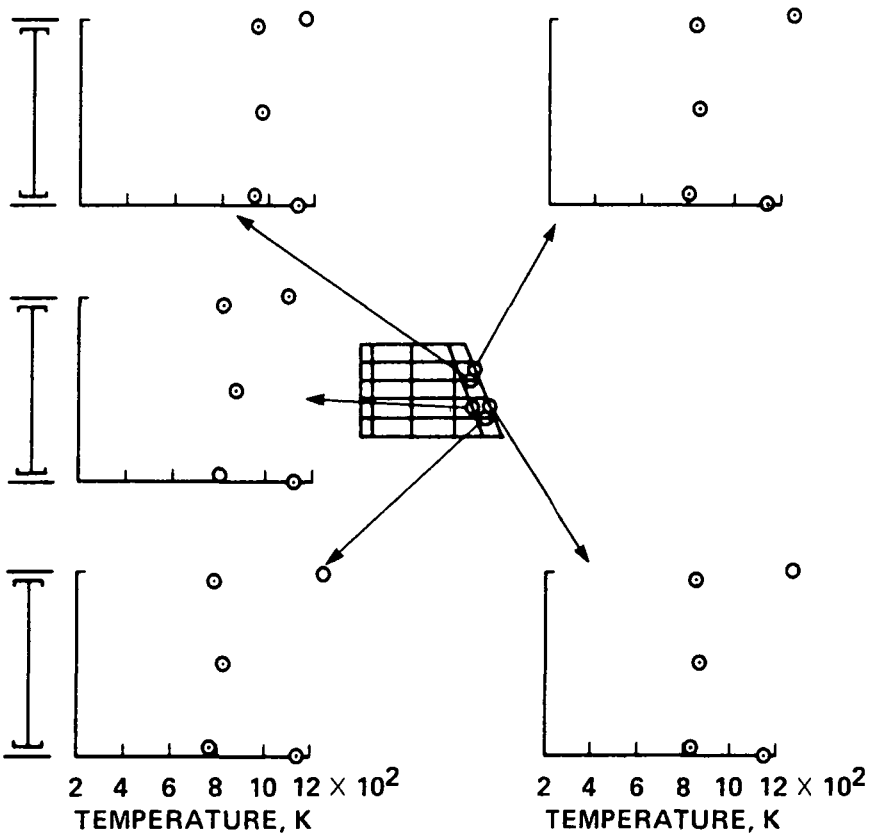

(f) Time = 1250 sec.

Figure 23.- Continued.

ORIGINAL PAGE IS
OF POOR QUALITY

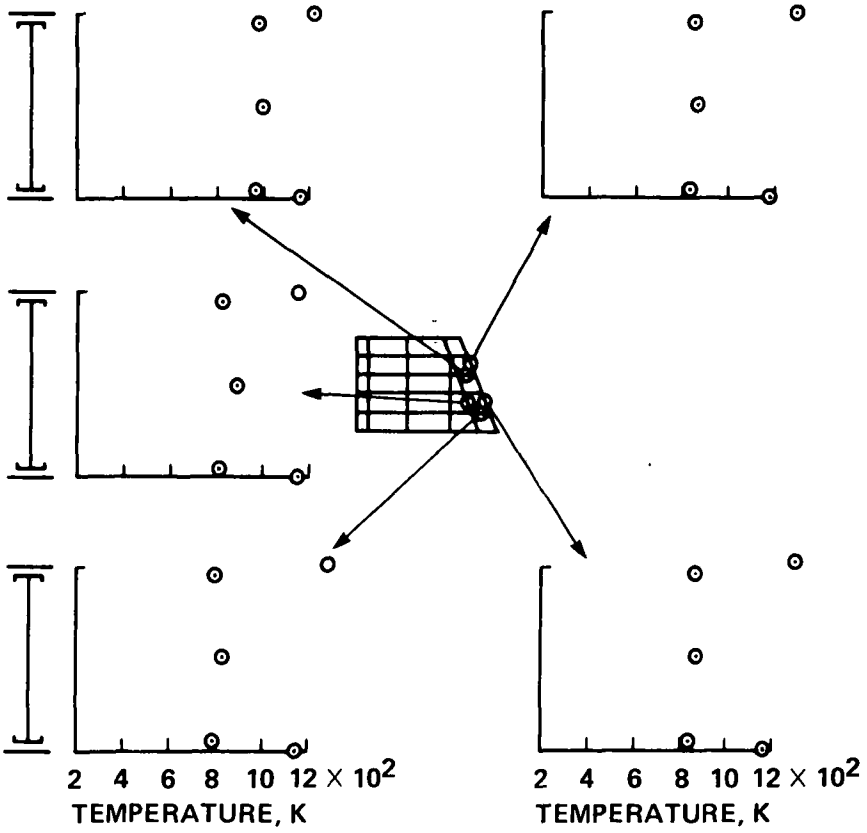

(g) Time = 1270 sec.

Figure 23.- Concluded.

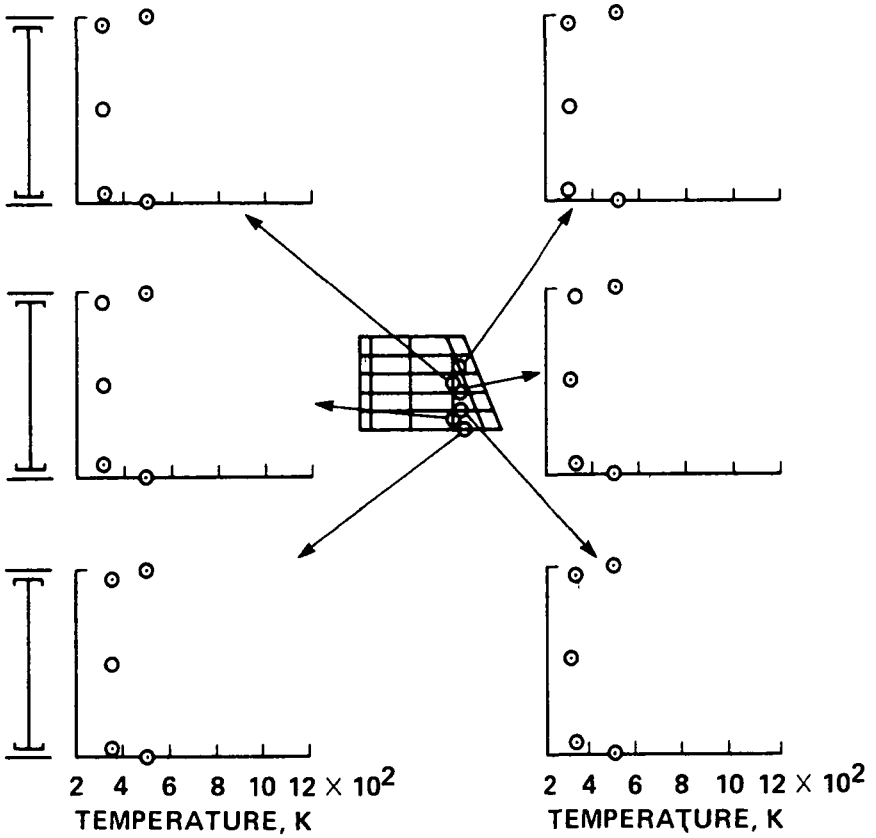

(a) Time = 400 sec.

Figure 24.- Measured spar, rib, and heat shield temperatures.

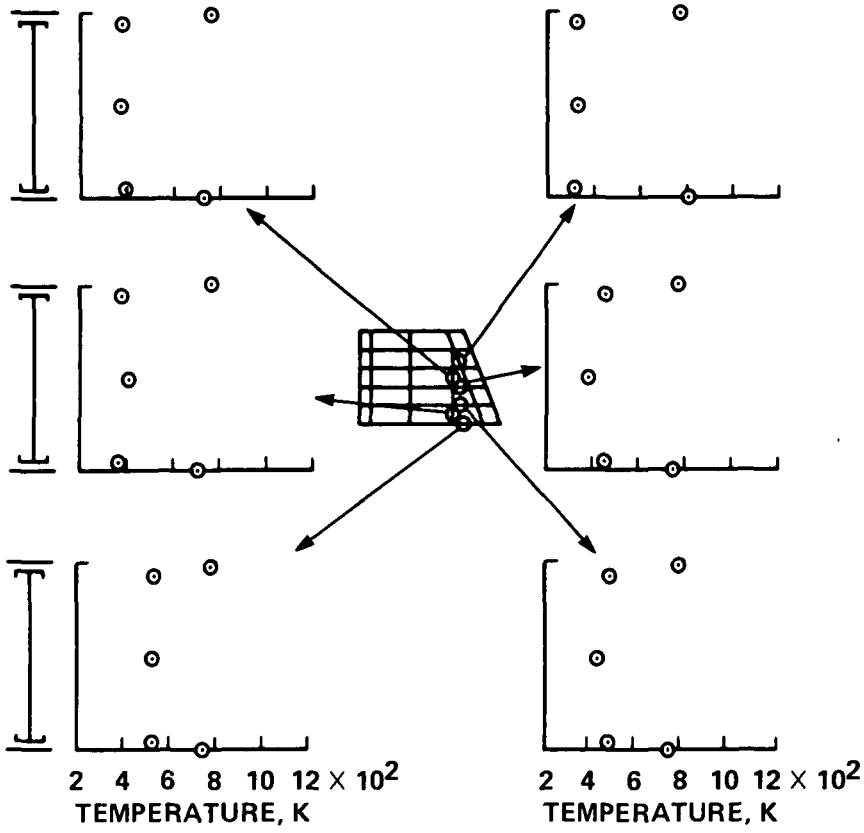

(b) Time = 600 sec.

Figure 24.- Continued.

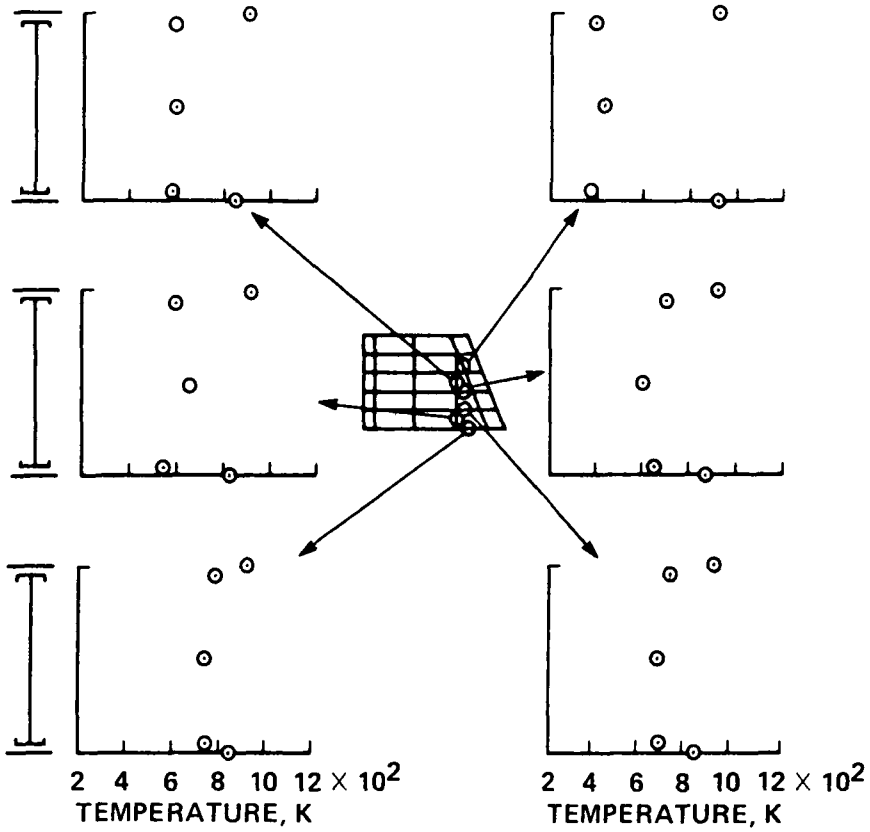

(c) Time = 800 sec.

Figure 24.- Continued.

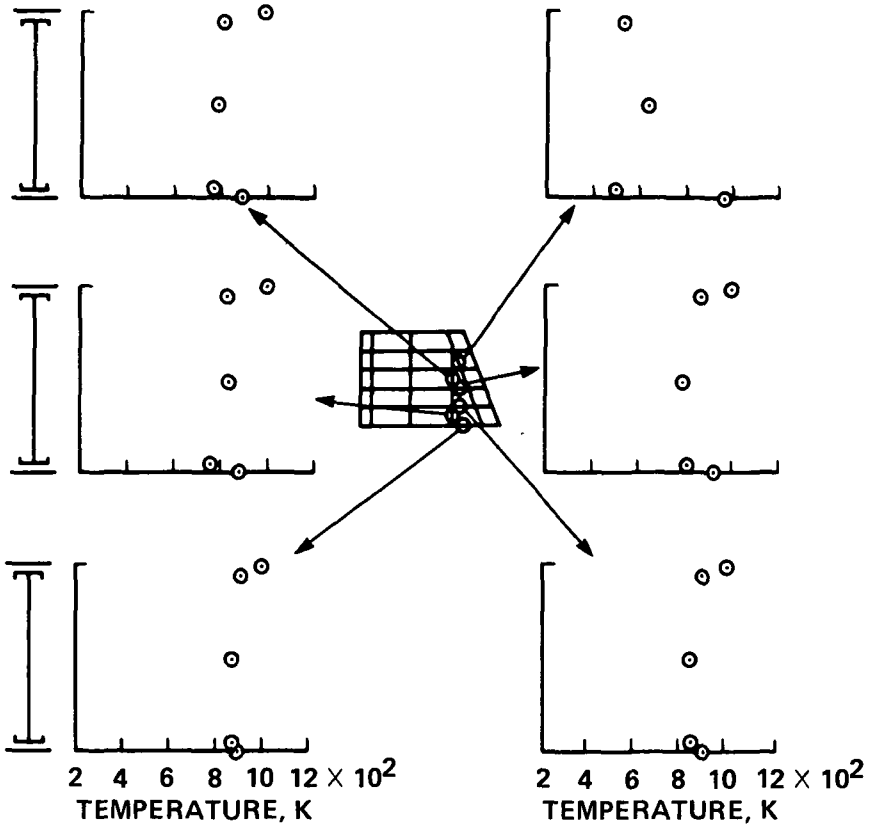

(d) Time = 1000 sec.

Figure 24.- Continued.

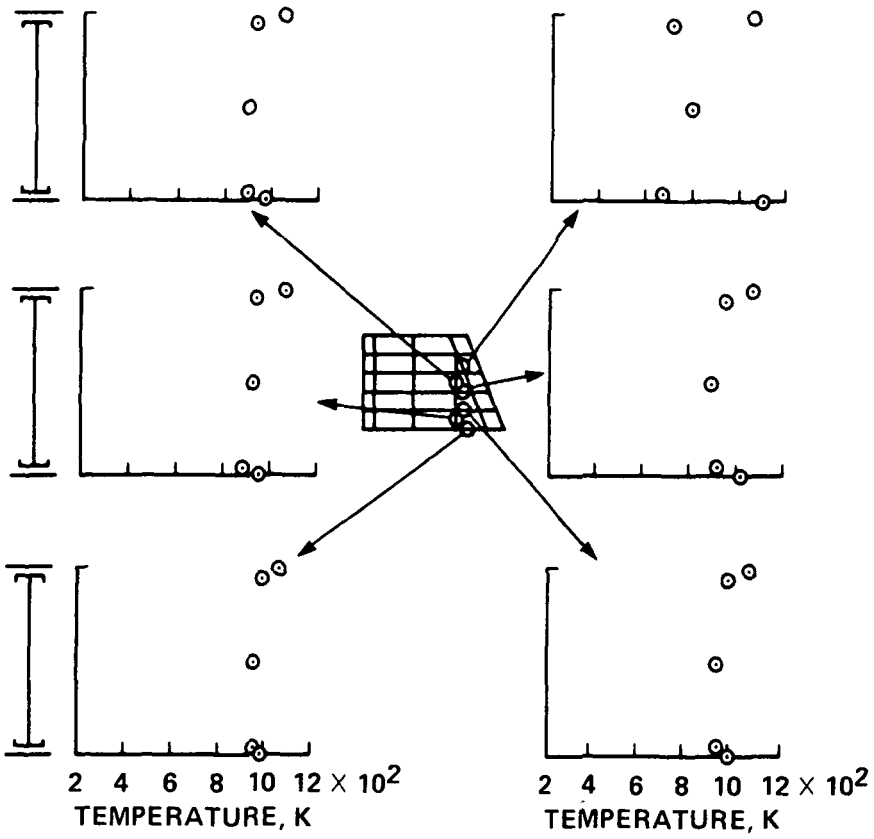

(e) Time = 1200 sec.

Figure 24.- Continued.

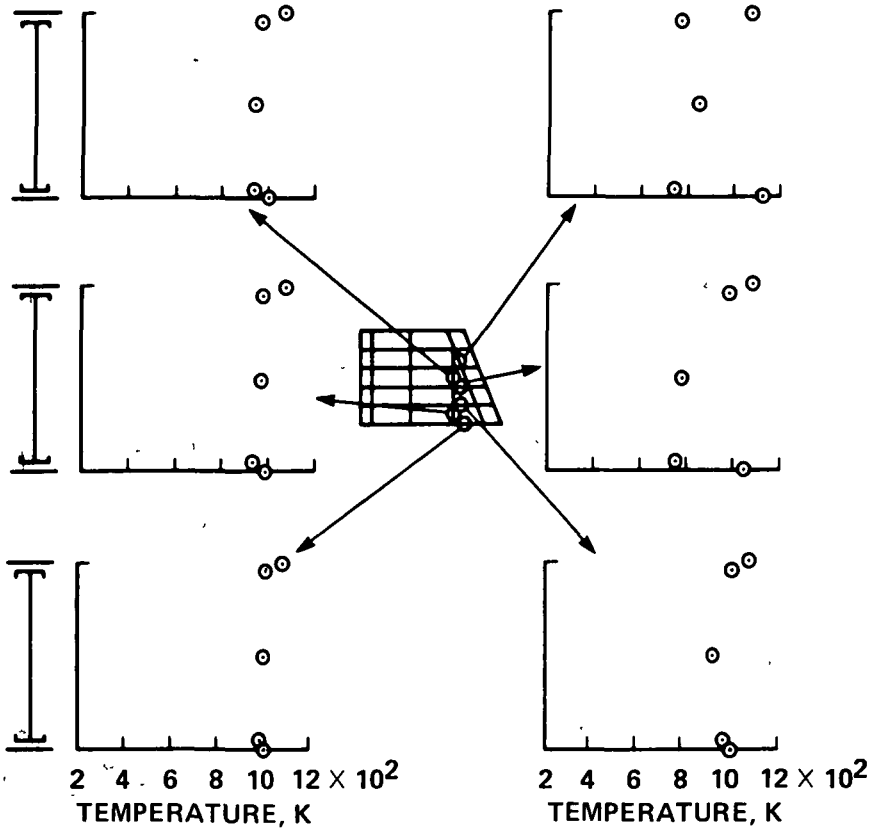

(f) Time = 1250 sec.

Figure 24.- Continued.

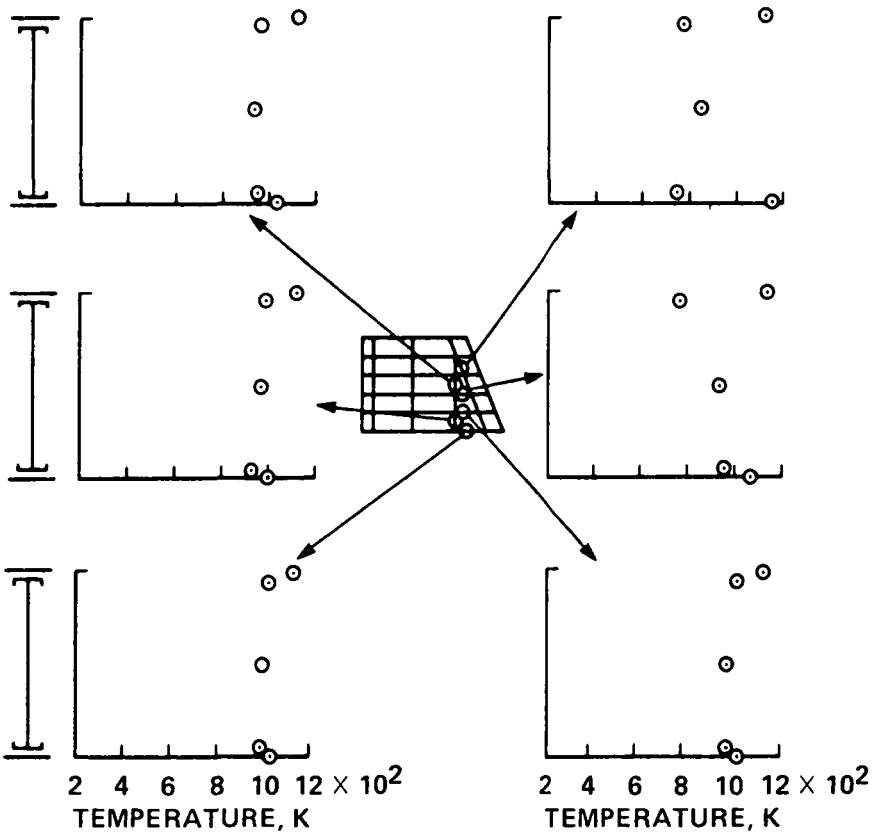

(g) Time = 1270 sec.

Figure 24.- Concluded.

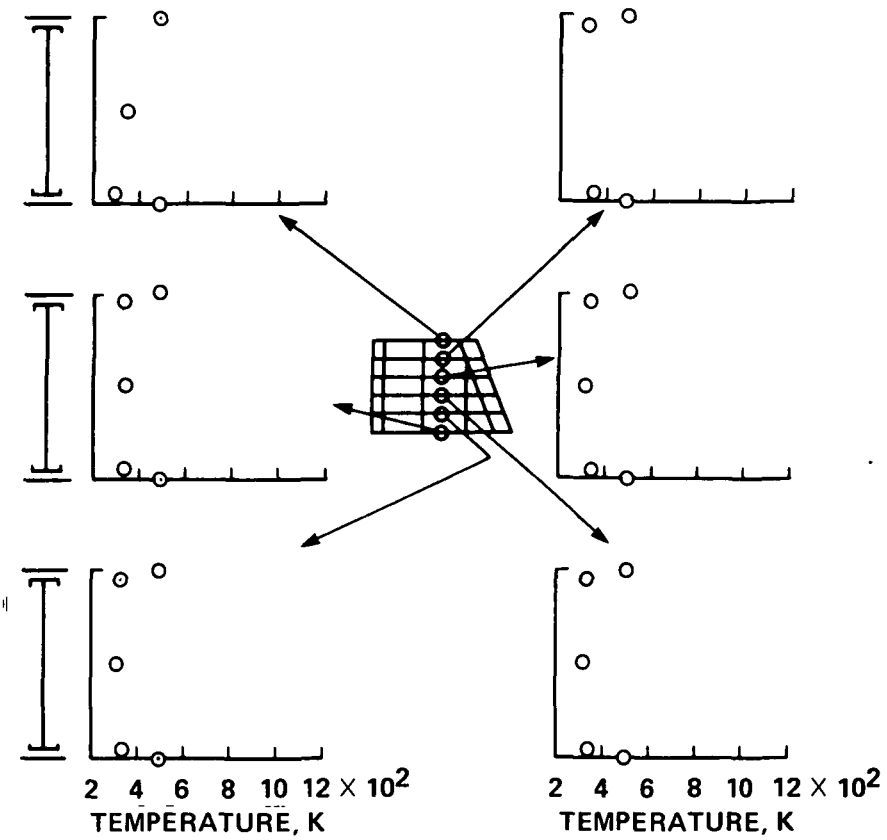

(a) Time = 400 sec.

Figure 25.- Measured spar, rib, and heat shield temperatures.

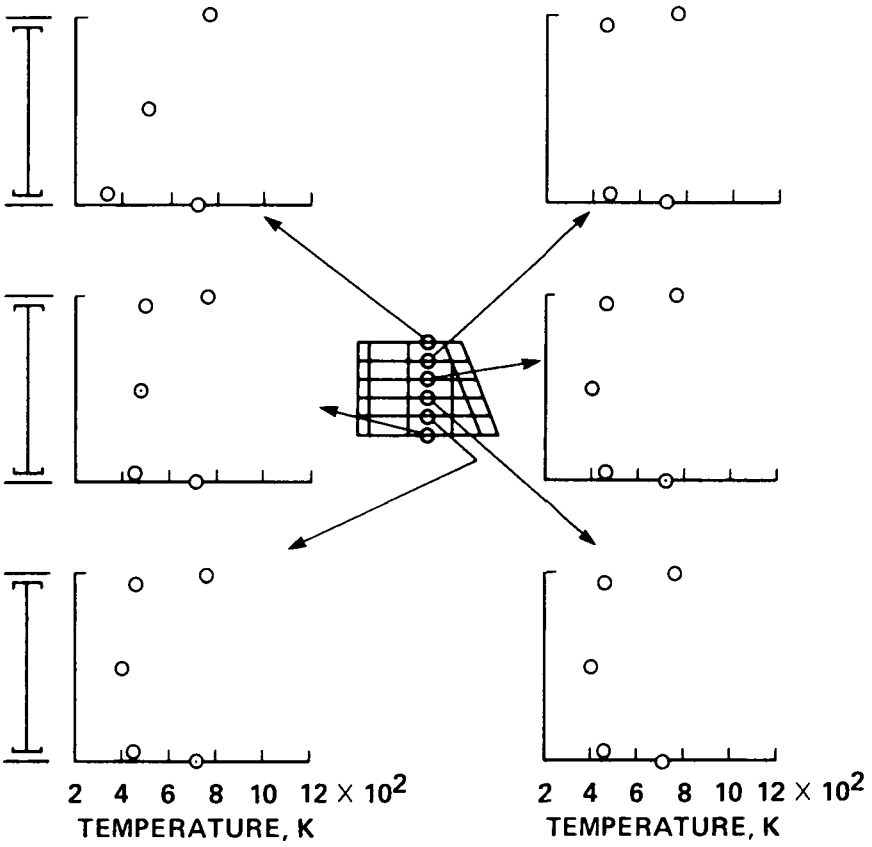

(b) Time = 600 sec.

Figure 25.- Continued.

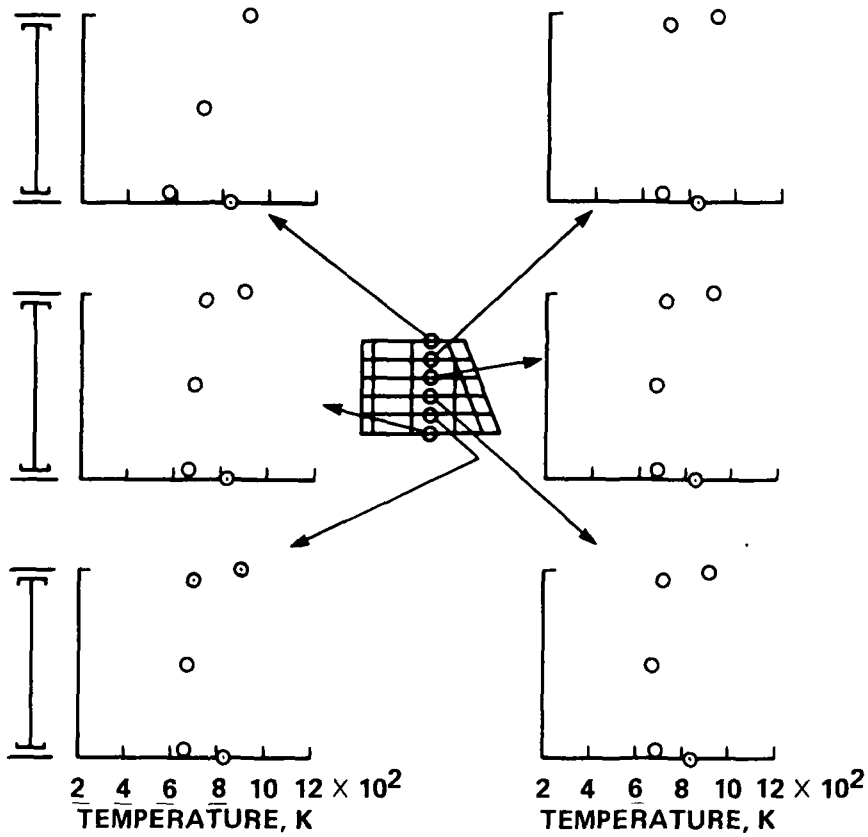

(c) Time = 800 sec.

Figure 25.- Continued.

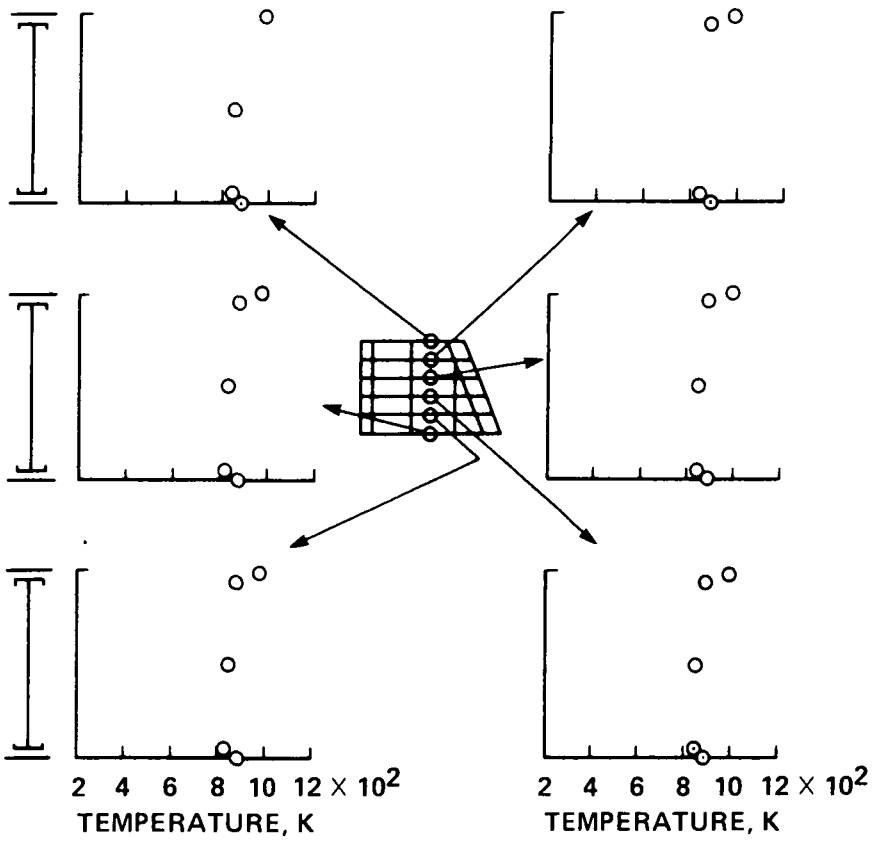

(d) Time = 1000 sec.

Figure 25.- Continued.

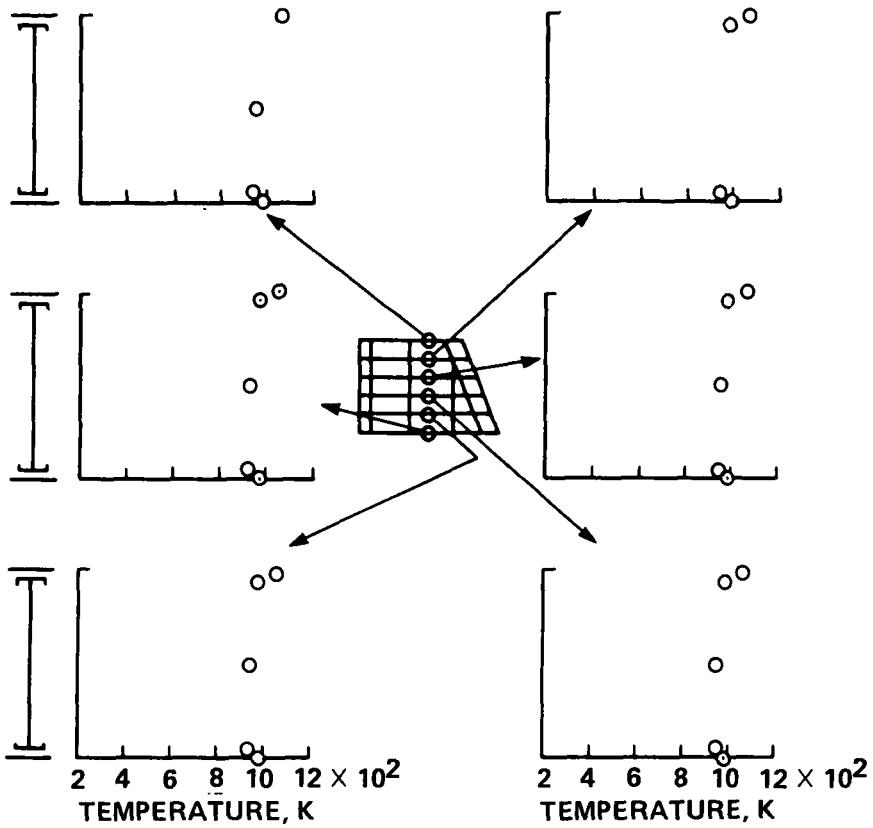

(e) Time = 1200 sec.

Figure 25.- Continued.

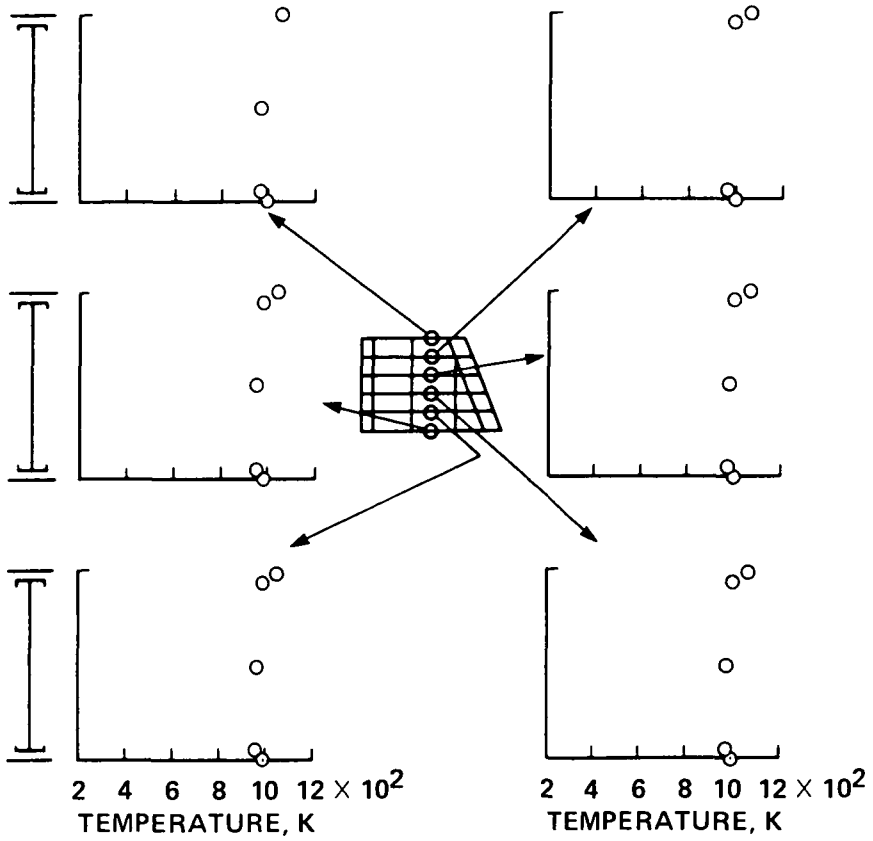

(f) Time = 1250 sec.

Figure 25.- Continued.

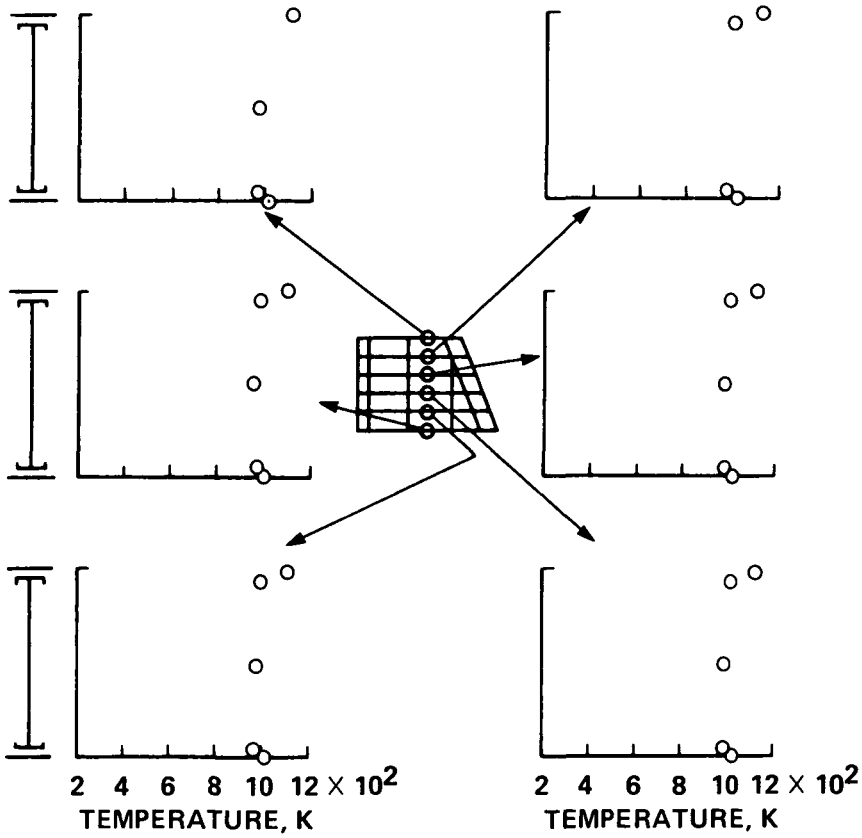

(g) Time = 1270 sec.

Figure 25.- Concluded.

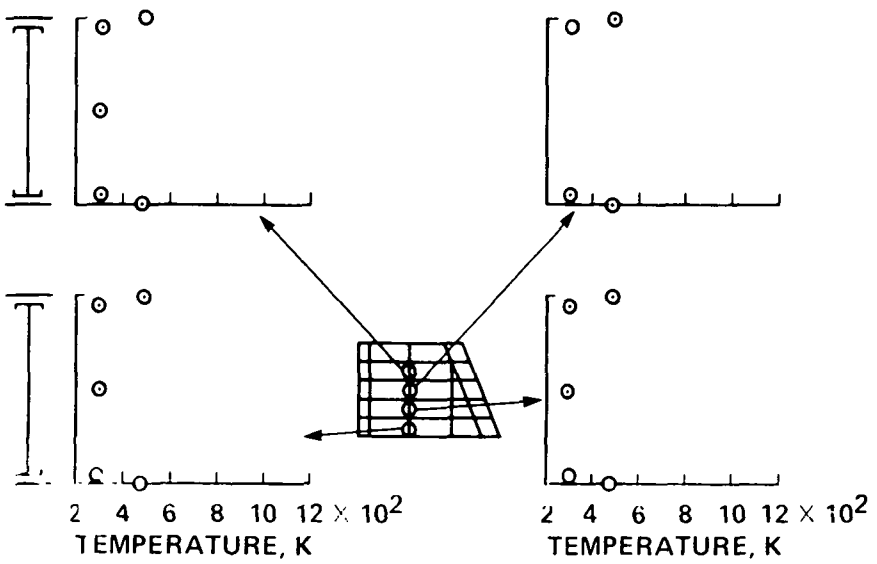

(a) Time = 400 sec.

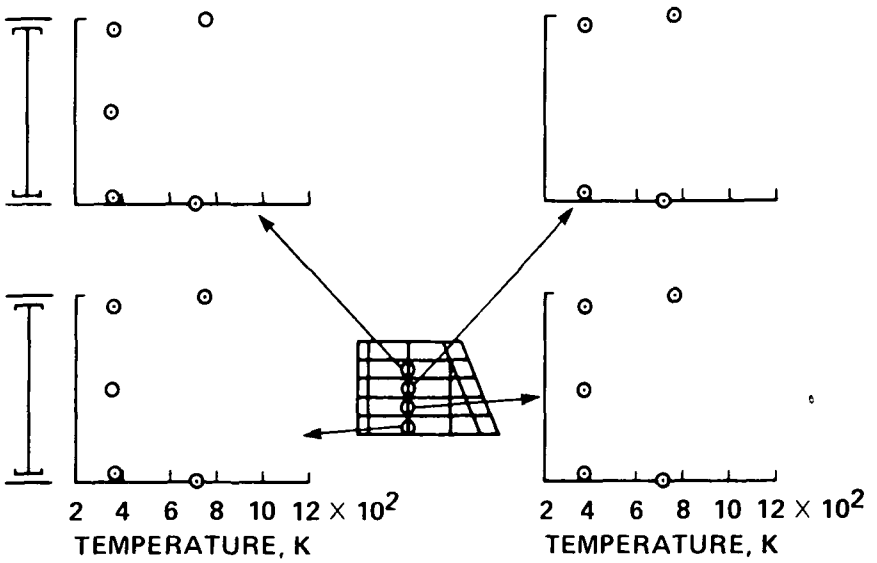

(b) Time = 600 sec.

Figure 26. - Measured spar, rib, and heat shield temperatures.

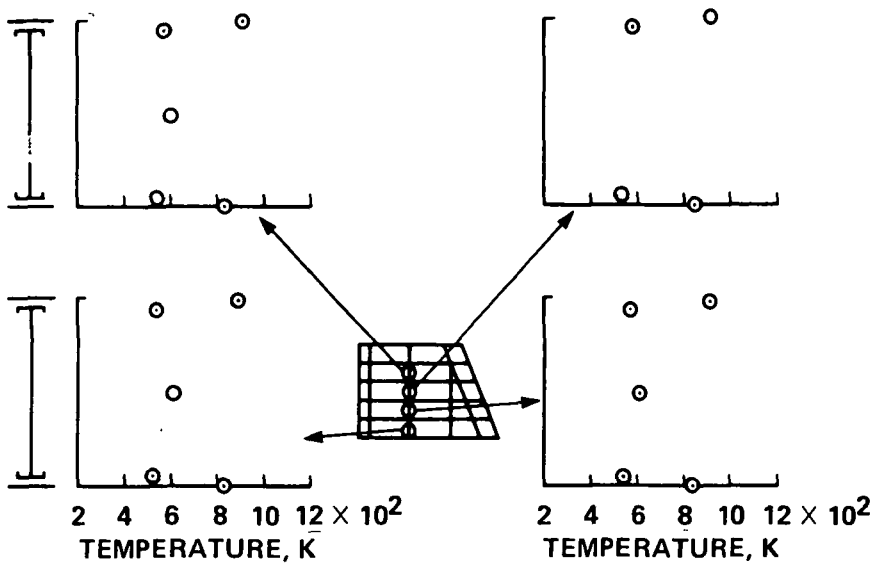

(c) Time = 800 sec.

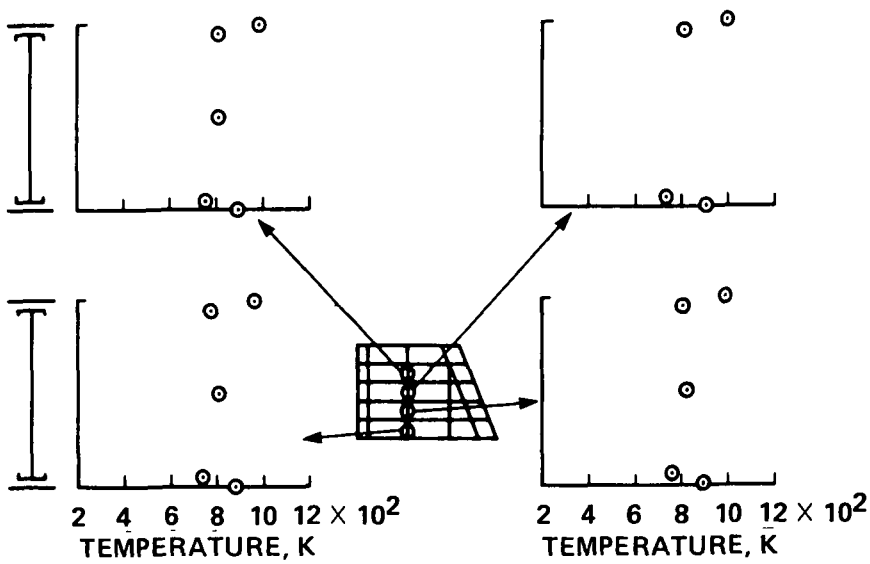

(d) Time = 1000 sec.

Figure 26.- Continued.

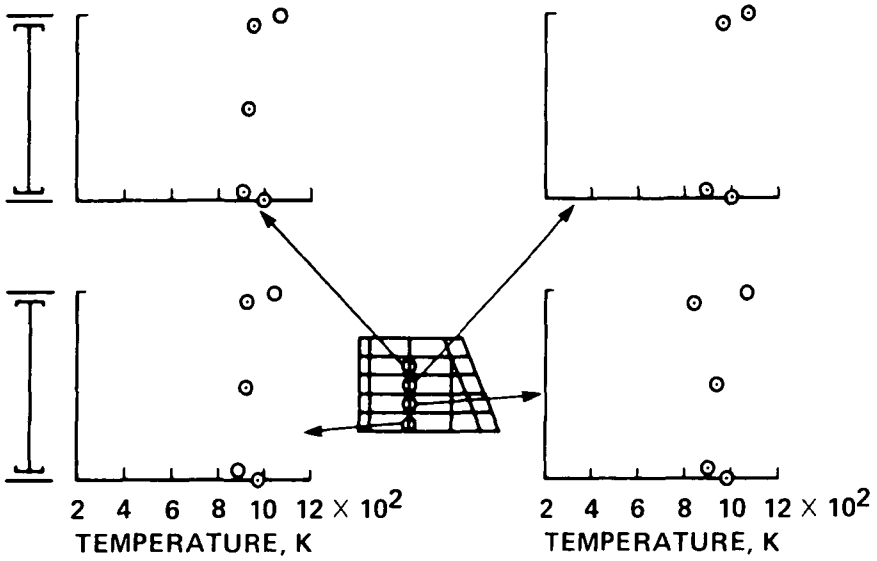

(e) Time = 1200 sec.

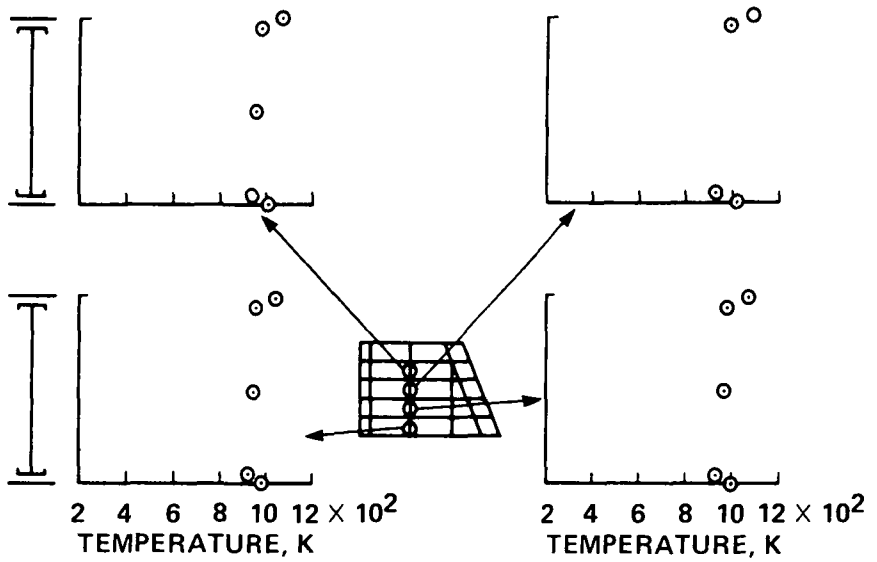

(f) Time = 1250 sec.

Figure 26.- Continued.

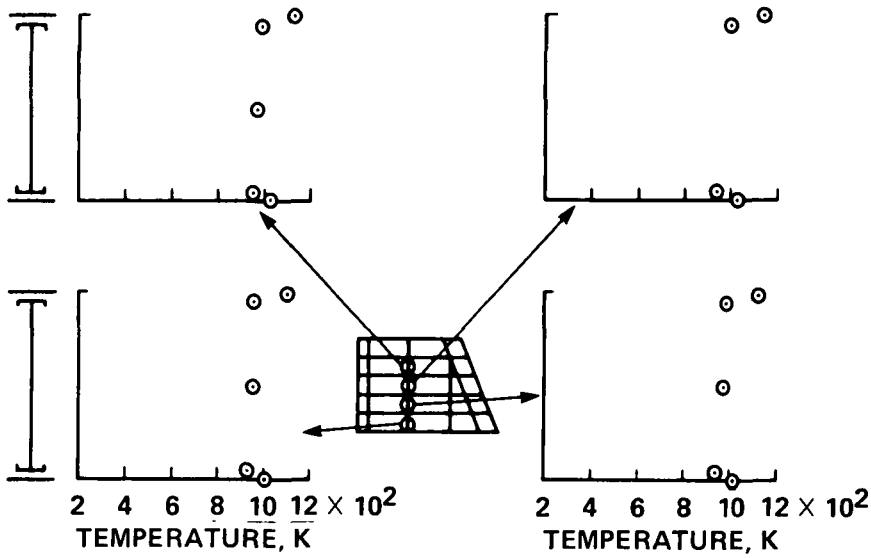

(g) Time = 1270 sec.

Figure 26.- Concluded.

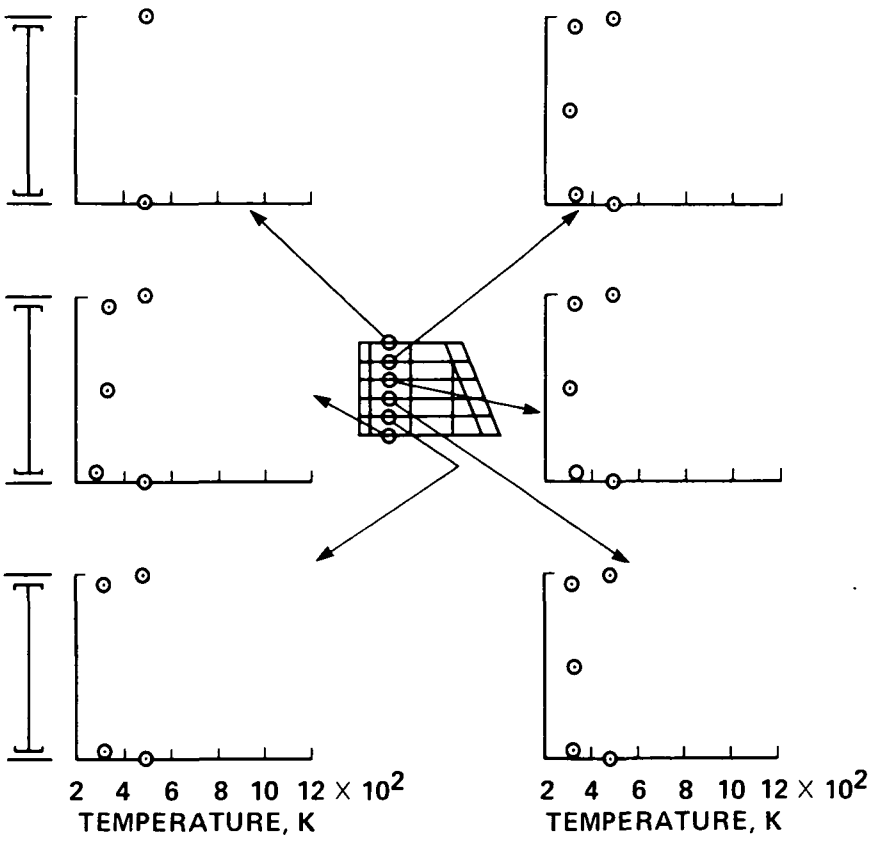

(a) Time = 400 sec.

Figure 27.- Measured spar, rib, and heat shield temperatures.

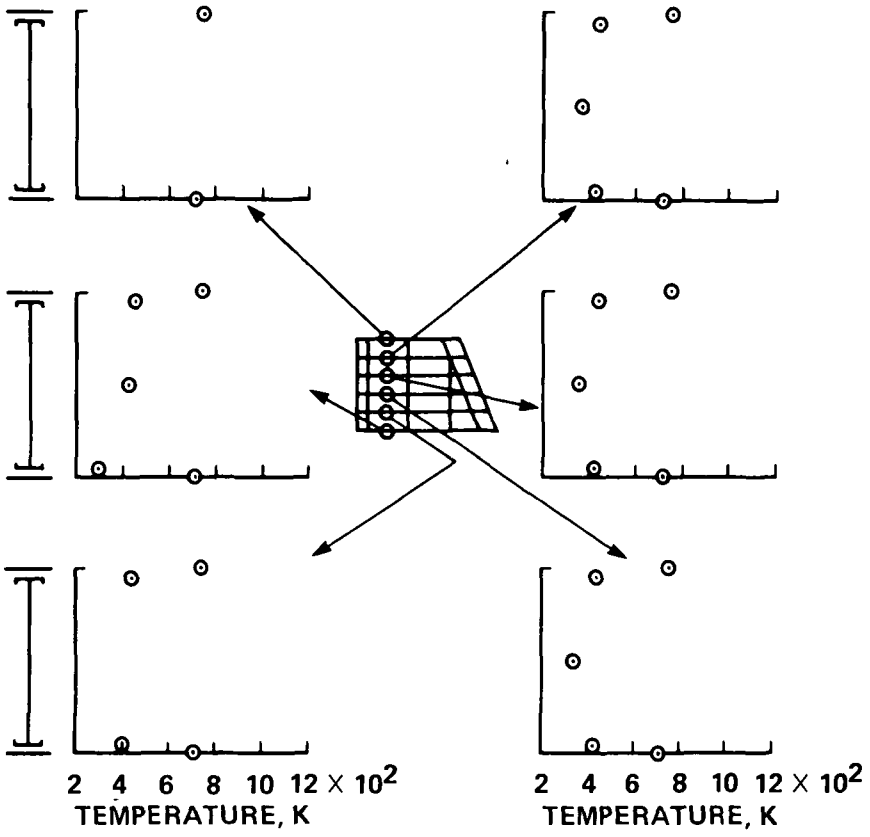

(b) Time = 600 sec.

Figure 27.- Continued.

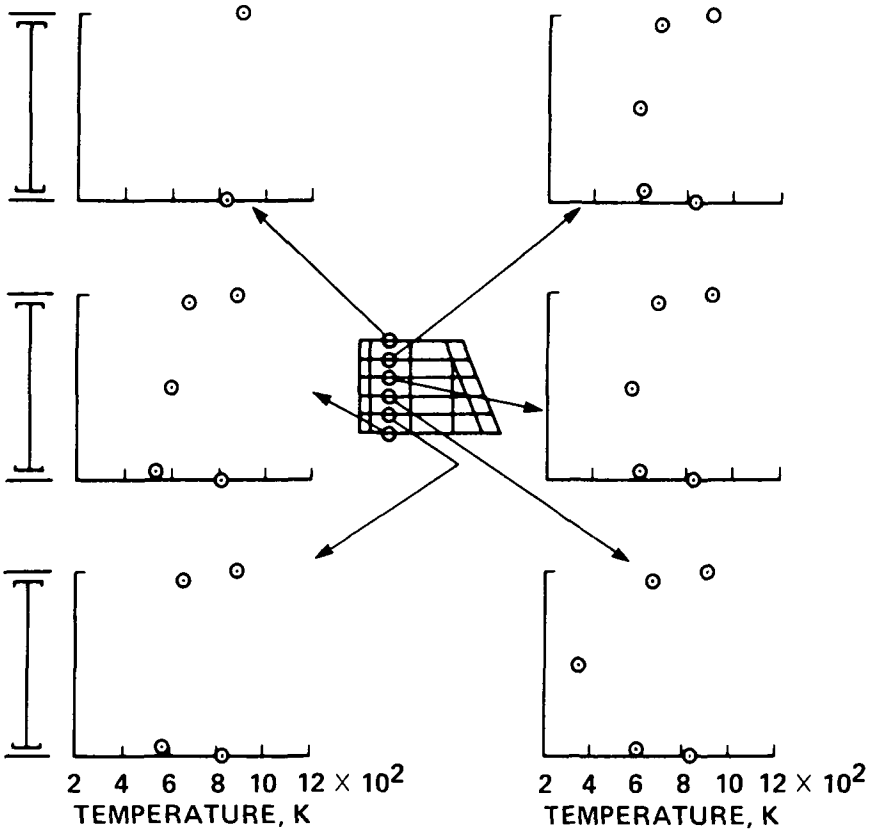

(c) Time = 800 sec.

Figure 27.- Continued.

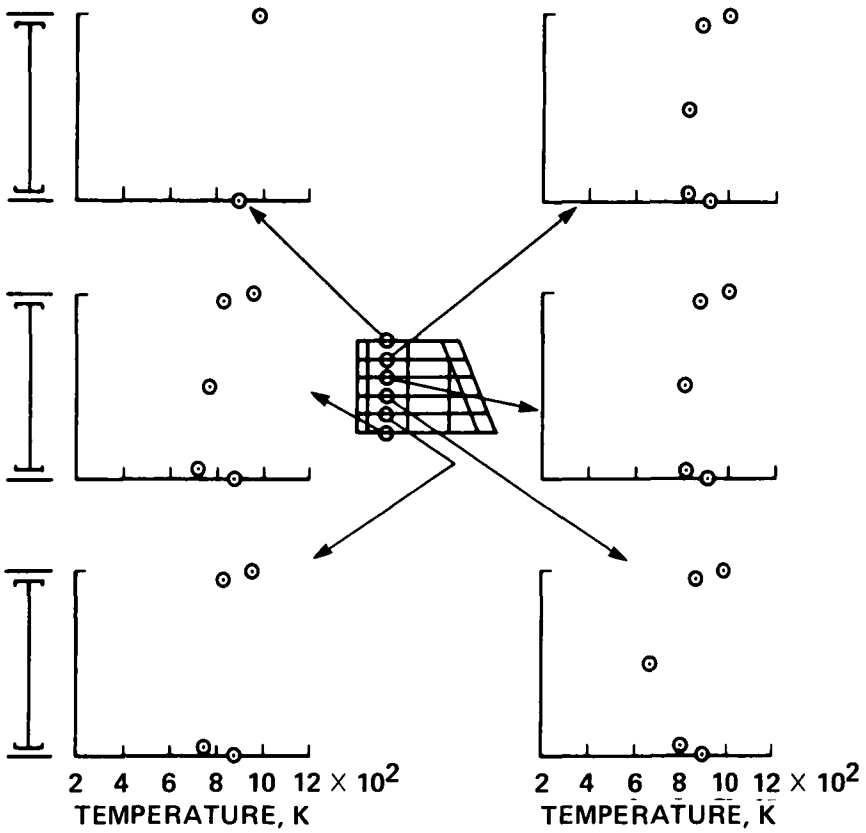

(d) Time = 1000 sec.

Figure 27.- Continued.

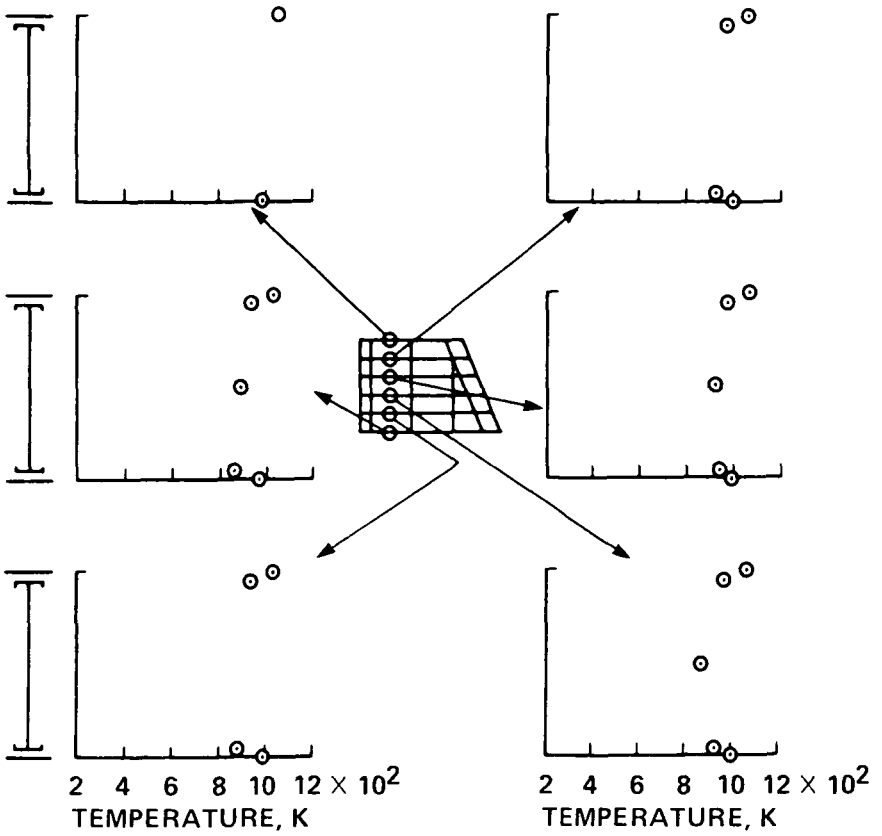

(e) Time = 1200 sec.

Figure 27.- Continued.

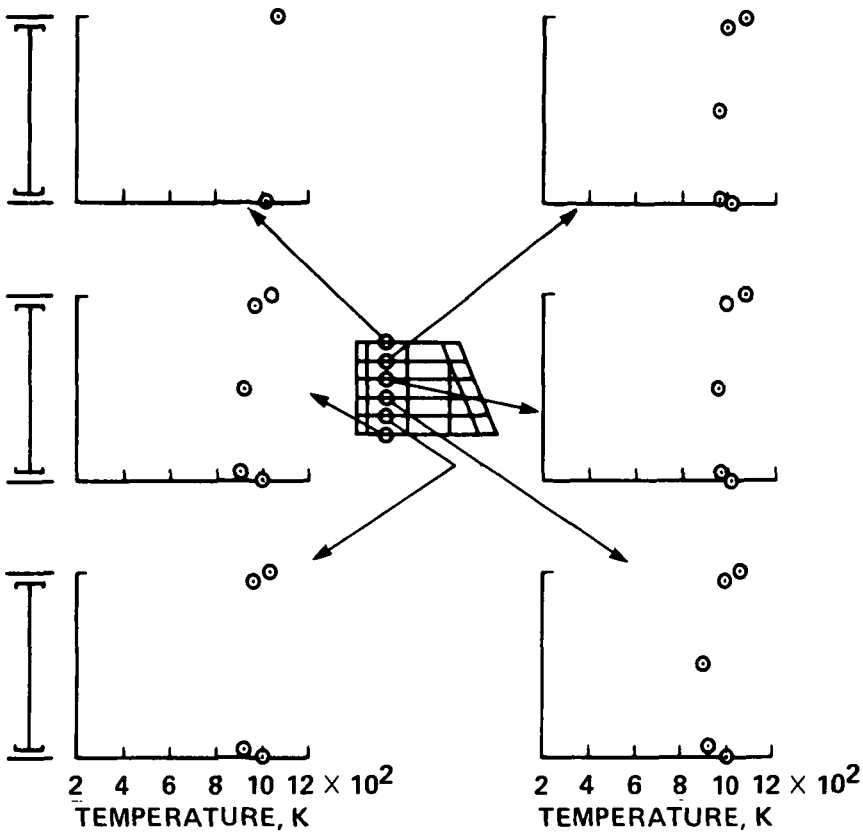

(f) Time = 1250 sec.

Figure 27.- Continued.

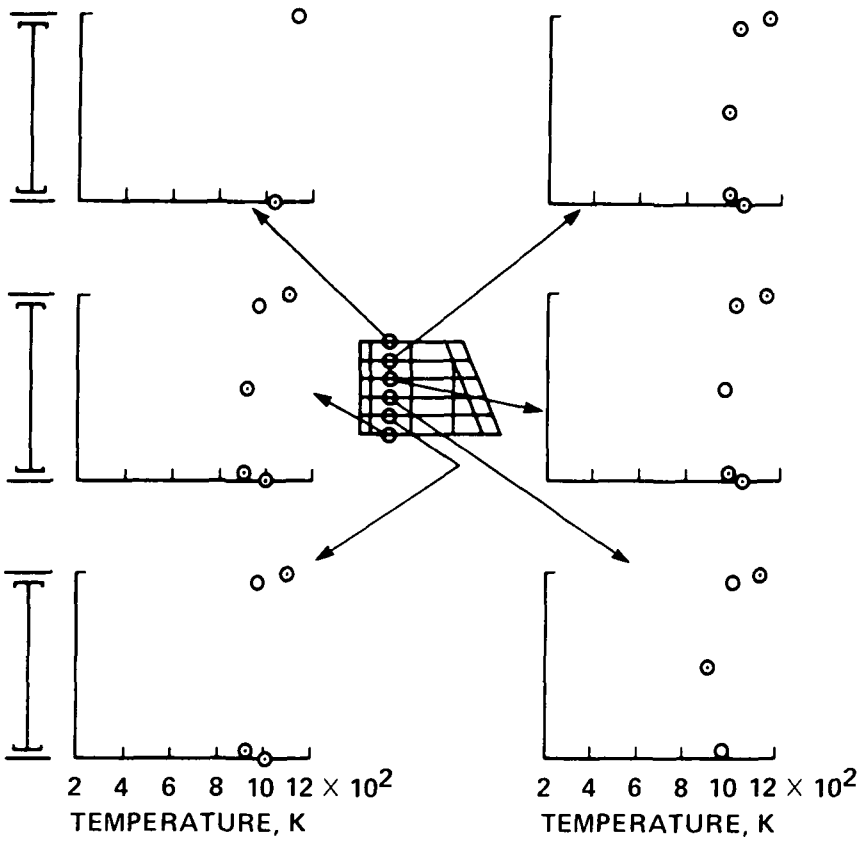

(g) Time = 1270 sec.

Figure 27.- Concluded.

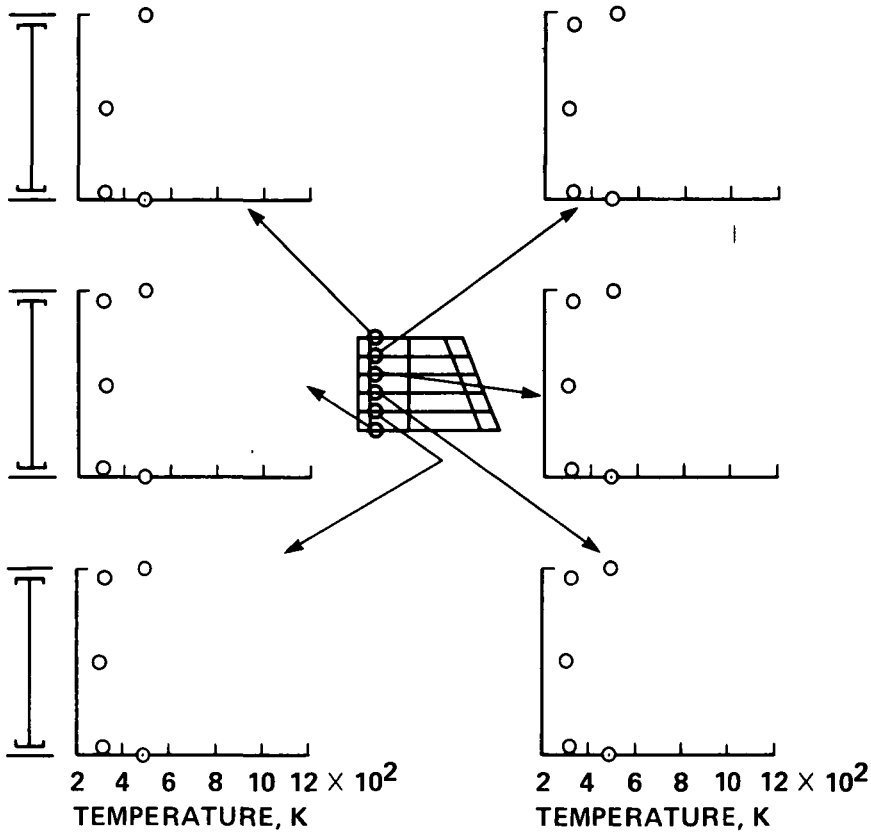

(a) Time = 400 sec.

Figure 28.- Measured spar, rib, and heat shield temperatures.

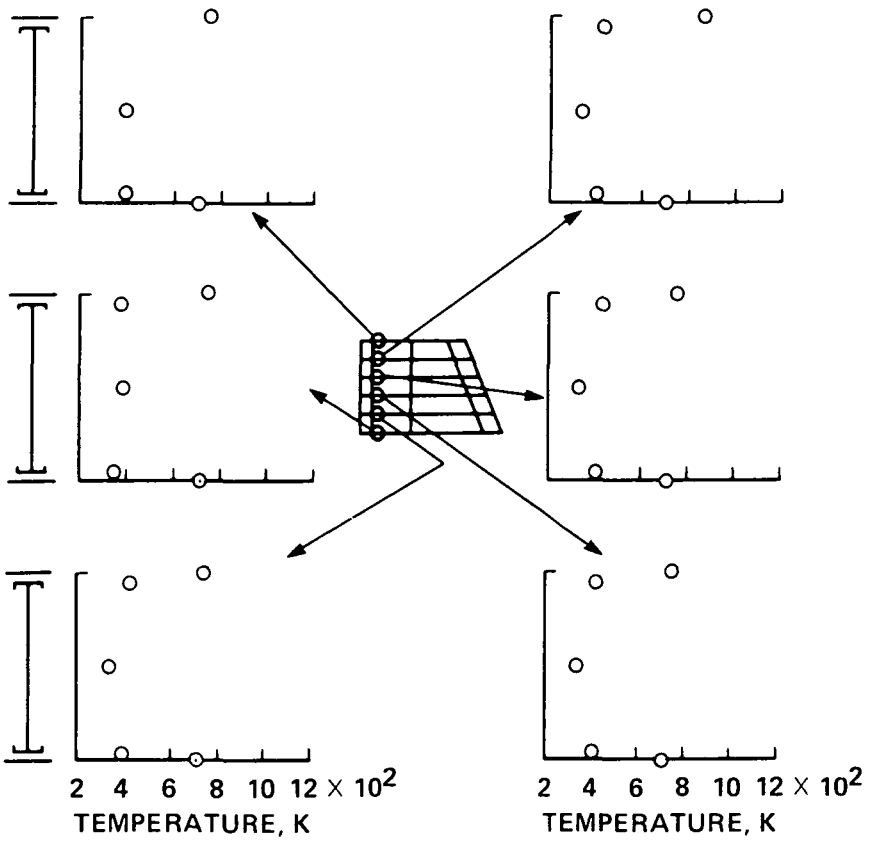

(b) Time = 600 sec.

Figure 28.- Continued.

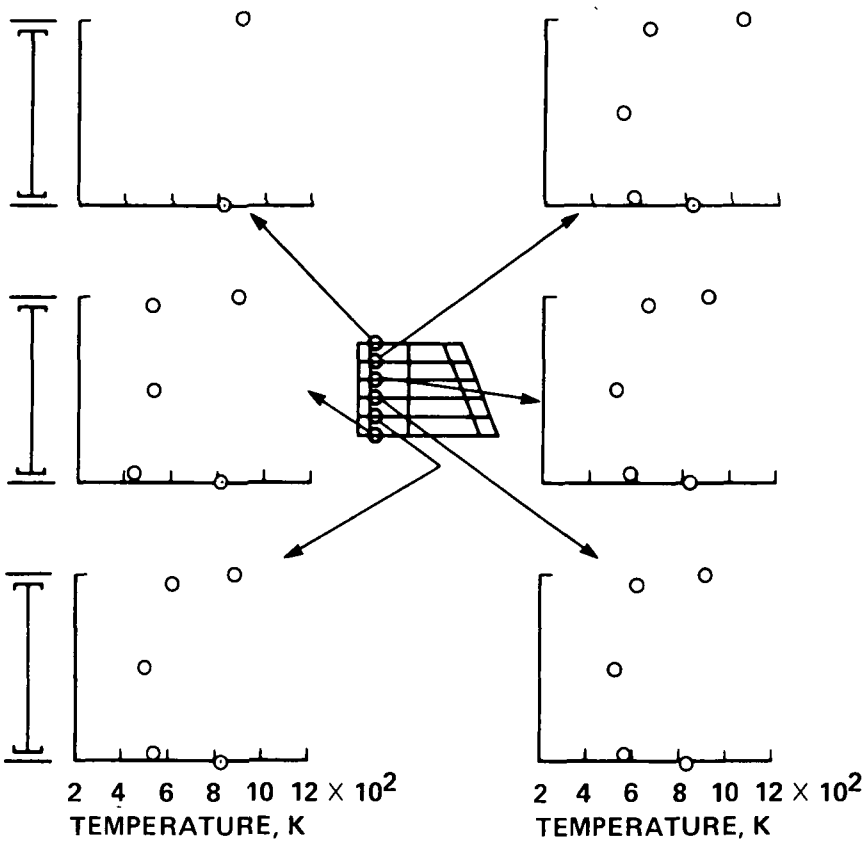

(c) Time = 800 sec.

Figure 28.- Continued.

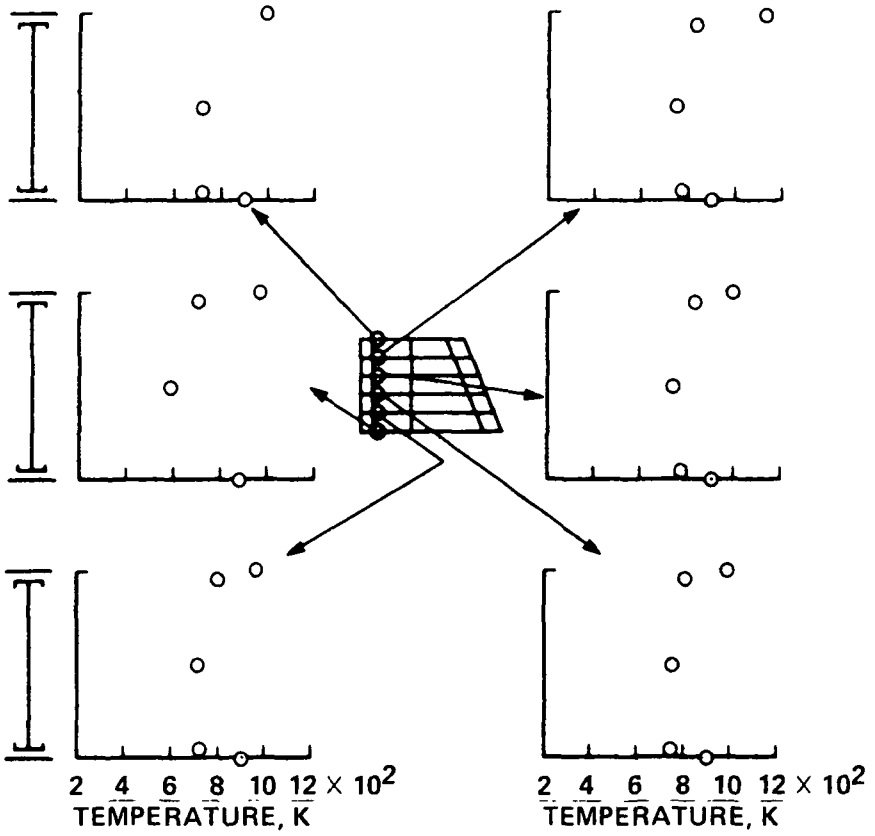

(d) Time = 1000 sec.

Figure 28.- Continued.

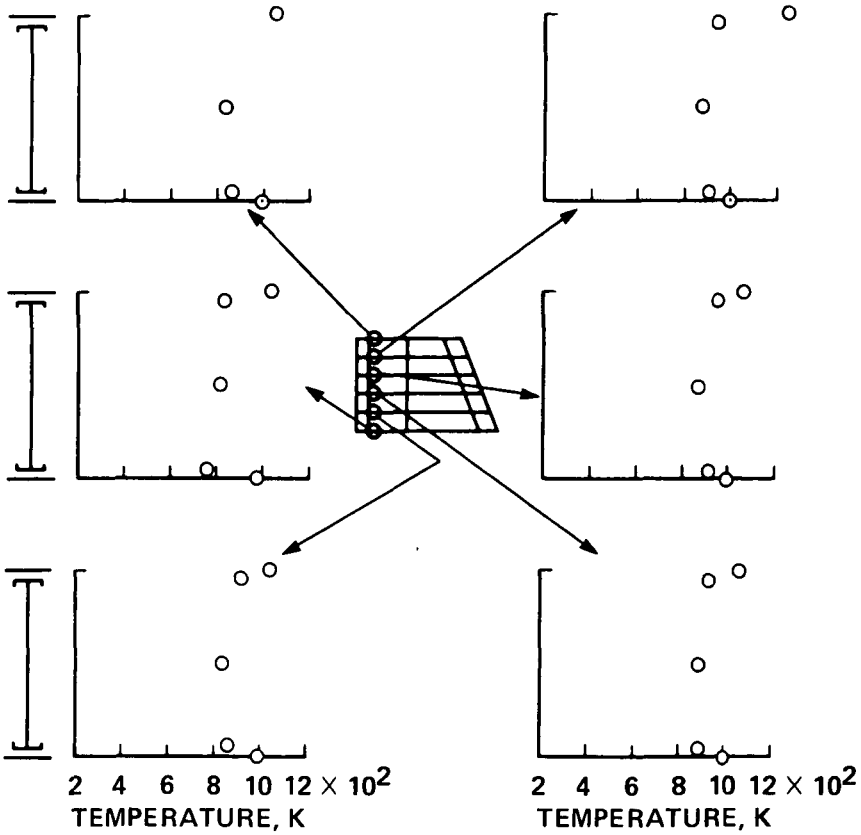

(e) Time = 1200 sec.

Figure 28.- Continued.

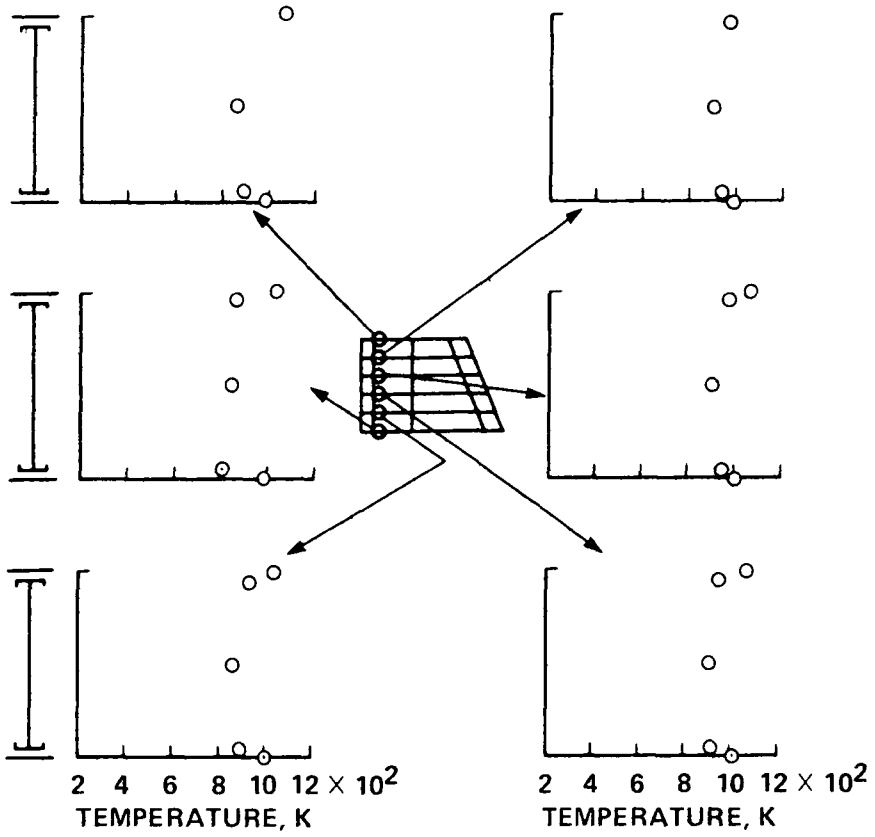

(f) Time = 1250 sec.

Figure 28.- Continued.

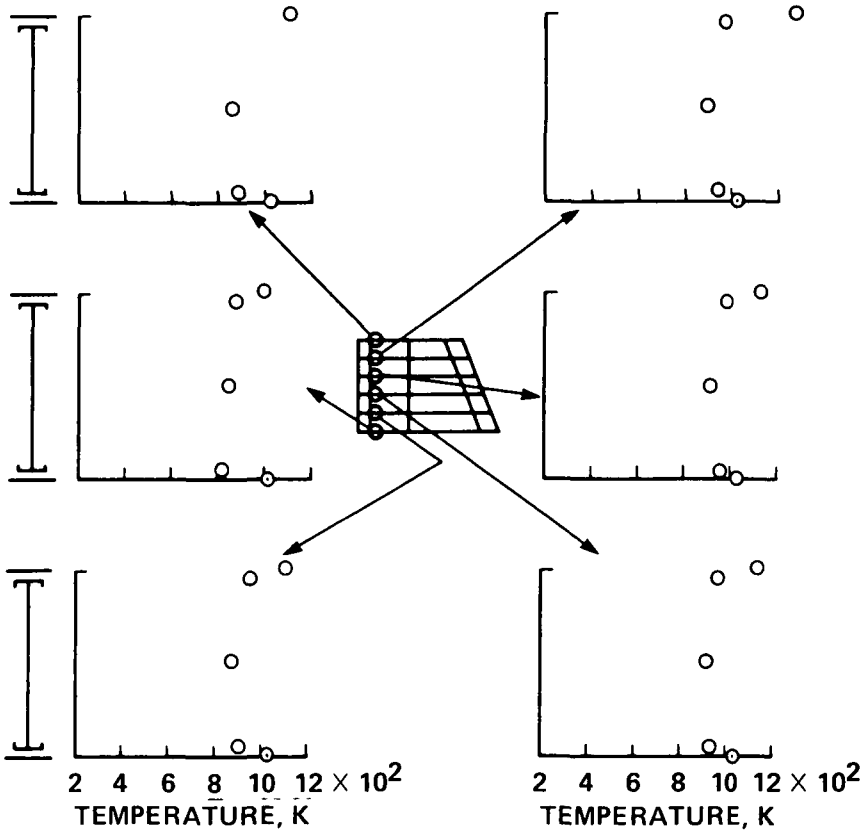

(g) Time = 1270 sec.

Figure 28.- Concluded.

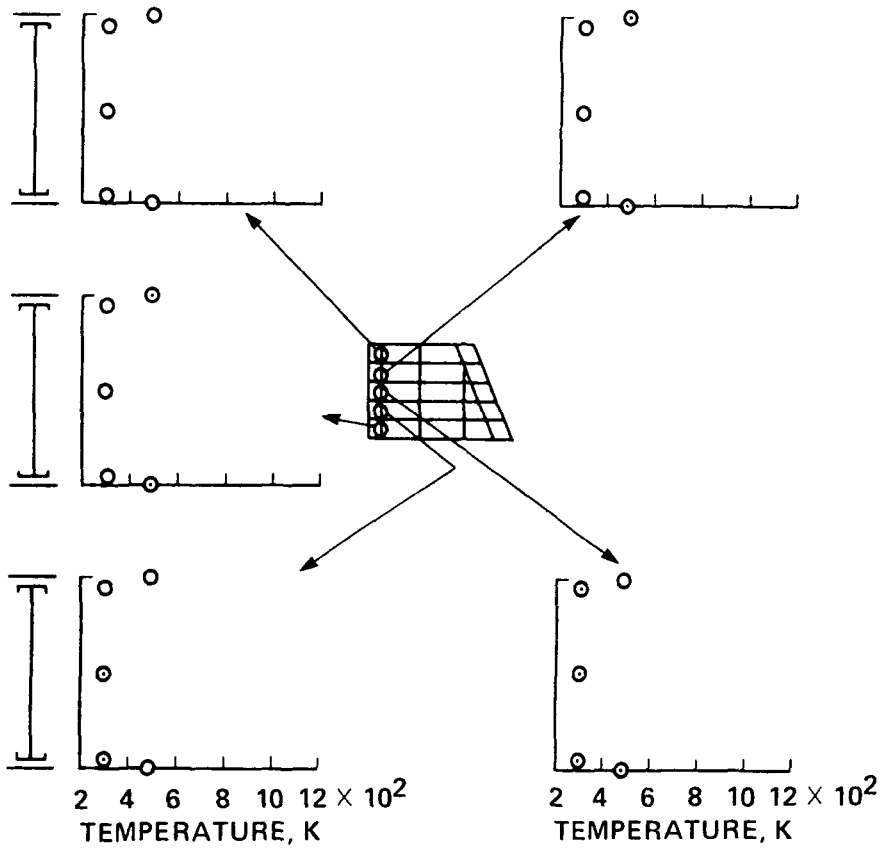

(a) Time = 400 sec.

Figure 29.- Measured spar, rib, and heat shield temperatures.

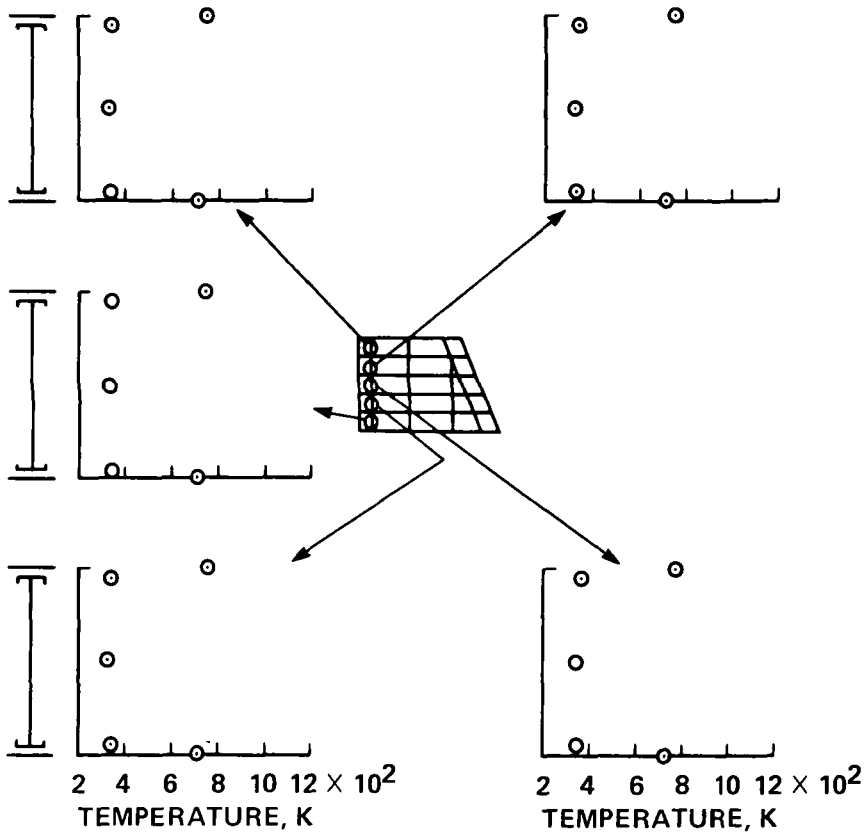

(b) Time = 600 sec.

Figure 29.- Continued.

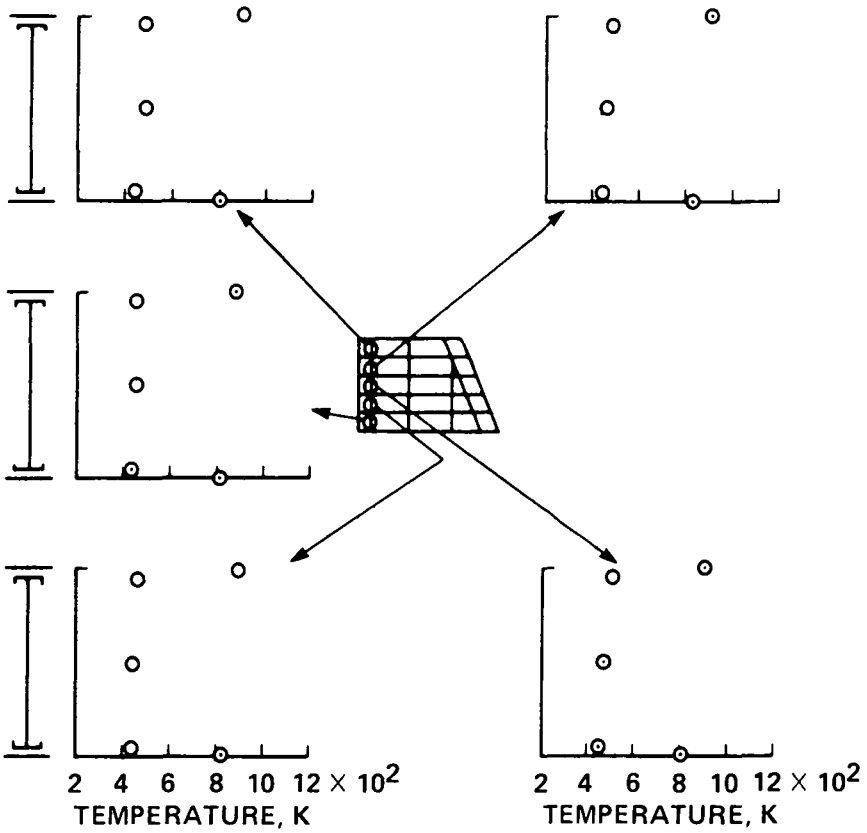

(c) Time = 800 sec.

Figure 29.- Continued.

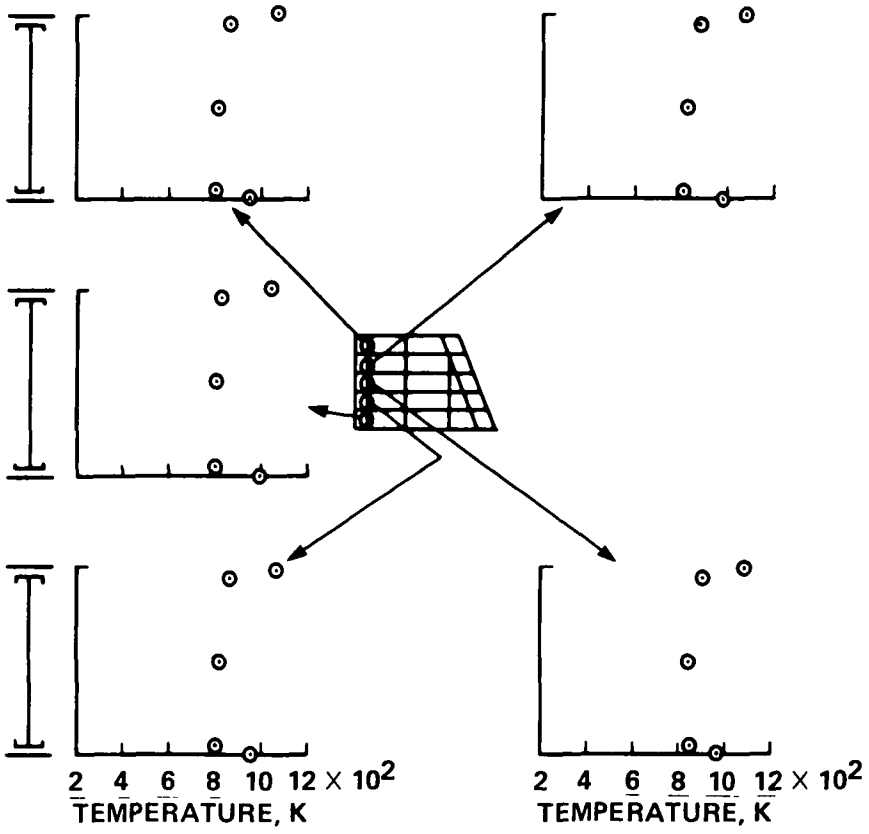

(d) Time = 1000 sec.

Figure 29.- Continued.

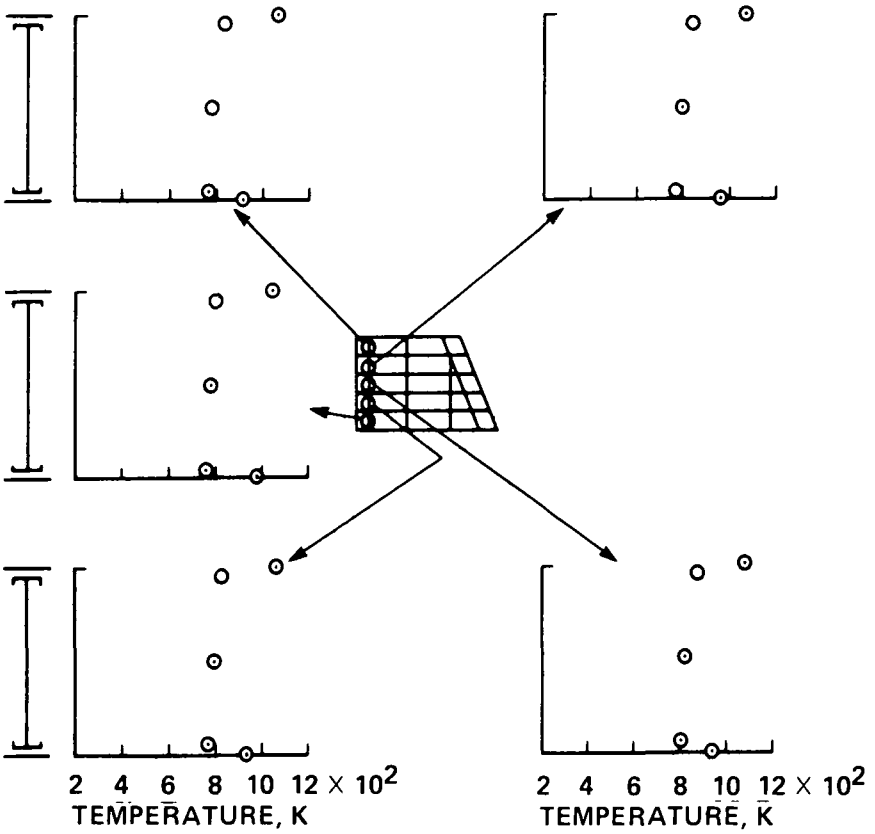

(e) Time = 1200 sec.

Figure 29.- Continued.

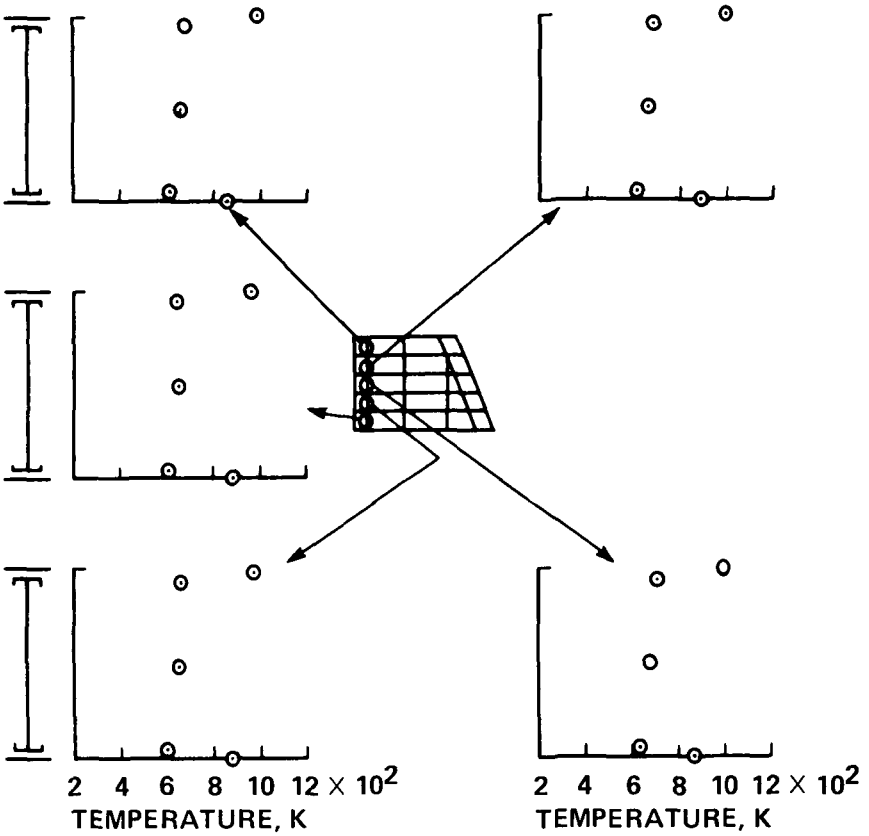

(f) Time = 1250 sec.

Figure 29.- Continued.

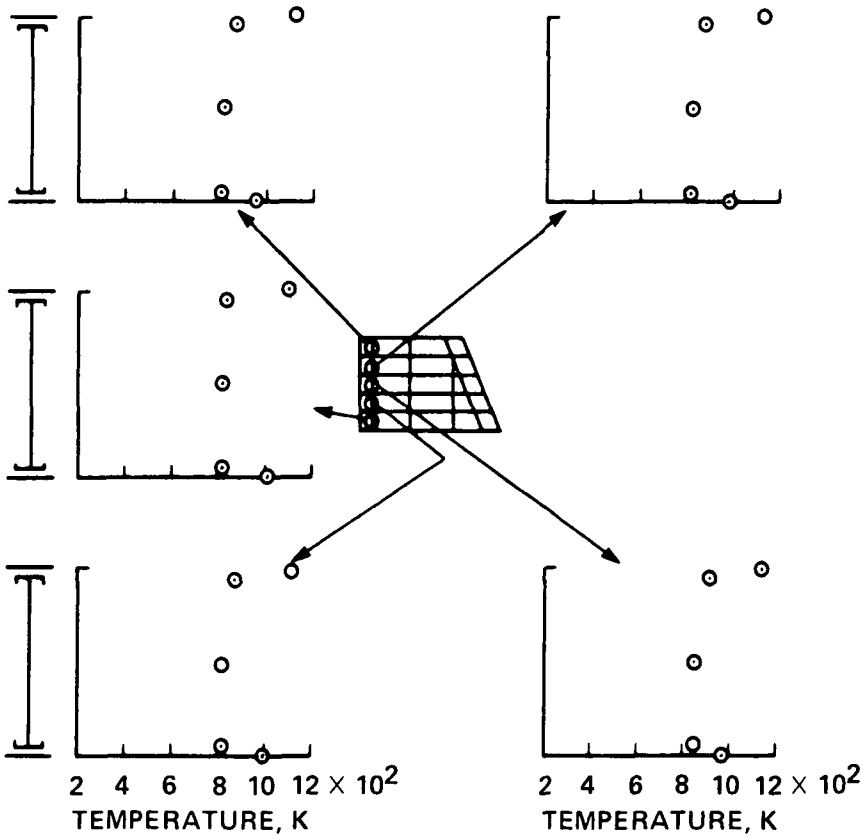

(g) Time = 1270 sec.

Figure 29.- Concluded.

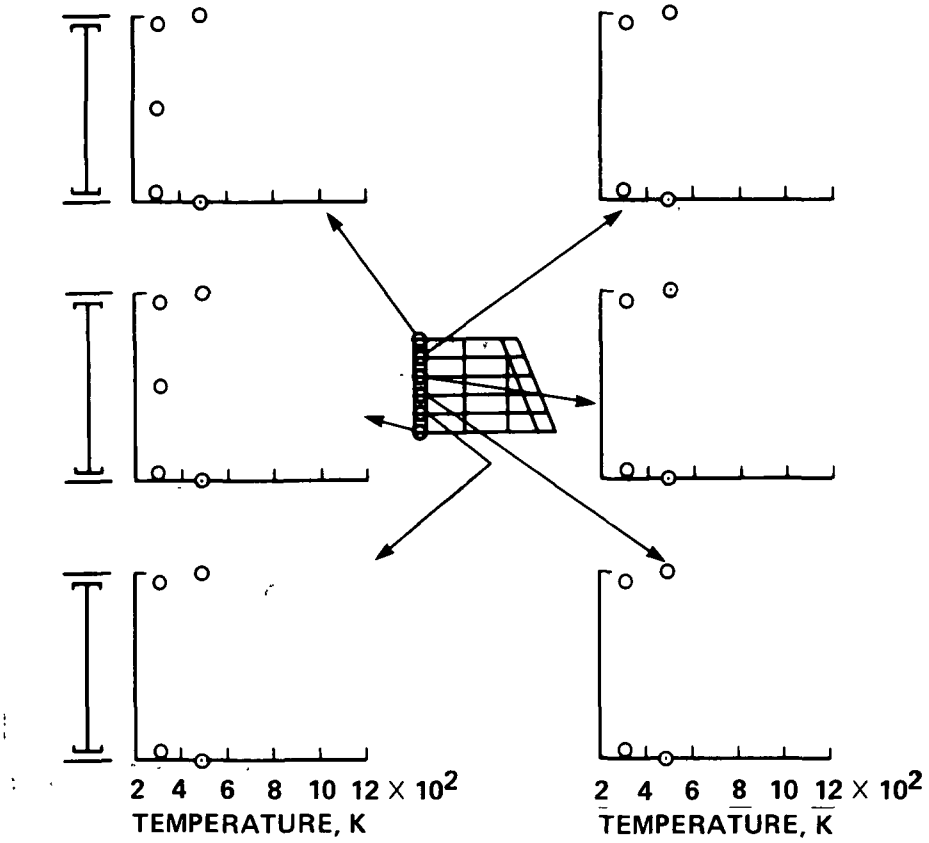

(a) Time = 400 sec.

Figure 30.- Measured spar, rib, and heat shield temperatures.

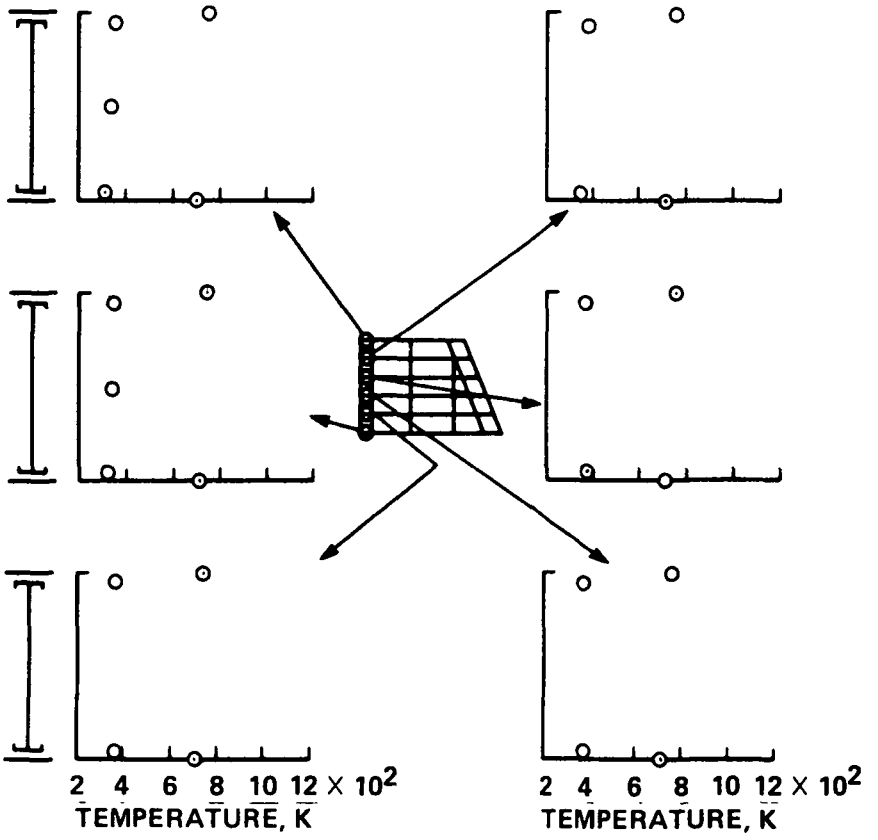

(b) Time = 600 sec.

Figure 30.- Continued.

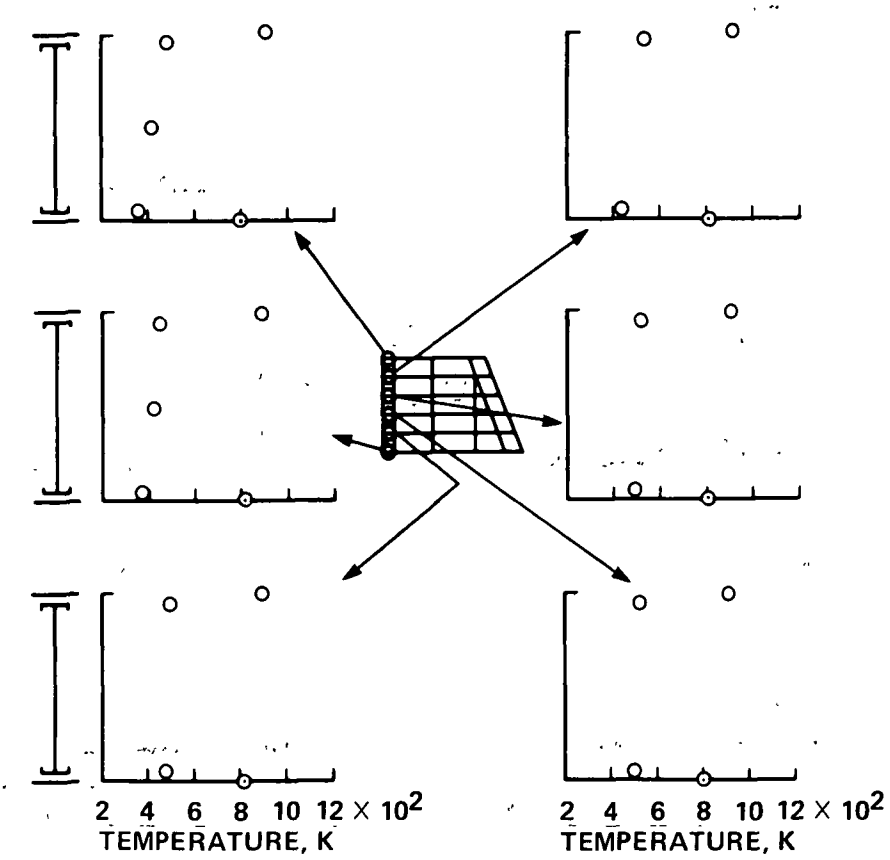

(c) Time = 800 sec.

Figure 30.- Continued.

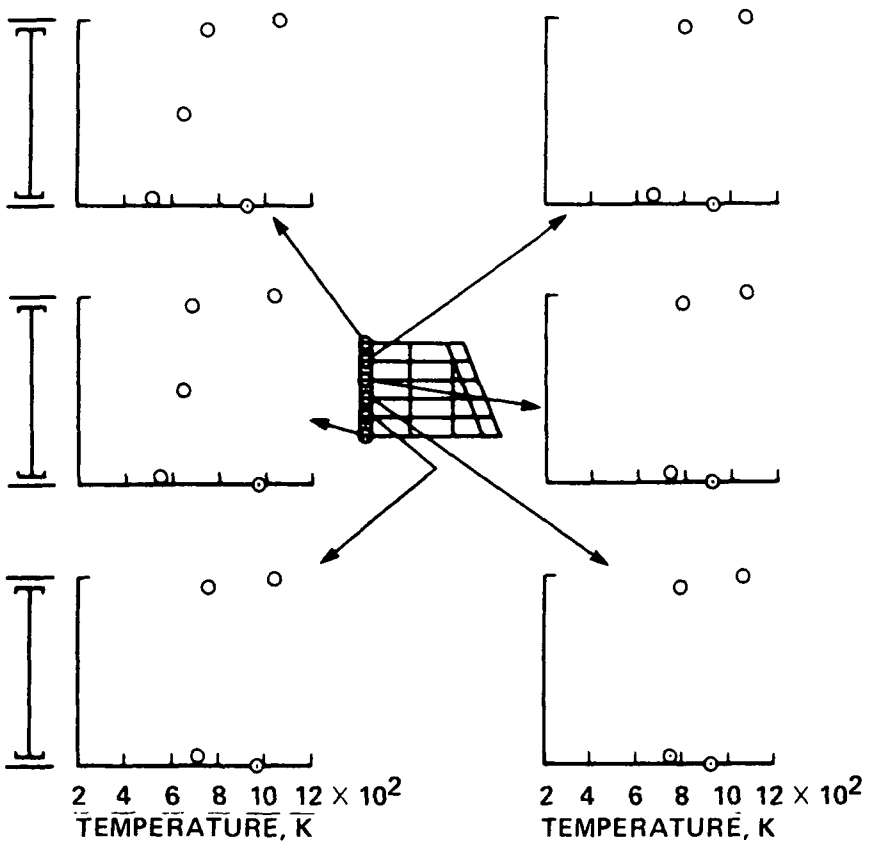

(d) Time = 1000 sec.

Figure 30.- Continued.

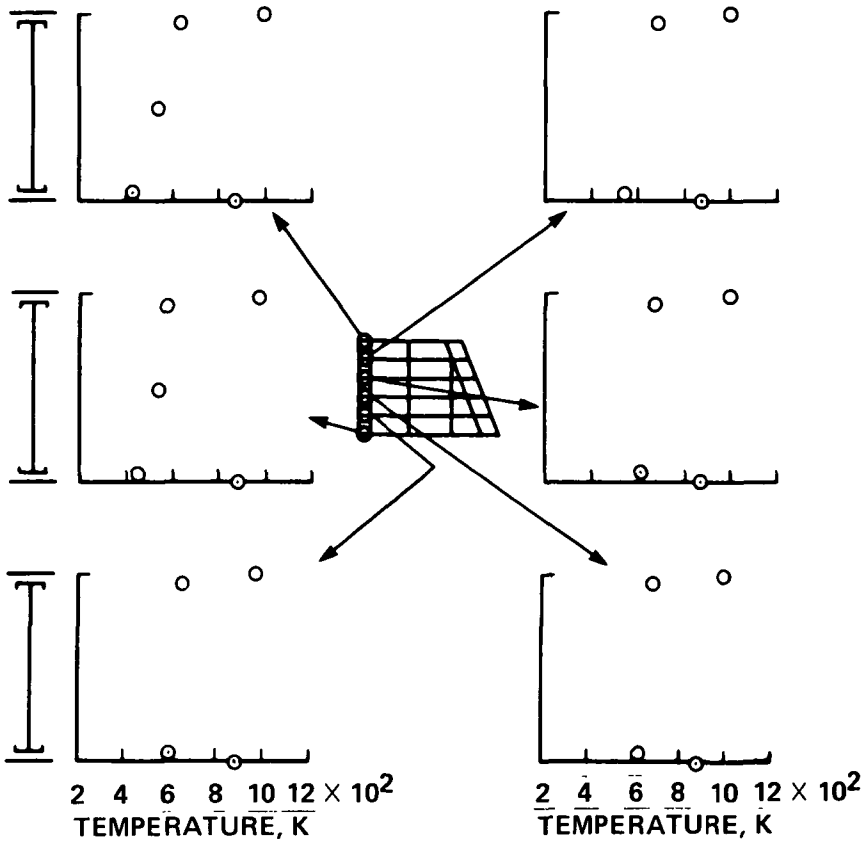

(e) Time = 1200 sec.

Figure 30.- Continued.

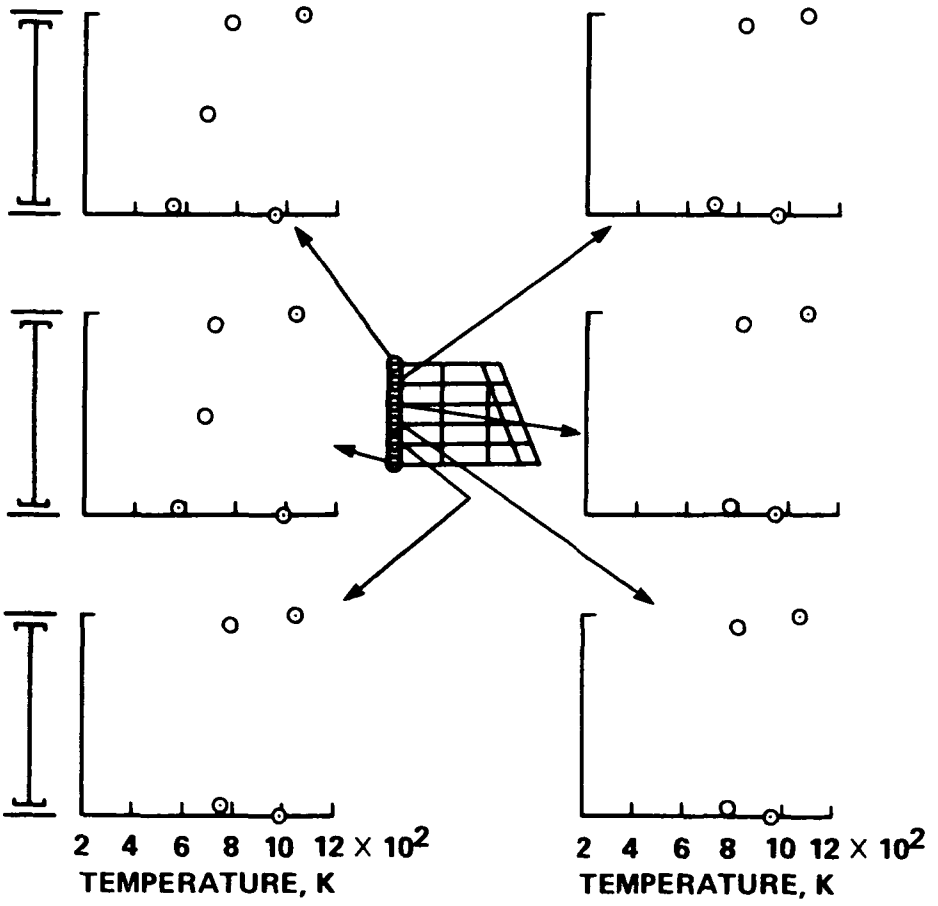

(f) Time = 1250 sec.

Figure 30.- Continued.

C-2

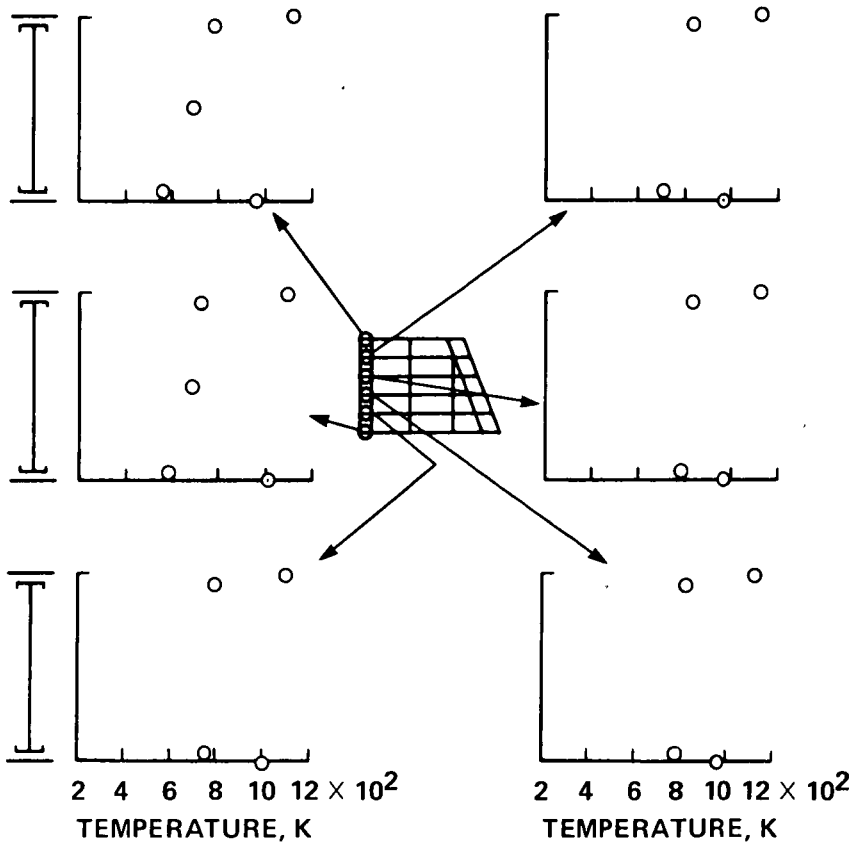

(g) Time = 1270 sec.

Figure 30.- Concluded.

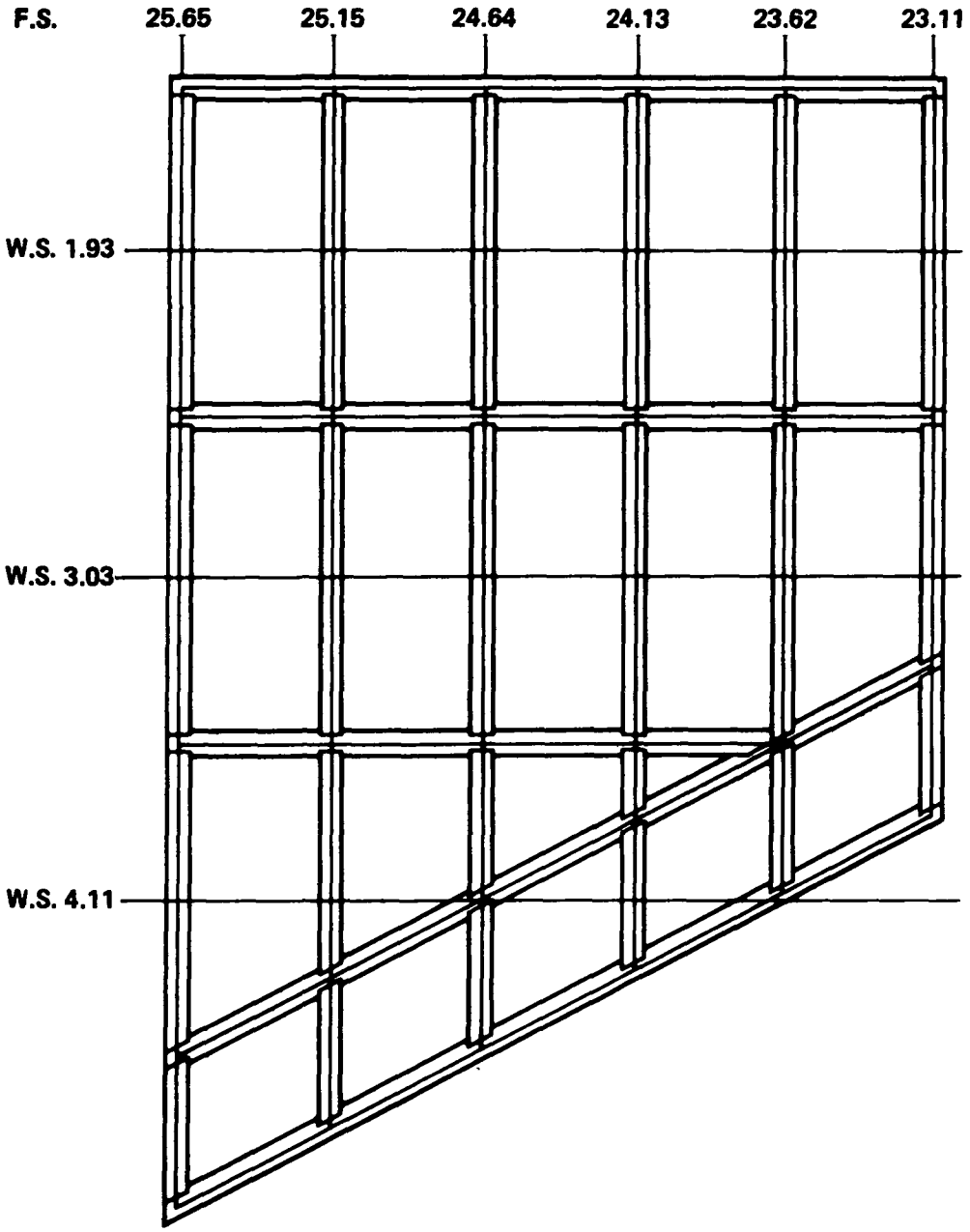

Figure 31.- Locations of design calculations. Fuselage station (F.S.), wing station (W.S.) in meters.

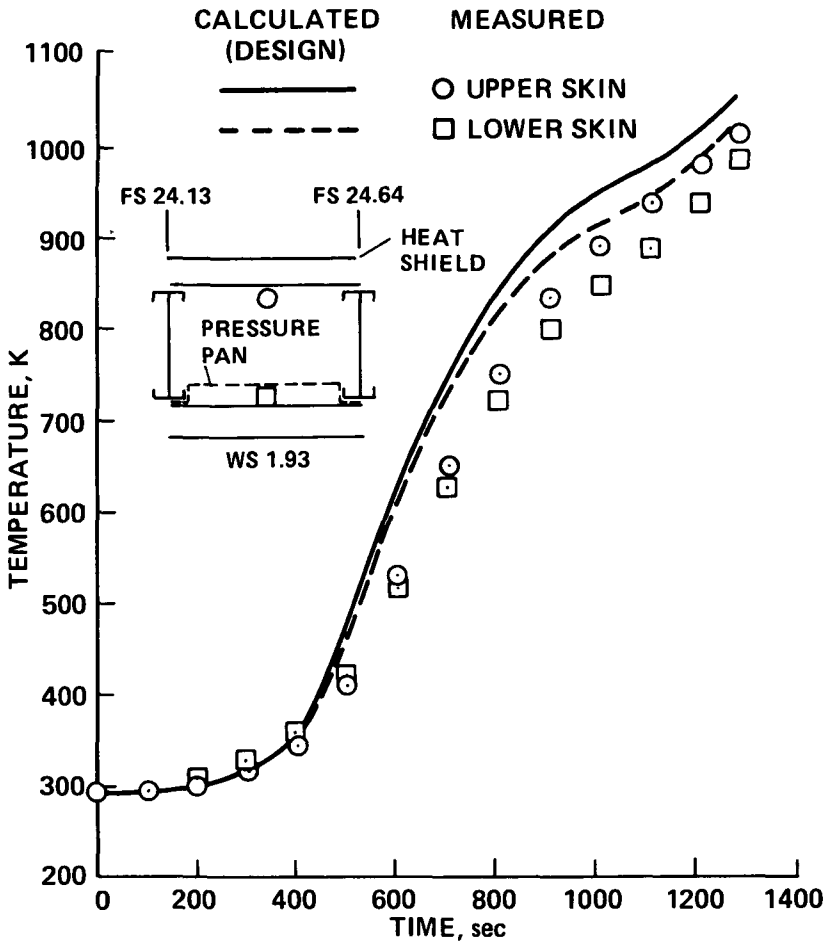

(a) Skin temperatures.

Figure 32.- Comparison of measured and design temperatures.

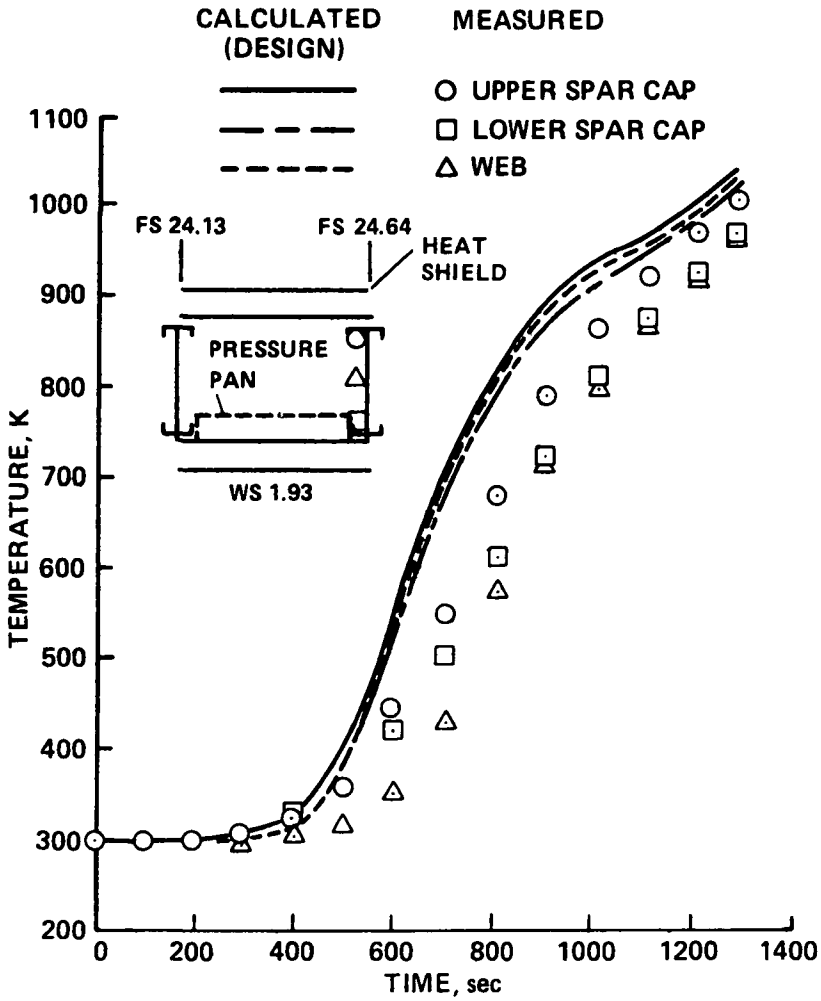

(b) Spar temperatures.

Figure 32.- Concluded.

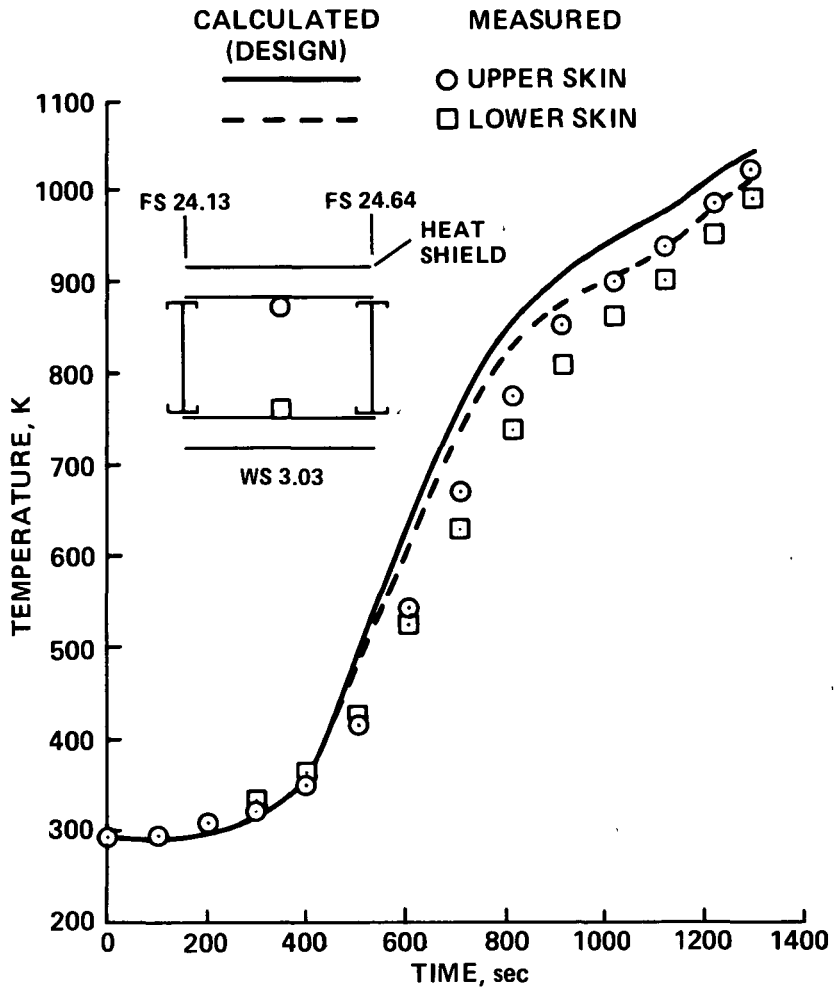

(a) Skin temperatures.

Figure 33.- Comparison of measured and design temperatures.

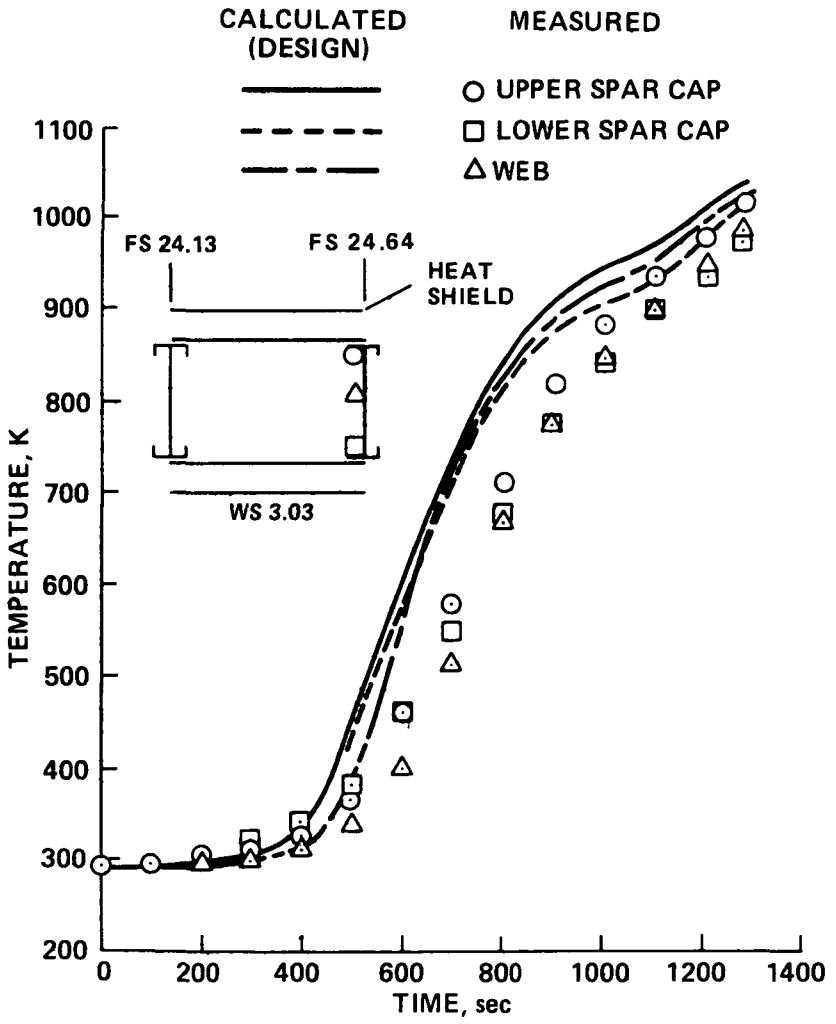

(b) Spar temperatures.

Figure 33.- Concluded.

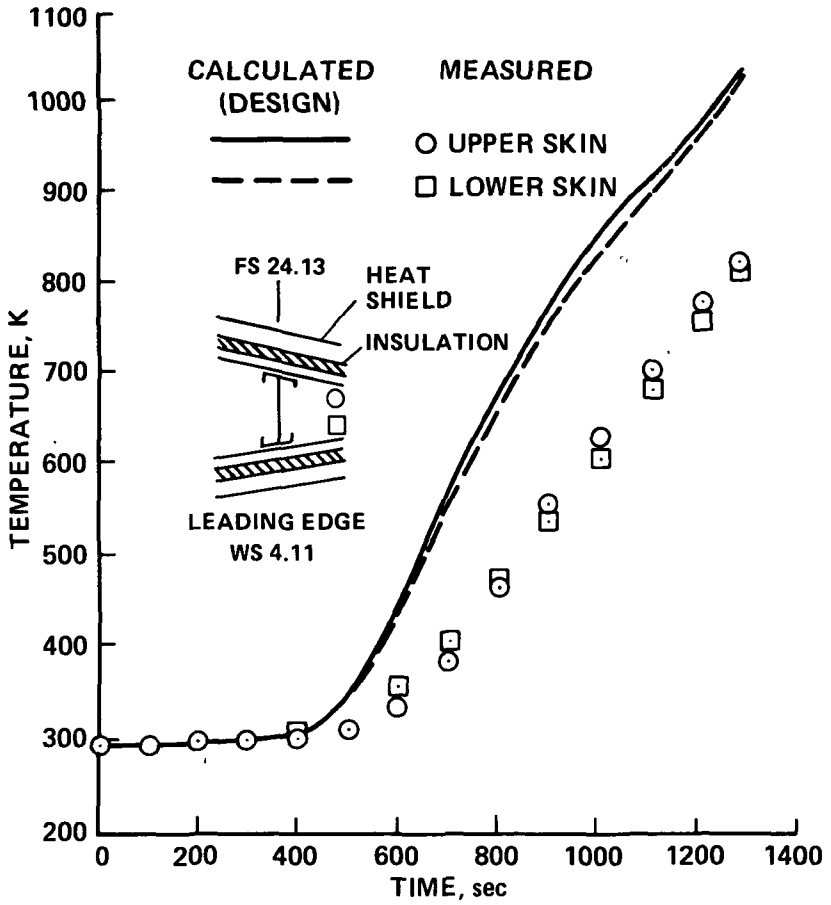

(a) Skin temperatures.

Figure 34.- Comparison of measured and design temperatures.

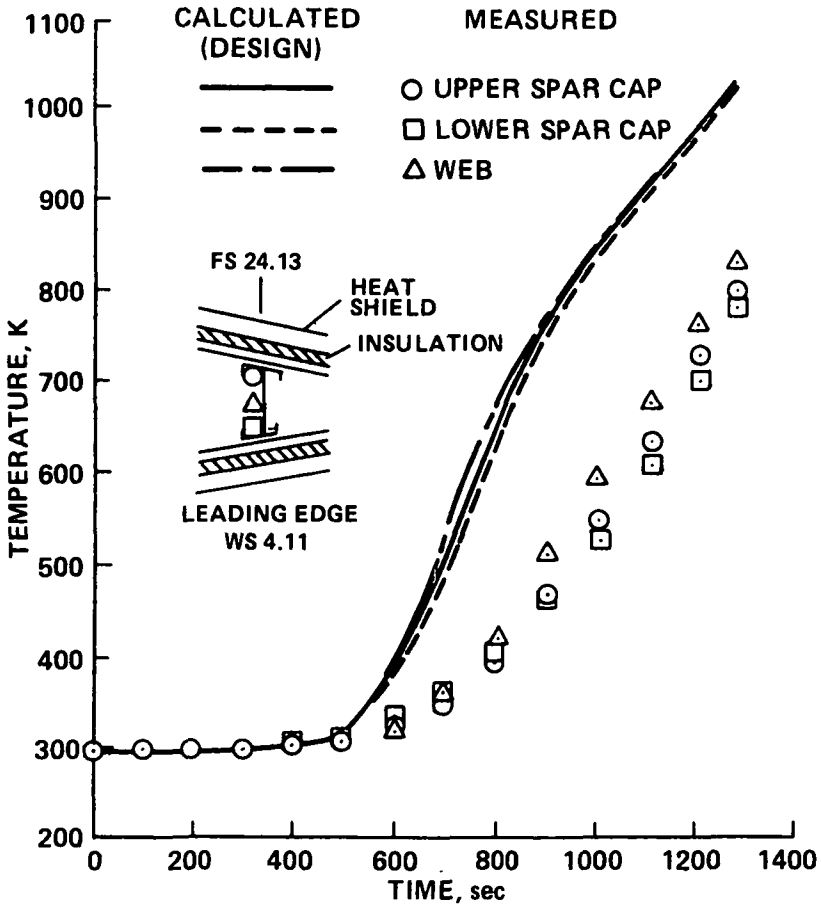

(b) Spar temperatures.

Figure 34.- Concluded.

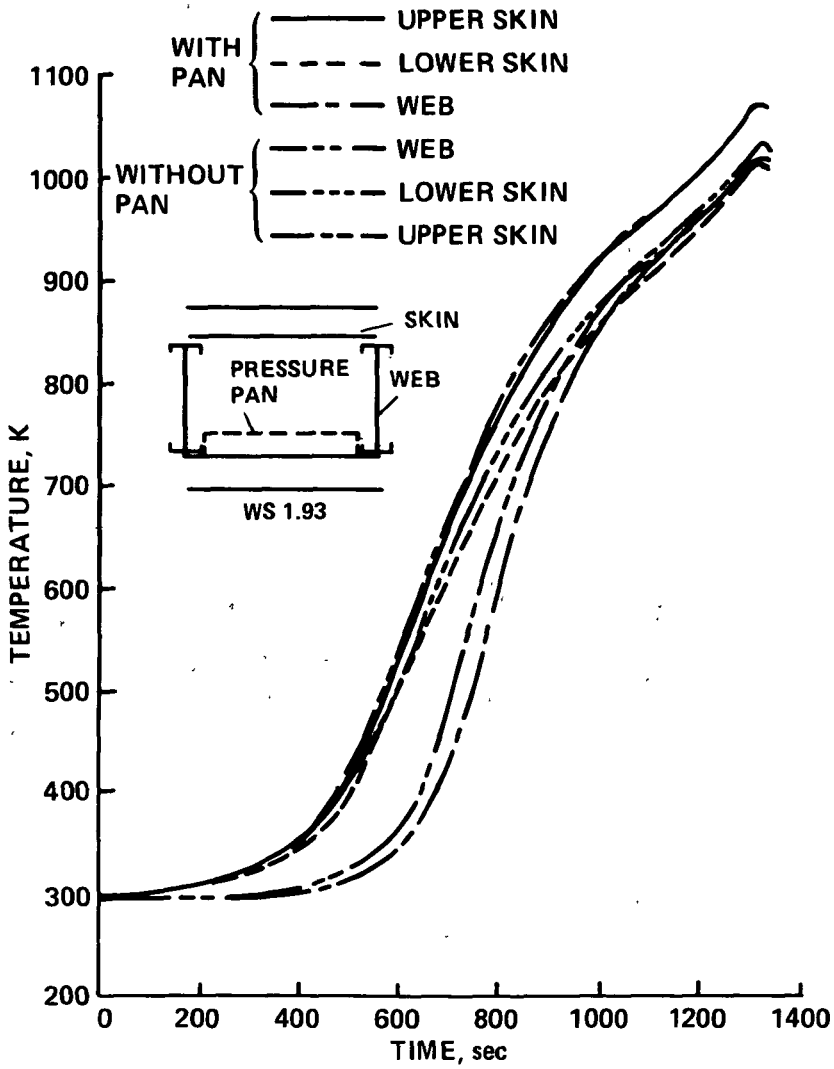

Figure 35.- Calculated HWTS temperatures with and without pressure pan. W.S. 1.93.

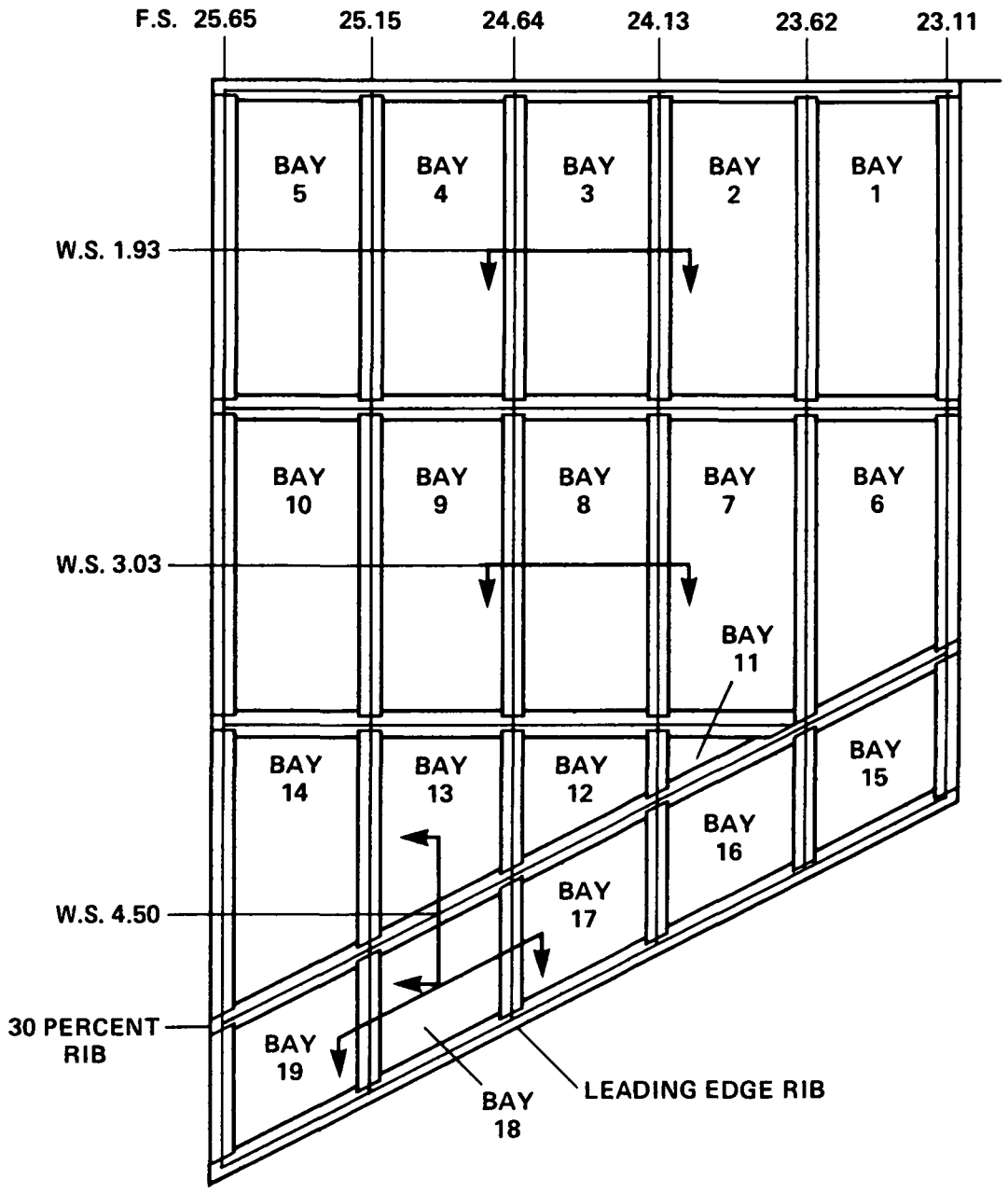

Figure 36.- Locations of thermal analysis; fuselage station (F.S.) and wing station (W.S.) in meters.

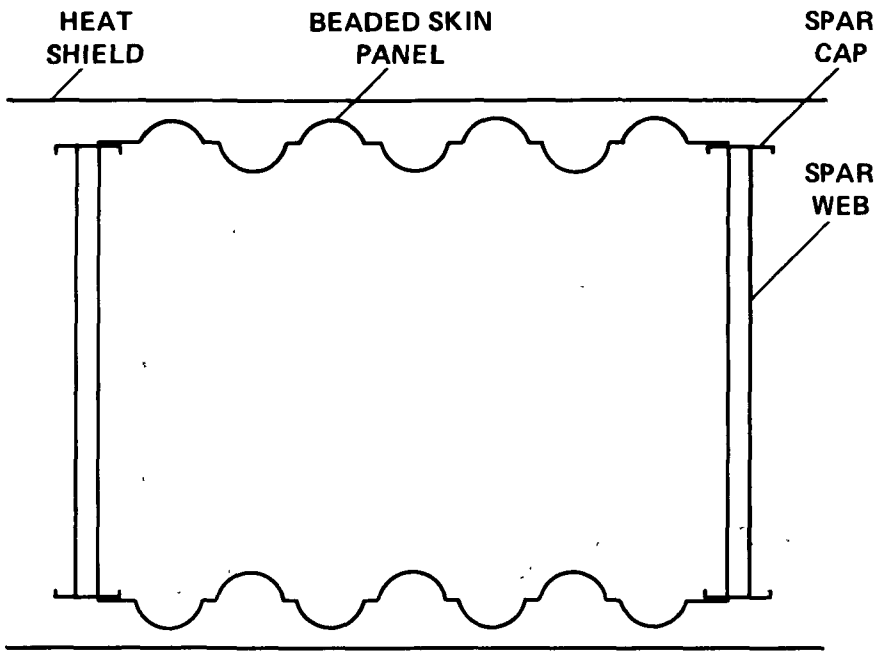

Figure 37.- Typical HWTS structure.

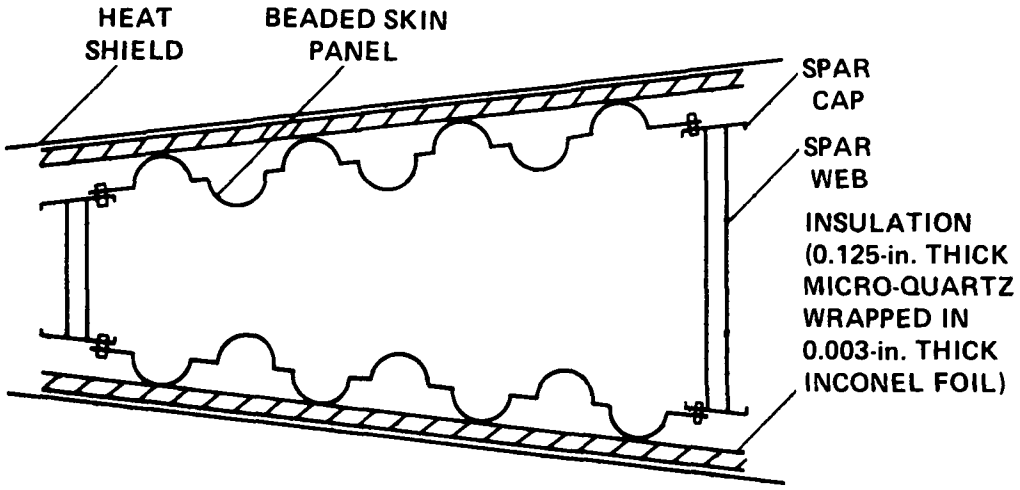

Figure 38.- Cross section of leading edge.

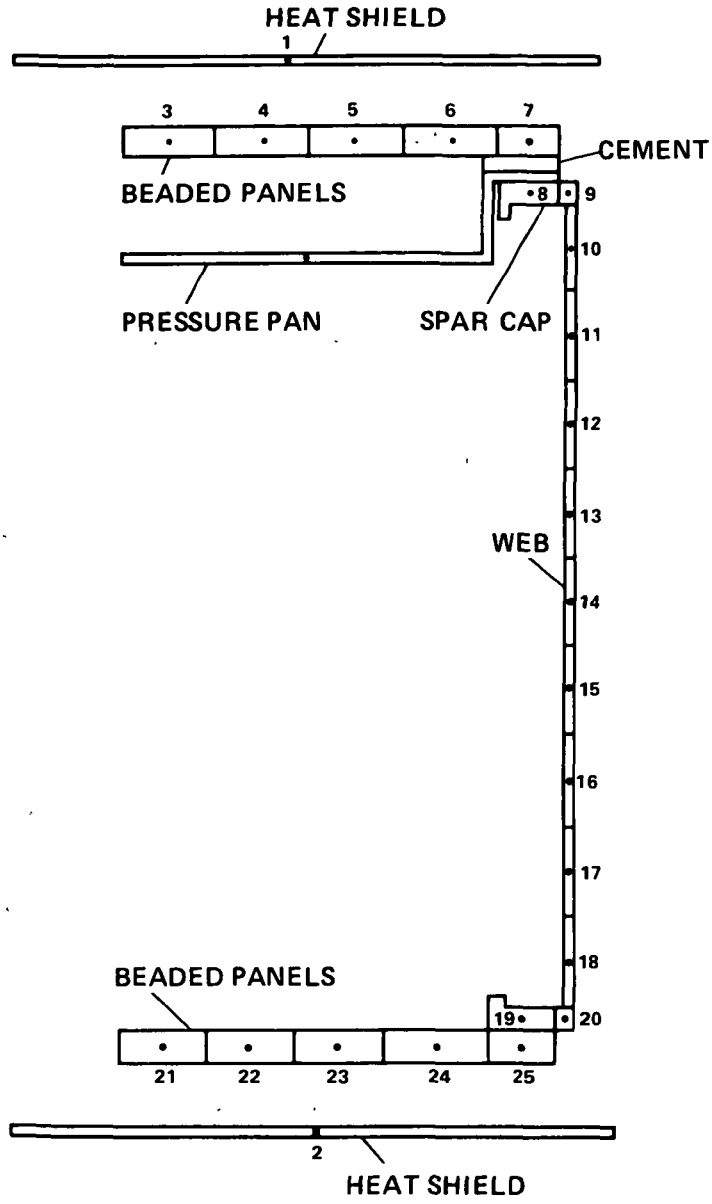

(a) Lumping and component identification.

Figure 39.- Thermal model 1 (Bay 3).

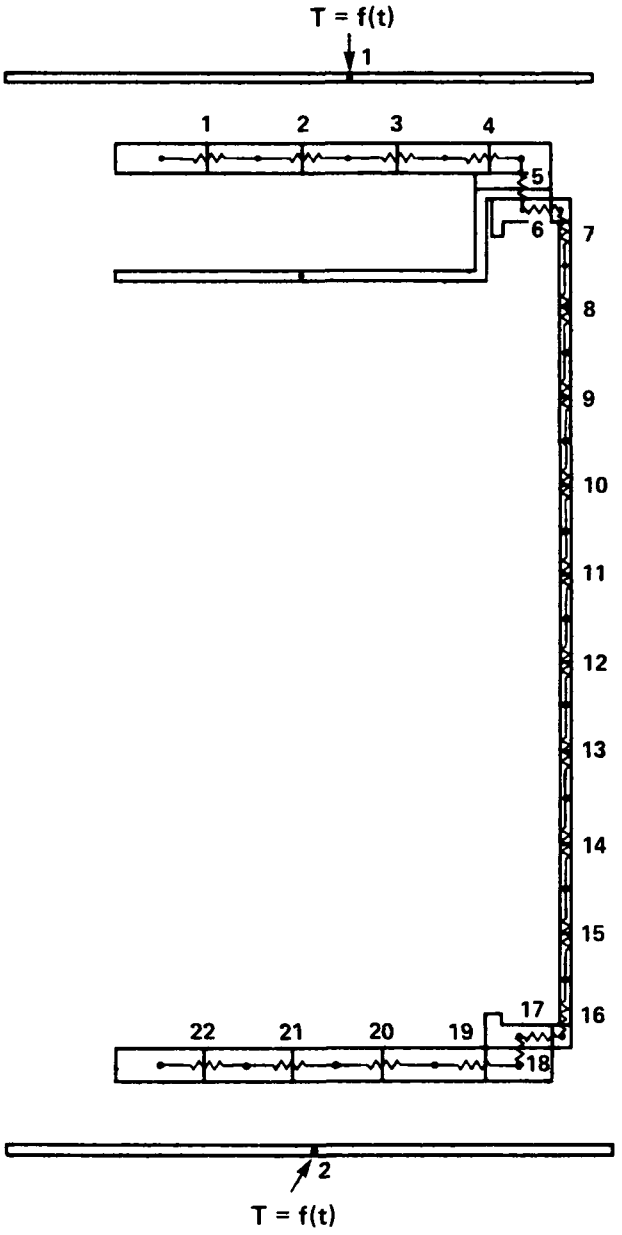

(b) Conduction resistors and temperatures inputs. Temperature = function of time [T = f(t)].

Figure 39.- Continued.

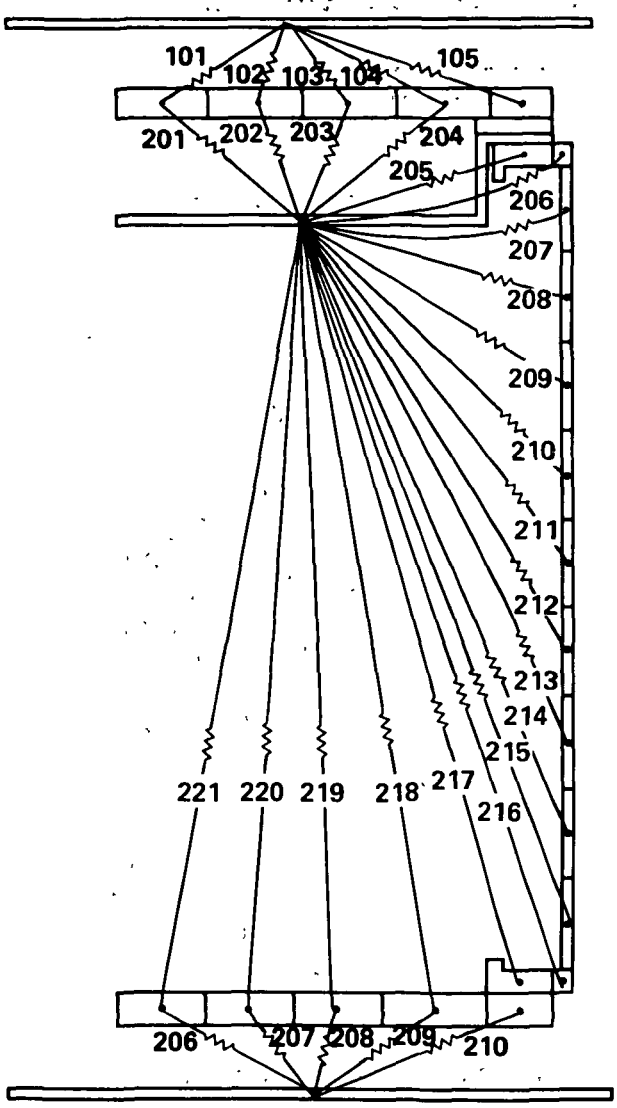

(c) Radiation resistors.

Figure 39.- Continued.

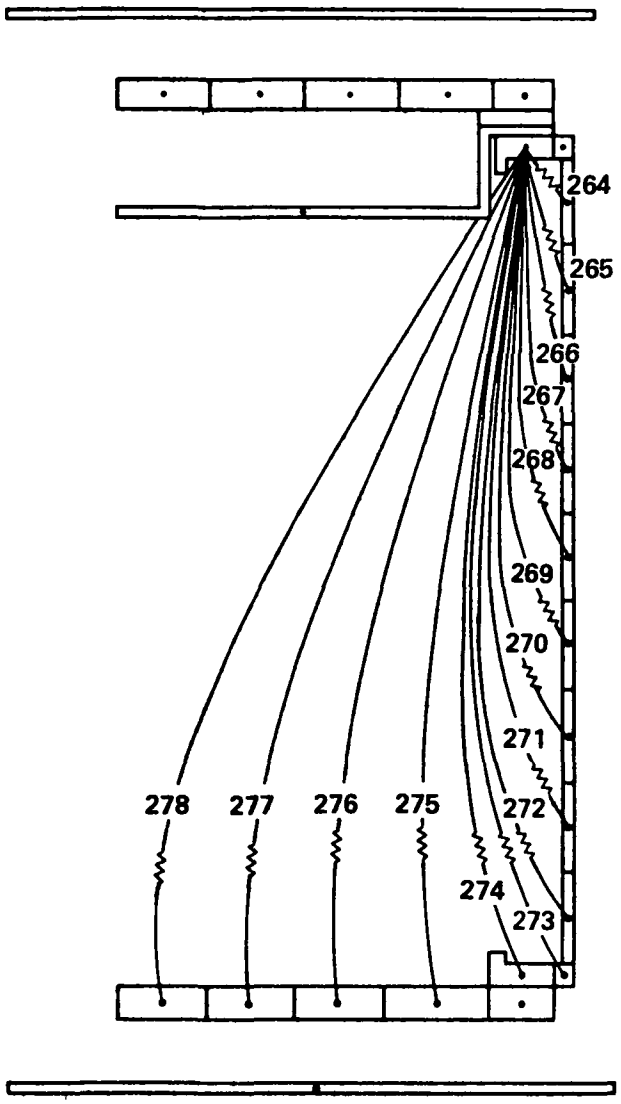

(d) Radiation resistors.

Figure 39.- Continued.

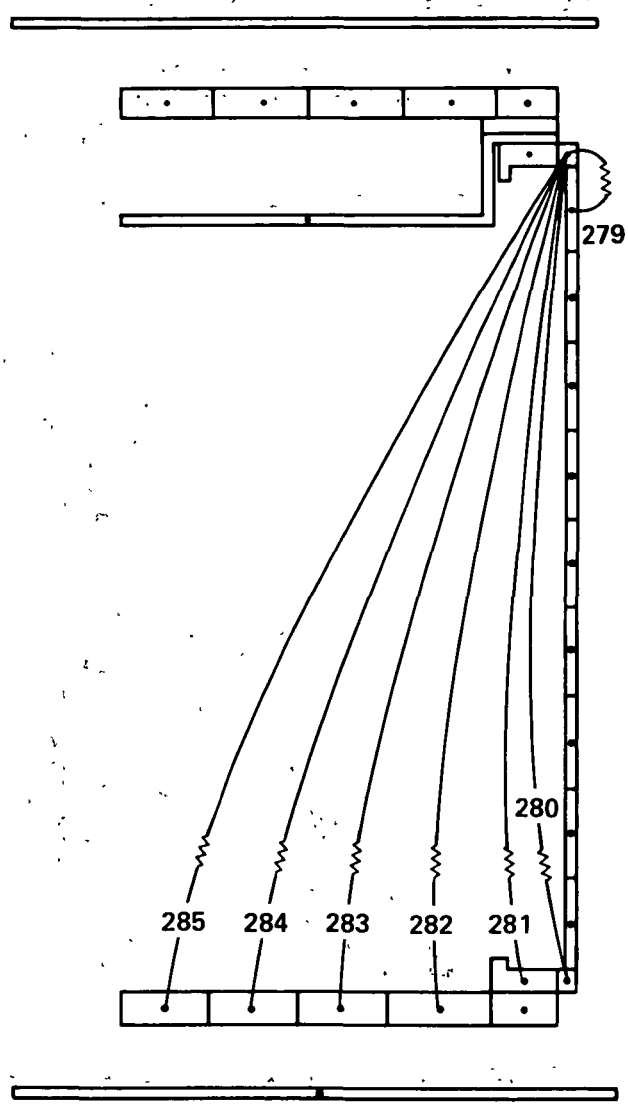

(e) Radiation resistors.

Figure 39.- Continued.

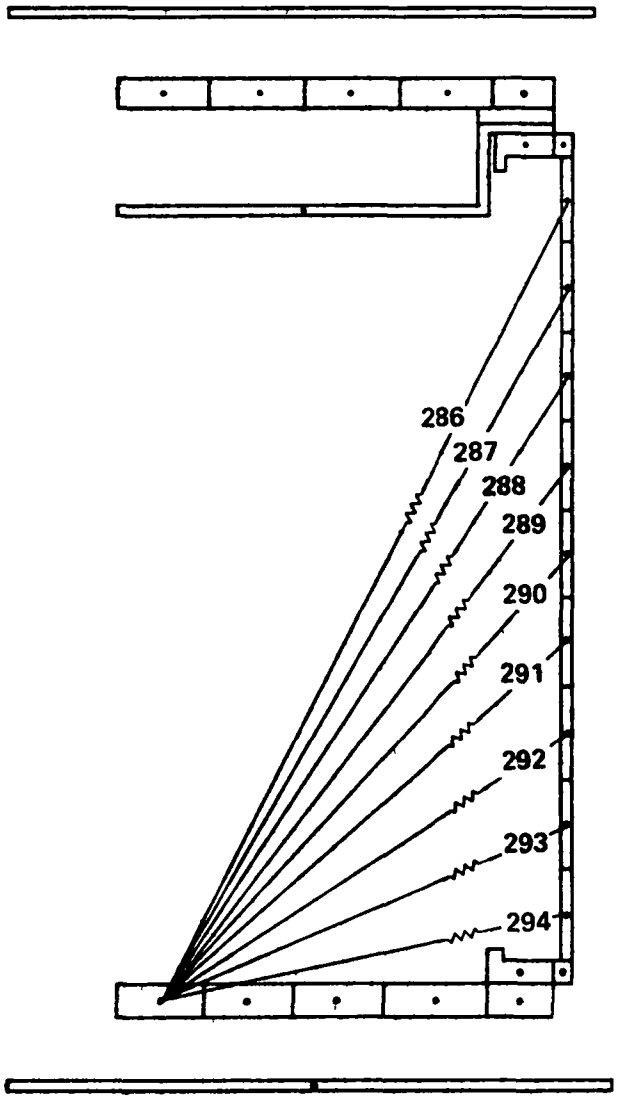

(f) Radiation resistors.

Figure 39.- Continued.

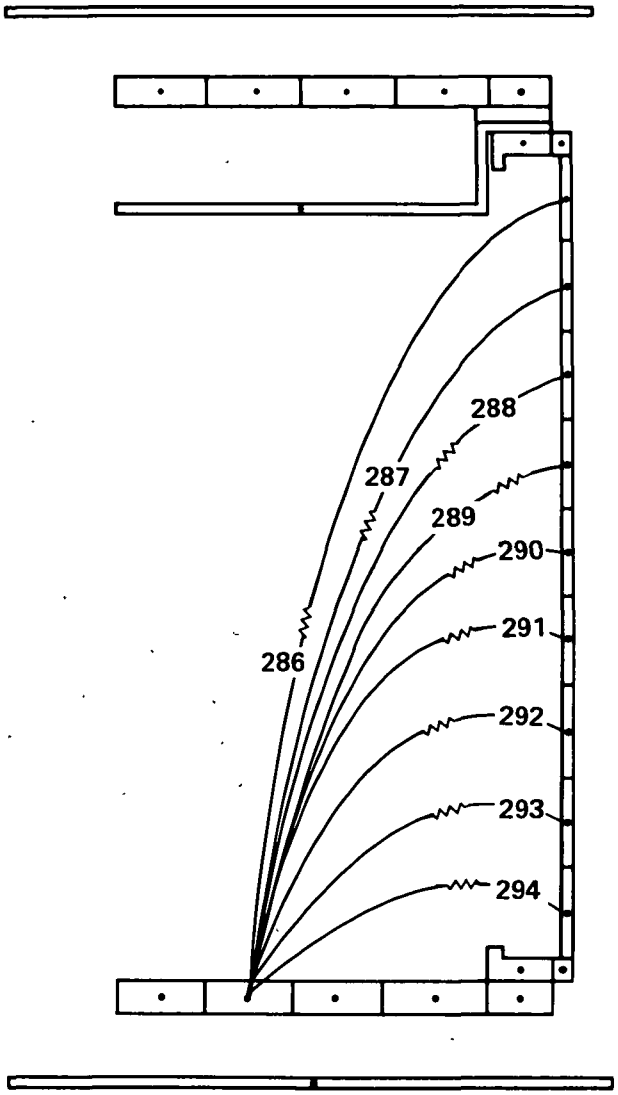

(g) Radiation resistors.

Figure 39.- Continued.

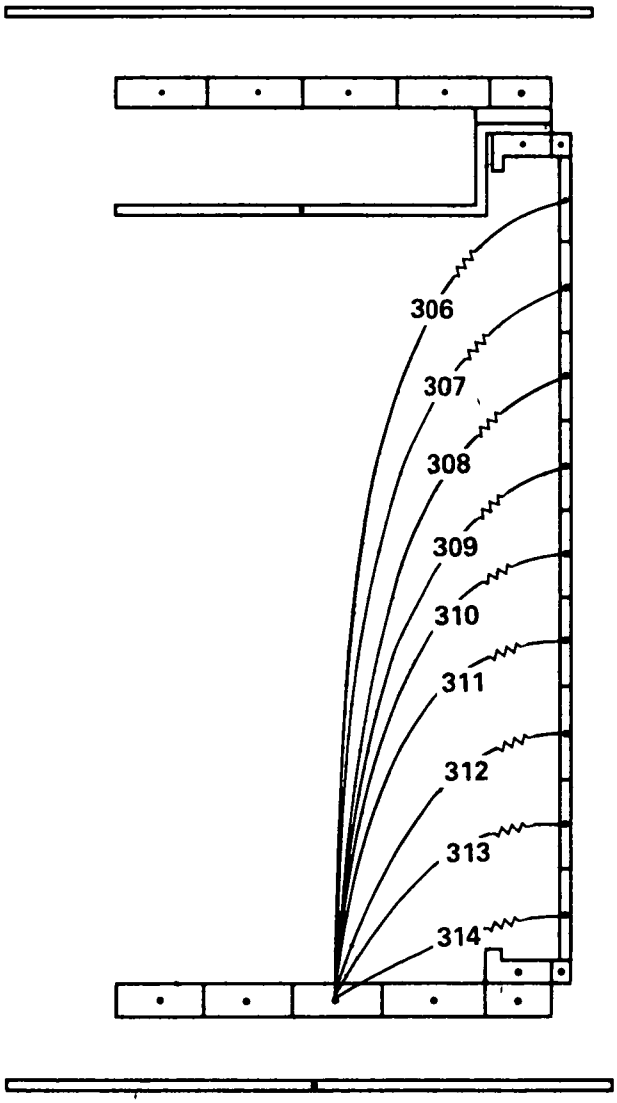

(h) Radiation resistors.

Figure 39.- Continued.

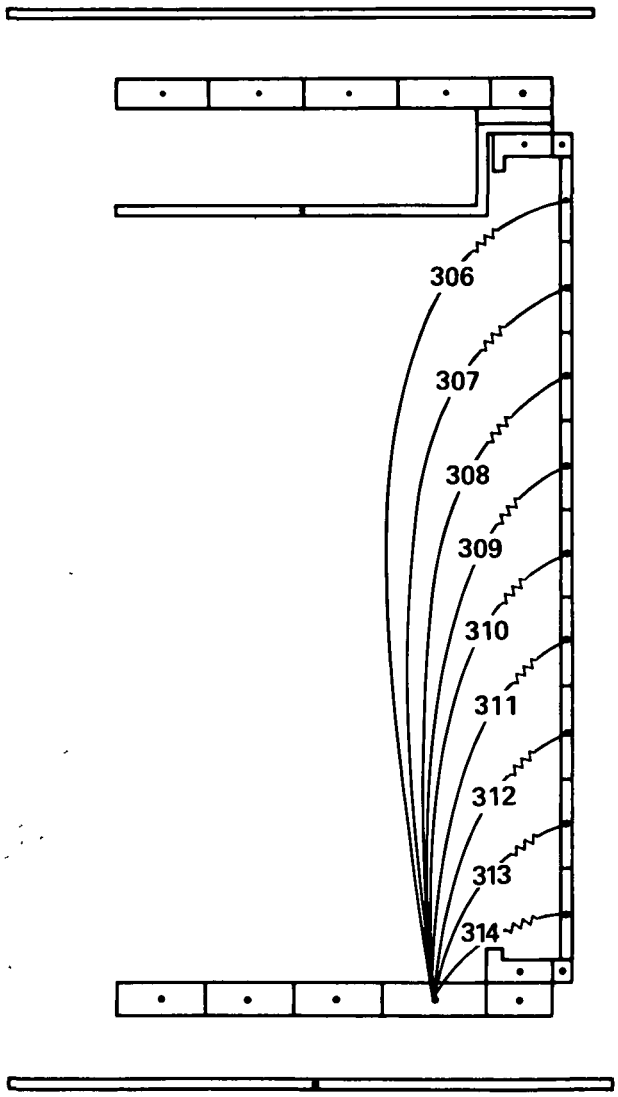

(i) Radiation resistors.

Figure 39.- Continued.

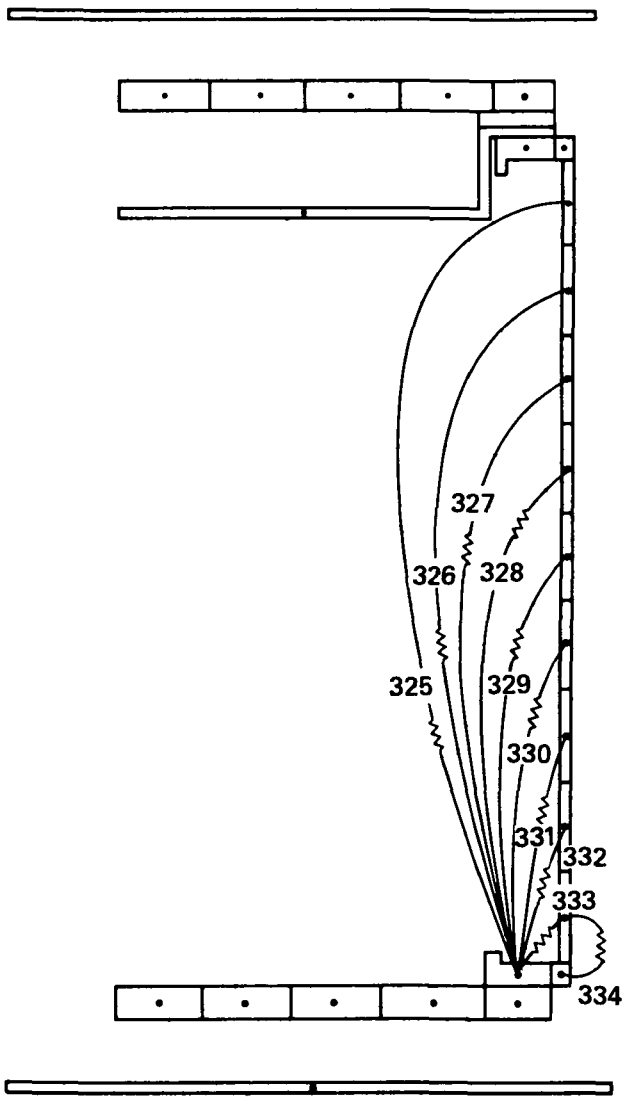

(j) Radiation resistors.

Figure 39.- Concluded.

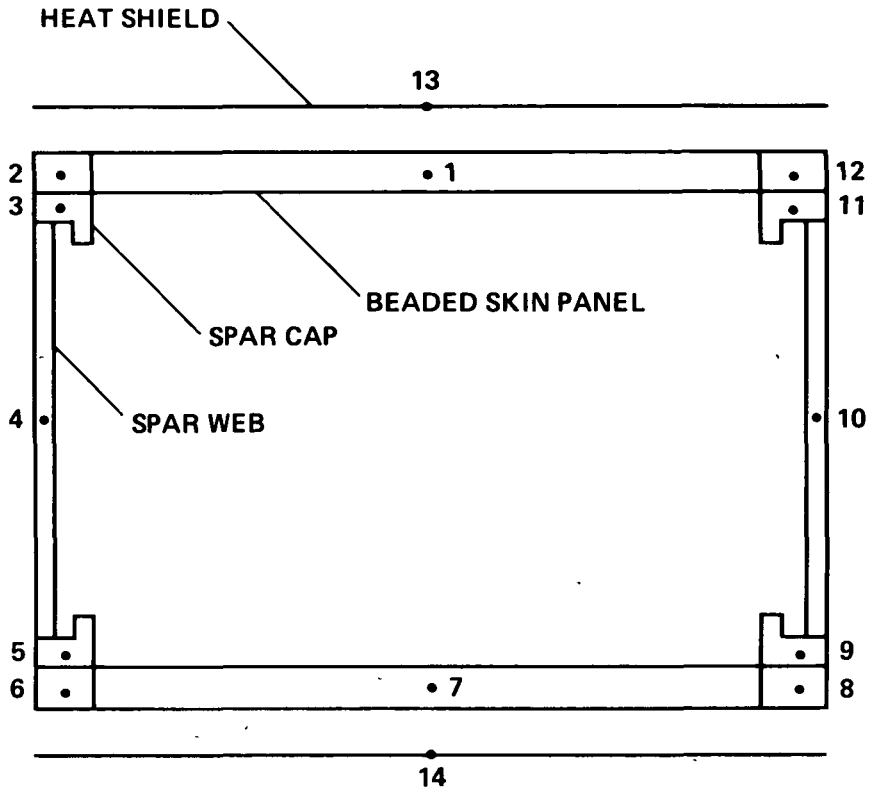

(a) Lumping and component identification.

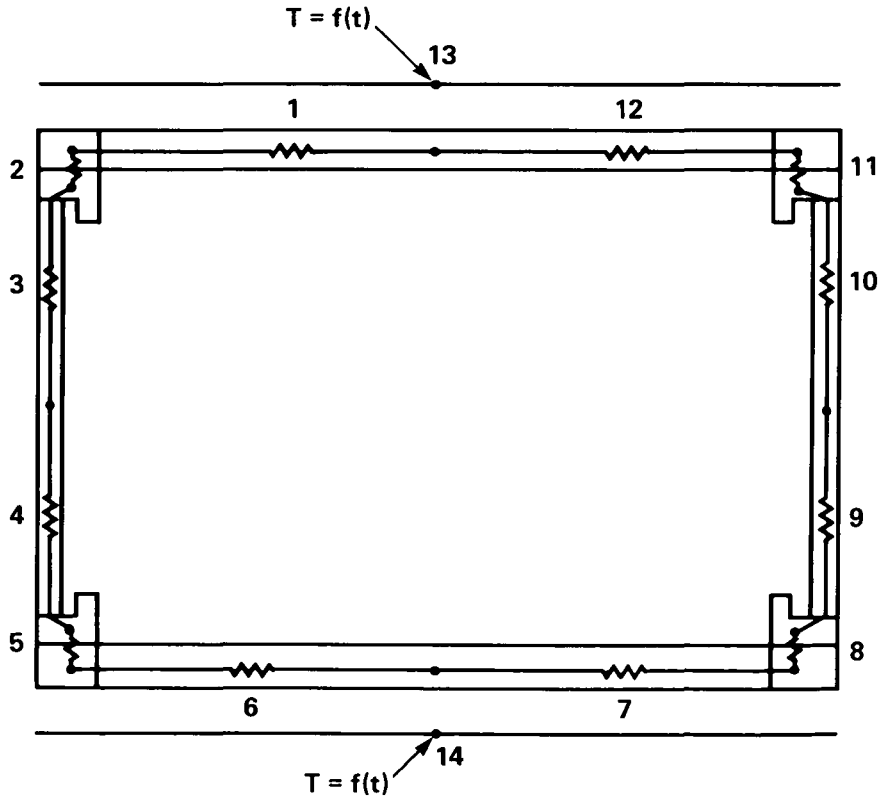

(b) Conduction resistors and temperature inputs.

Figure 40.- Thermal model 2, bay 8.

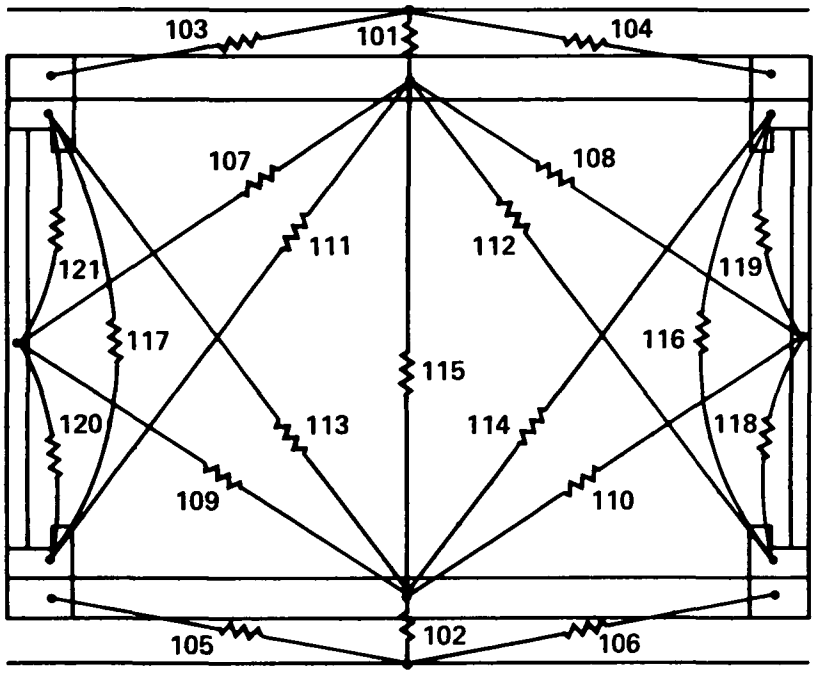

(c) Radiation resistors.

Figure 40.- Concluded.

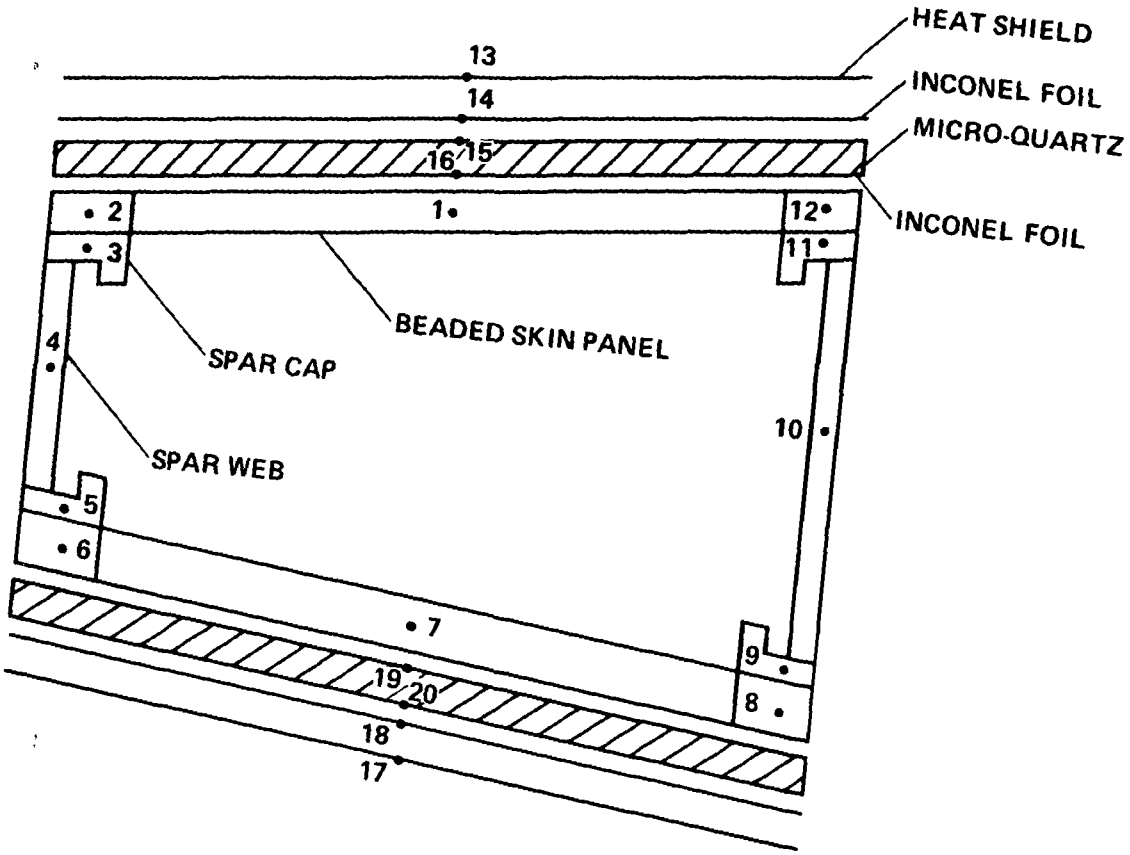

(a) Lumping and component identification.

Figure 41.- Thermal model 3, leading edge (bay 18).

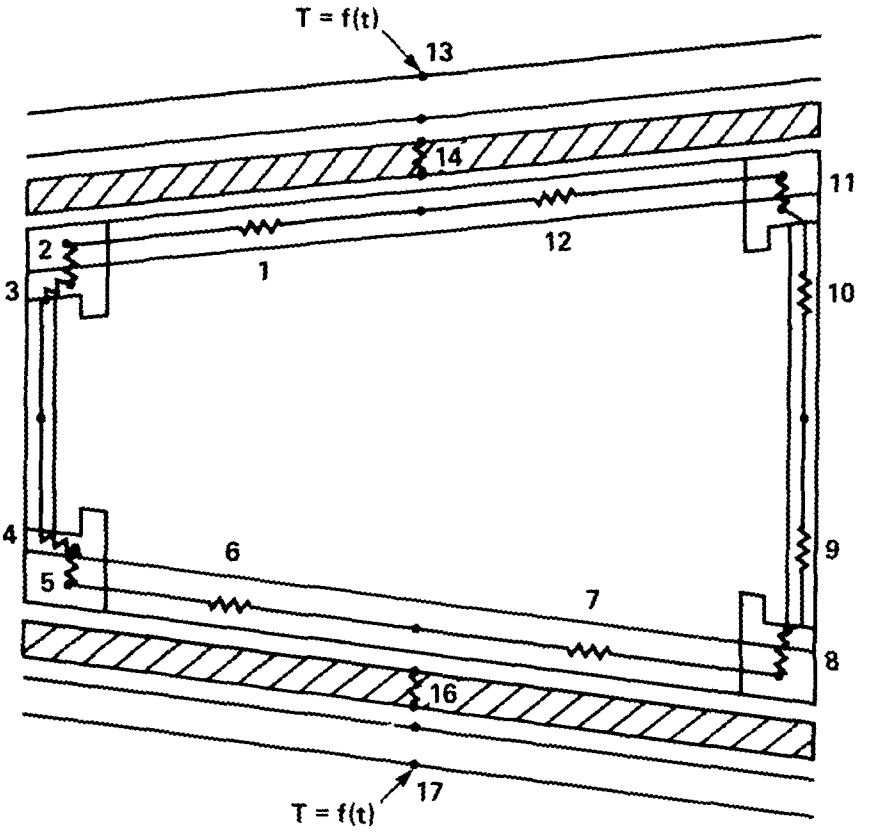

(b) Conduction resistors and temperature inputs.

Figure 41.- Continued.

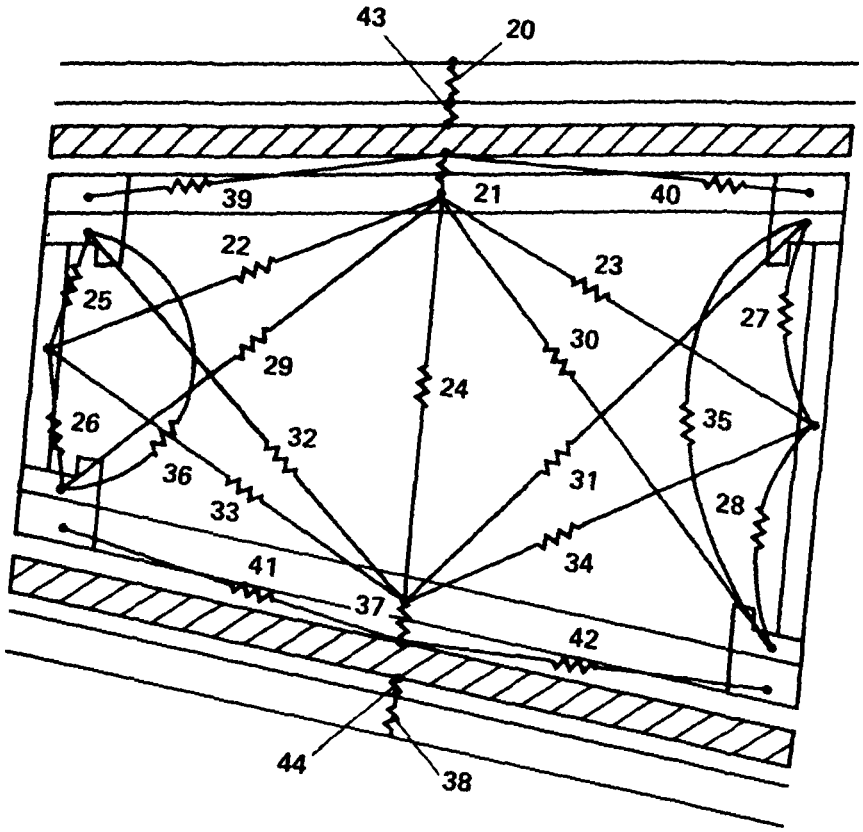

(c) Radiation resistors.

Figure 41.- Concluded.

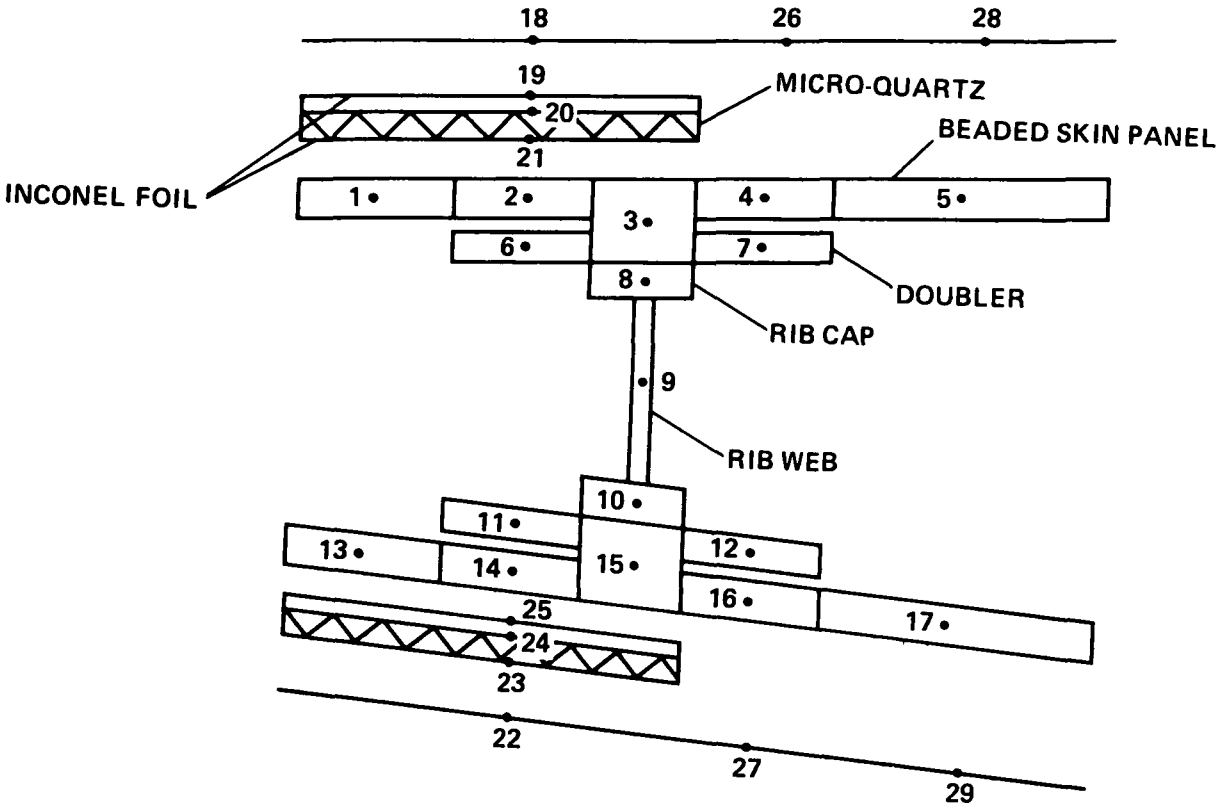

(a) Lumping and component identification.

Figure 42.- Thermal model of 30% rib.

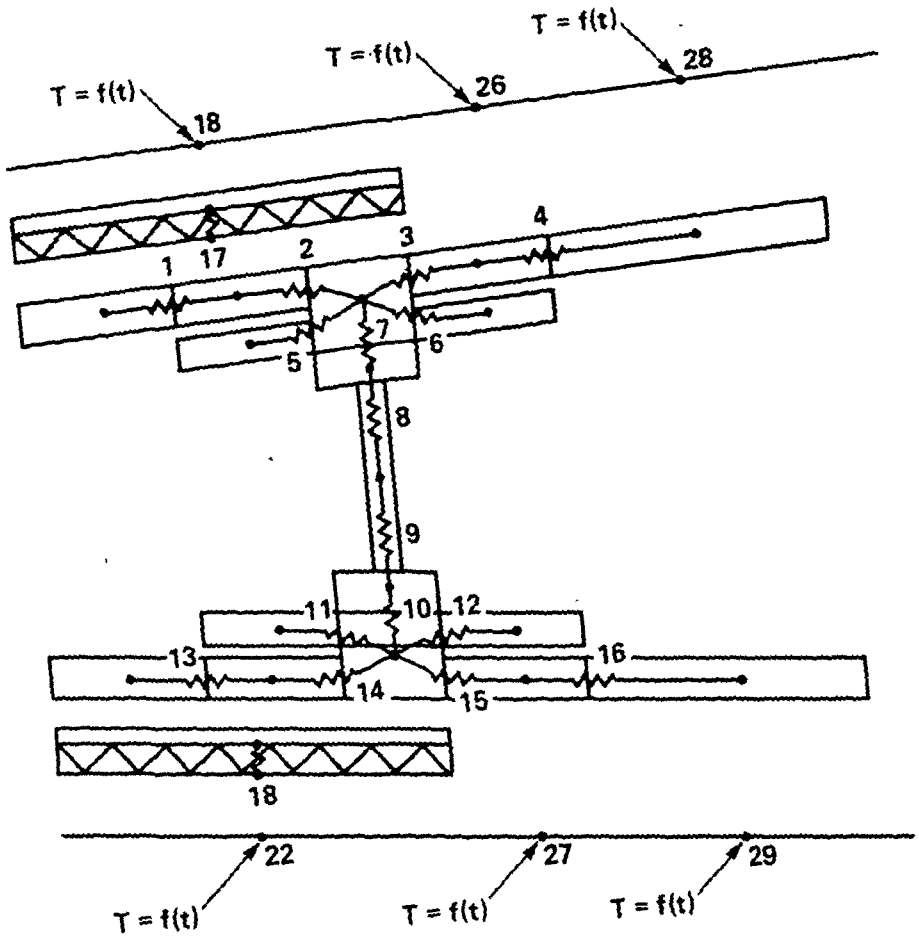

(b) Conduction resistors and temperature inputs.

Figure 42.- Continued.

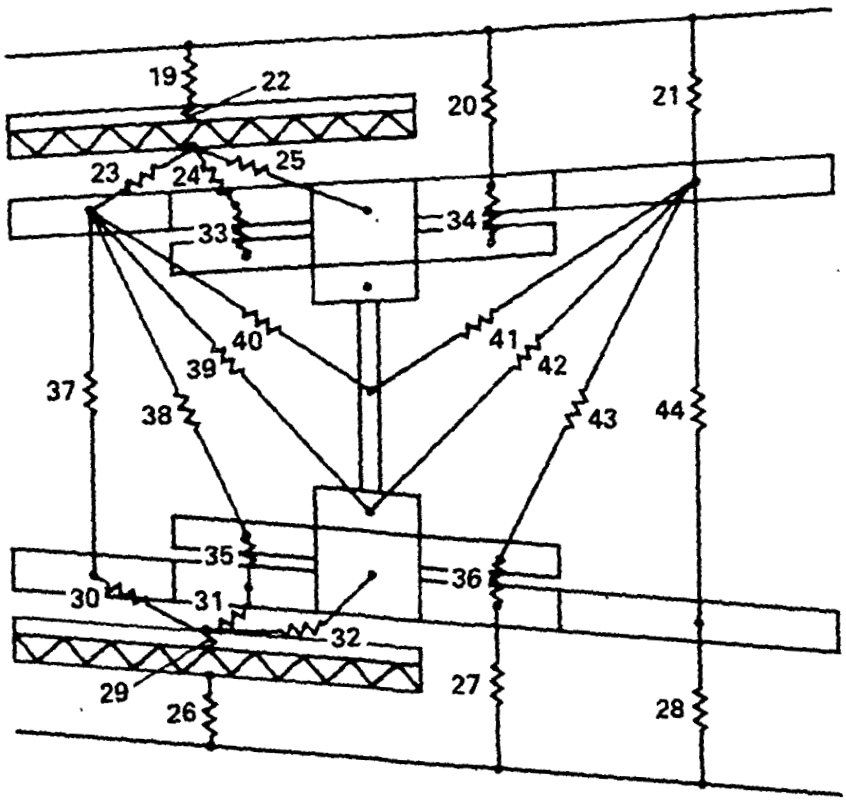

(c) Radiation resistors.

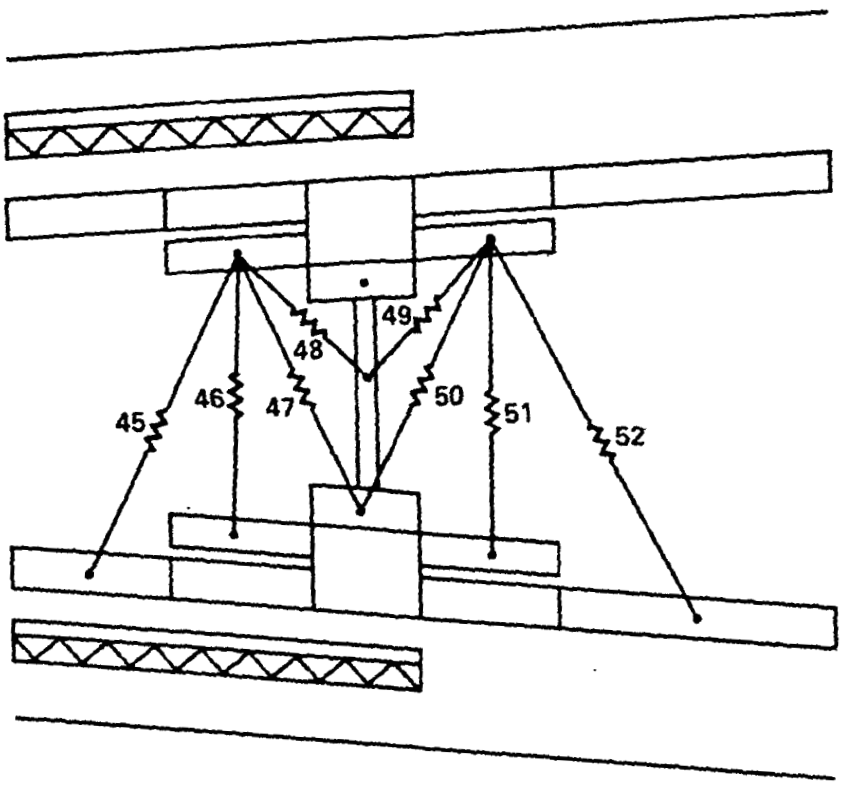

(d) Radiation resistors.

Figure 42.- Continued.

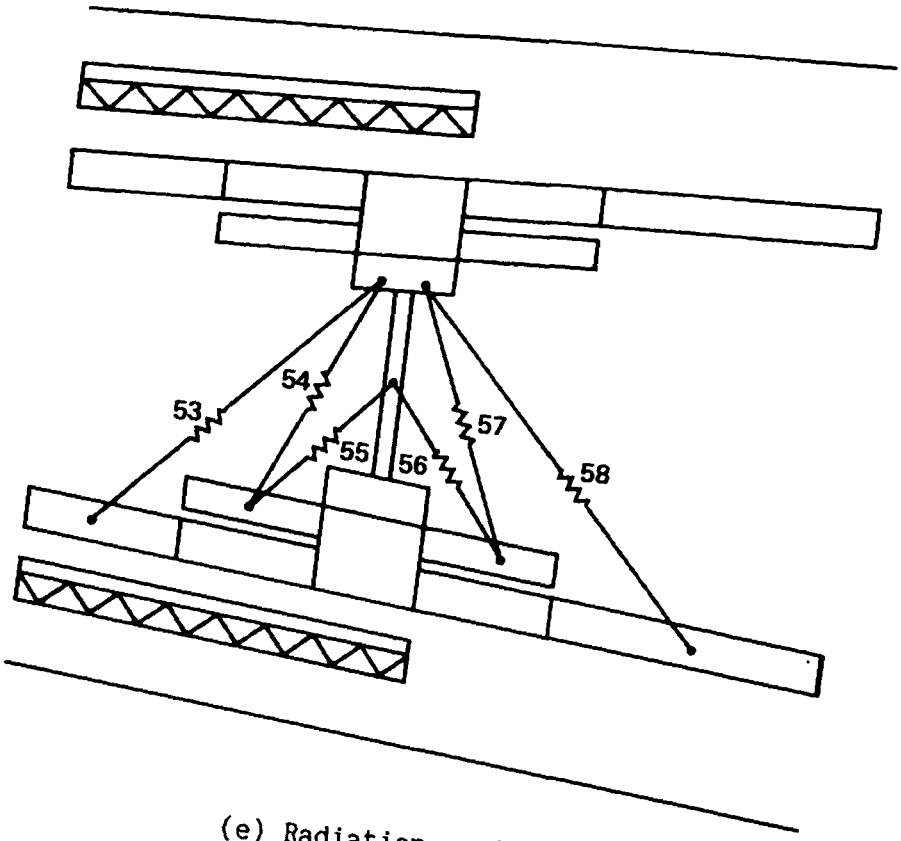

(e) Radiation resistors.

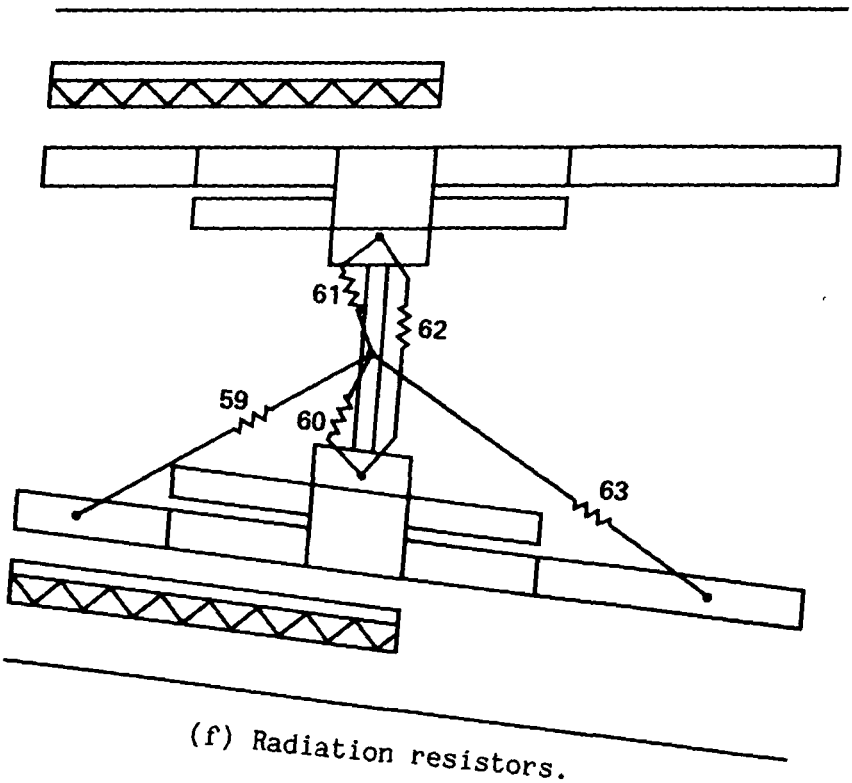

(f) Radiation resistors.

Figure 42.- Concluded.

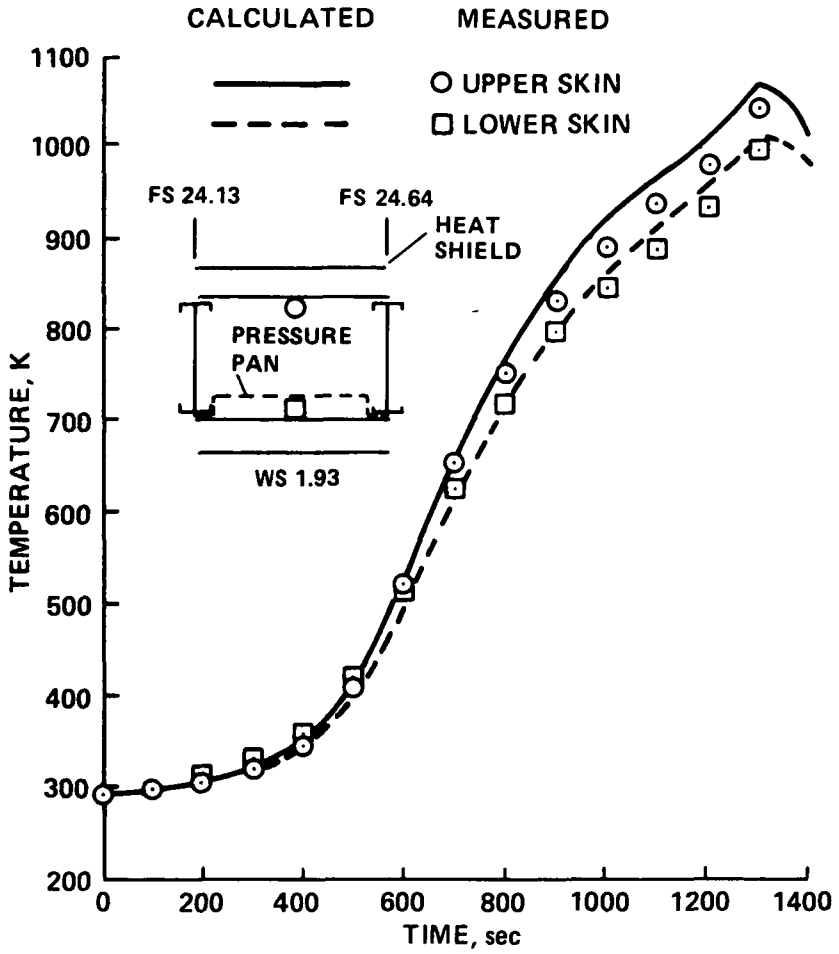

(a) Skin temperatures.

Figure 43.- Comparison of measured and calculated HWTS temperatures; fuselage stations (F.S.) and wing stations (W.S.) are in meters.

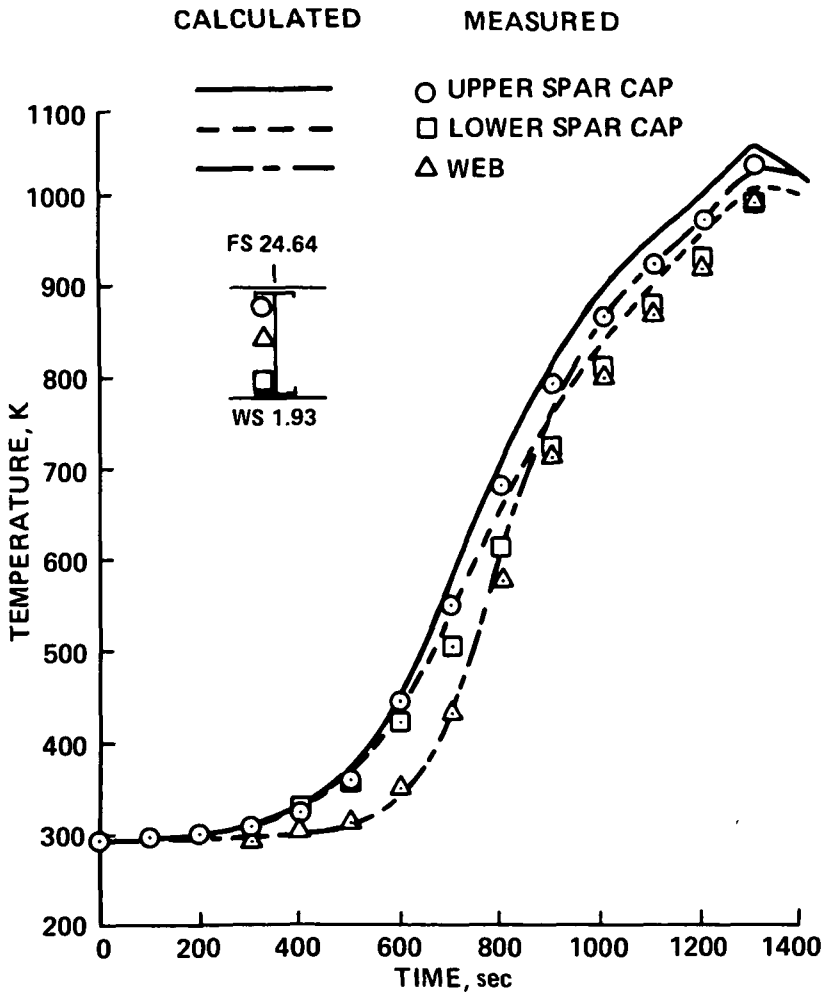

(b) Spar temperatures.

Figure 43.- Concluded.

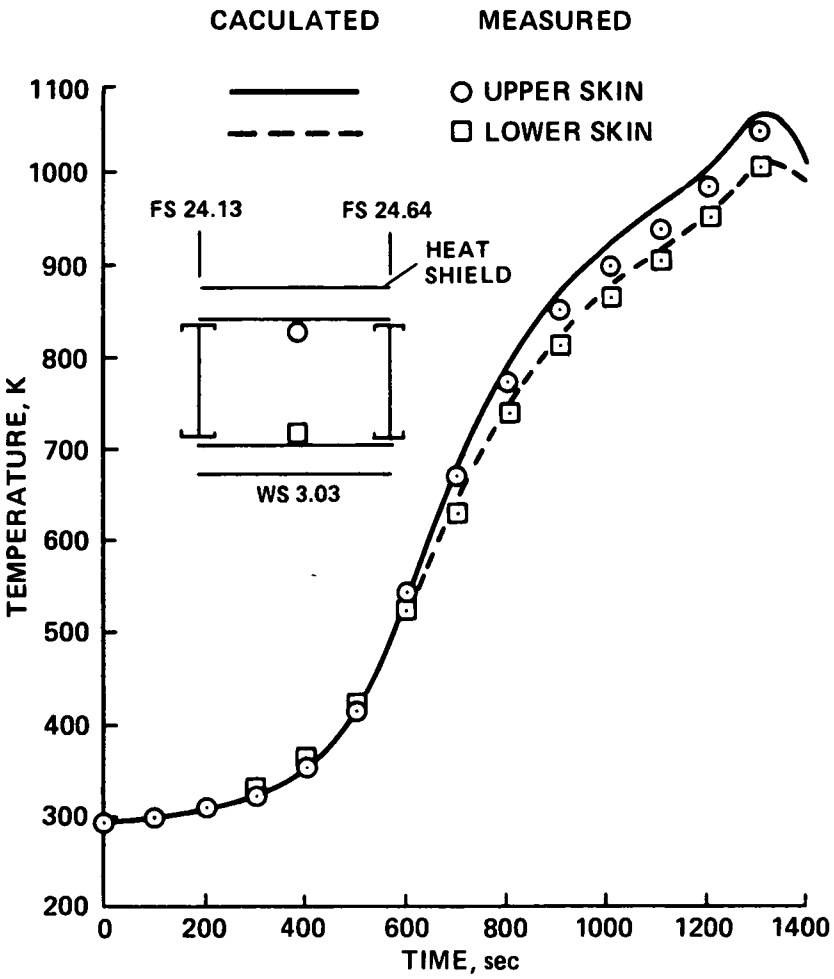

(a) Skin temperatures.

Figure 44.- Comparison of measured and calculated HWTS temperatures; fuselage stations (F.S.) and wing stations (W.S.) are in meters.

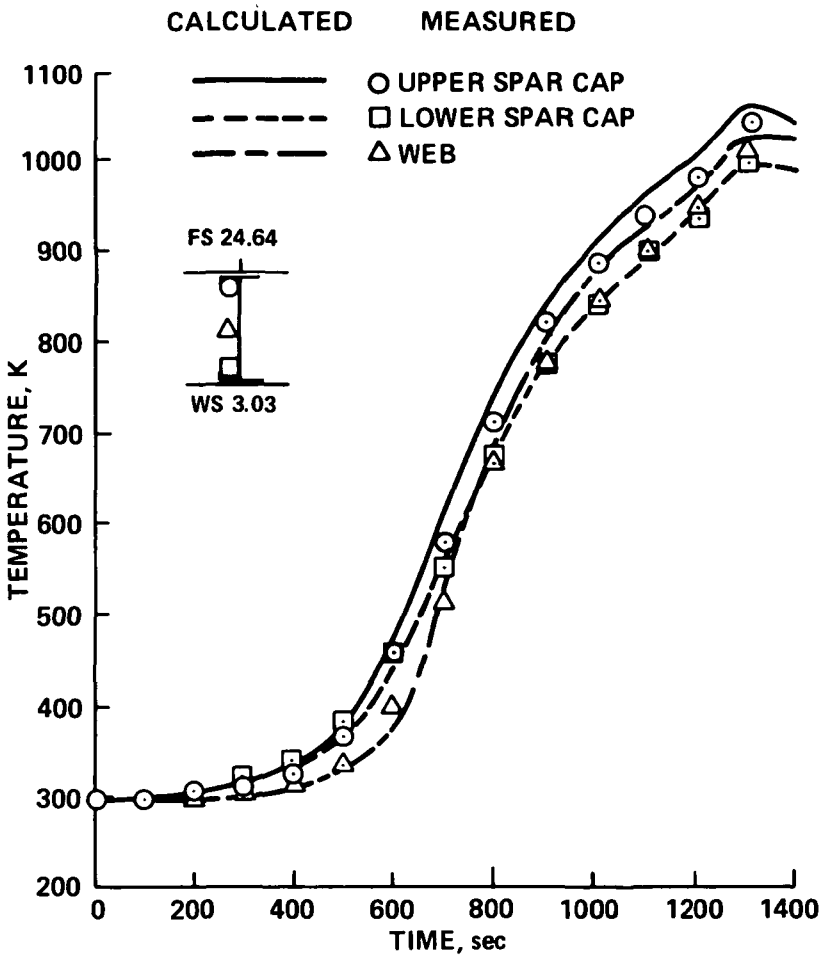

(b) Spar temperatures.

Figure 44.- Concluded.

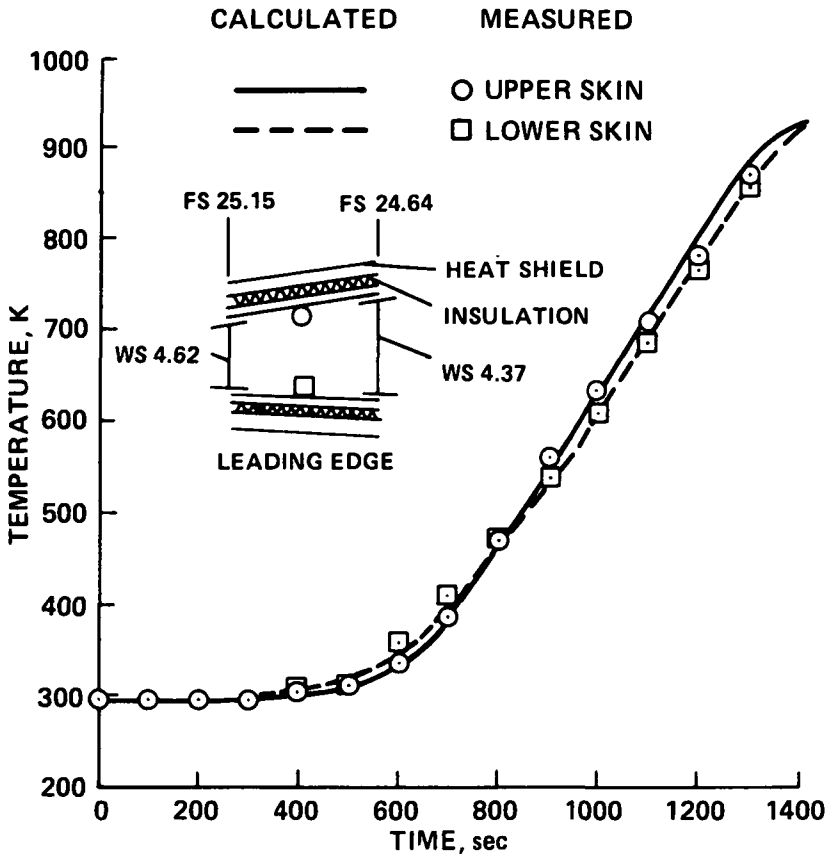

(a) Skin temperatures.

Figure 45.- Comparison of measured and calculated HWTS temperatures; fuselage stations (F.S.) and wing stations (W.S.) are in meters.

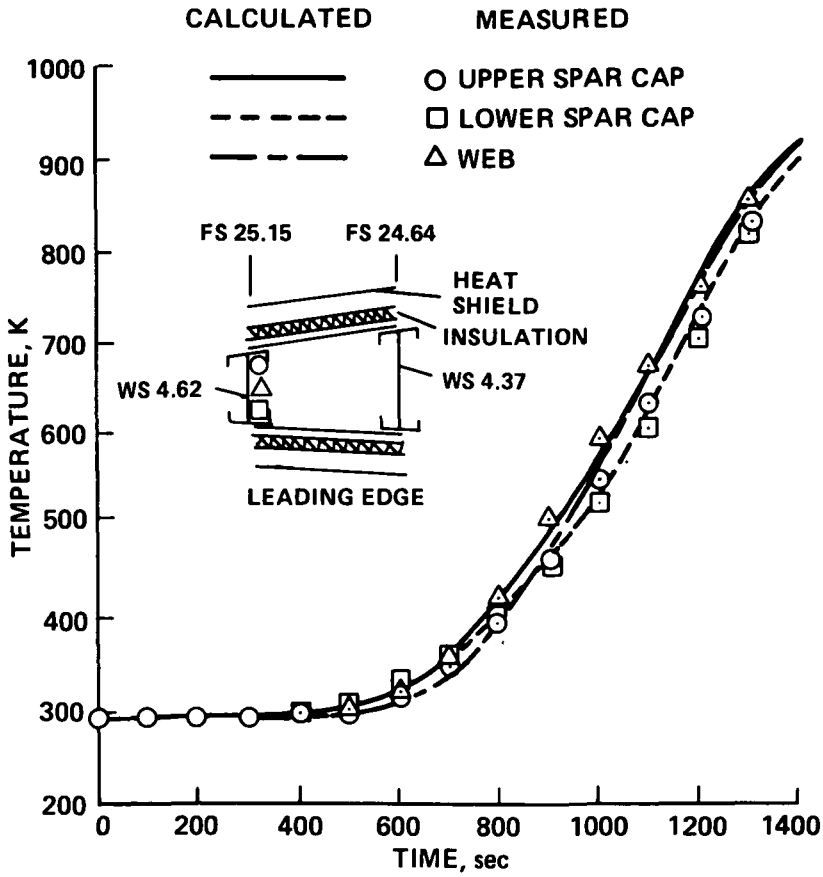

(b) Spar temperatures.

Figure 45.- Concluded.

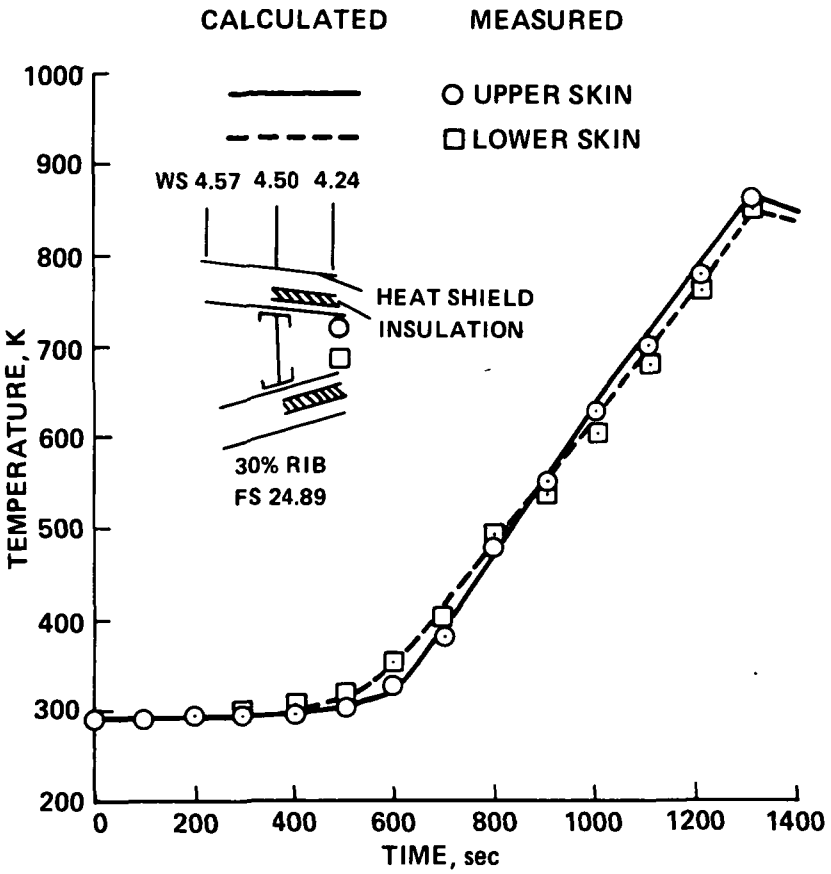

(a) Skin temperatures.

Figure 46.- Comparison of measured and calculated HWTS temperatures; fuselage stations (F.S.) and wing stations (W.S.) are in meters.

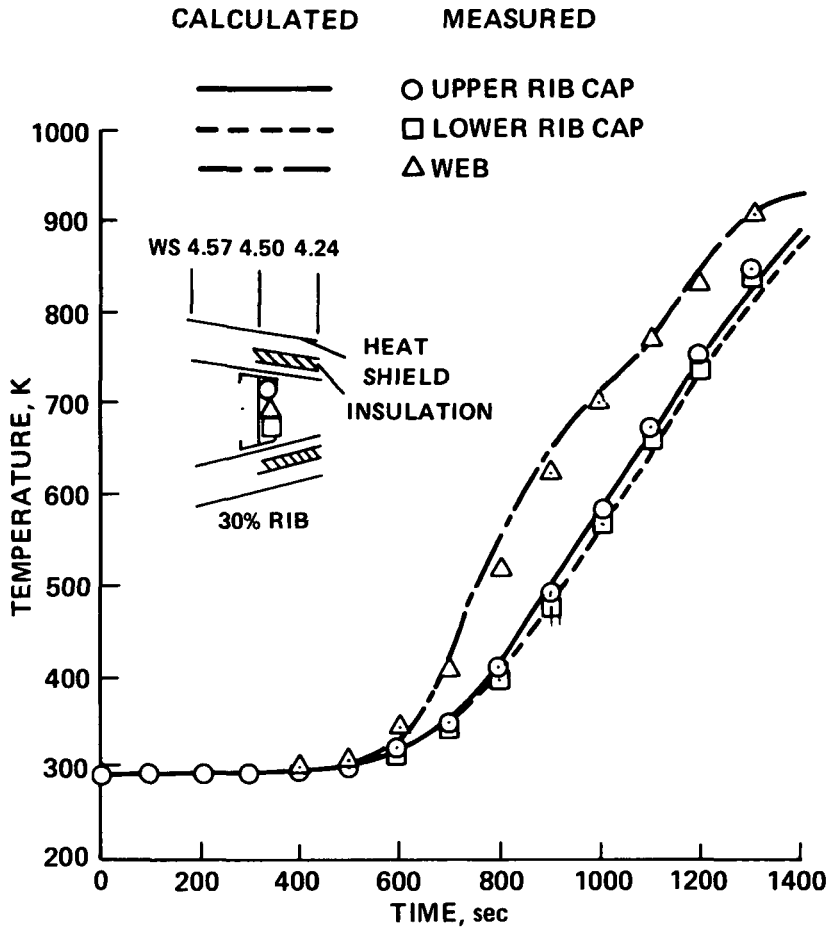

(b) Rib temperatures.

Figure 46.- Continued.

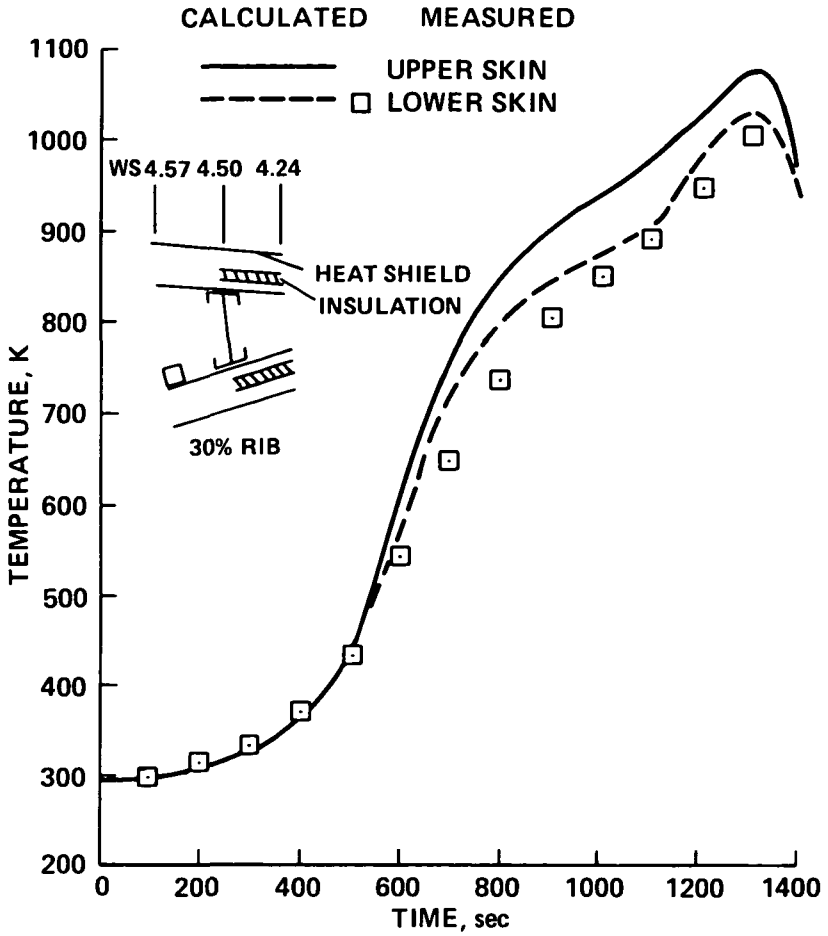

(c) Skin temperatures.

Figure 46.- Concluded.

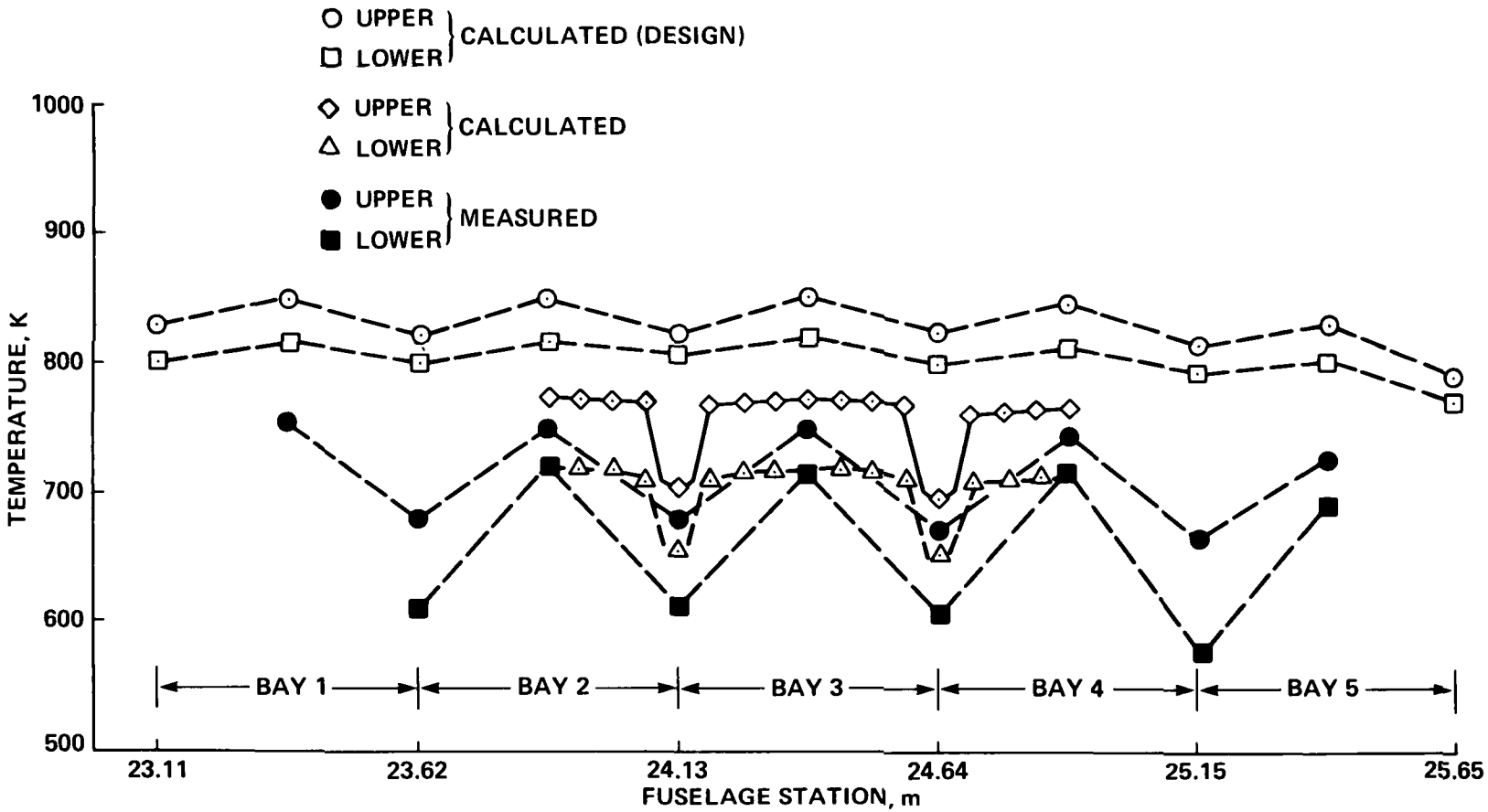

Figure 47.- Temperature distribution at W.S. 1.93, time = 800 sec.

1. Report No.	2. Government Accession No.	3. Recipient's Catalog No.
NASA TM-85918		

4. Title and Subtitle	5. Report Date
COMPARISON OF MEASURED AND CALCULATED TEMPERATURES FOR A MACH 8 HYPERSONIC WING TEST STRUCTURE	March 1986
	6. Performing Organization Code
7. Author(s)	8. Performing Organization Report No.
Robert D. Quinn and Roger A. Fields	H-1271, A-85137
	10. Work Unit No.
9. Performing Organization Name and Address	
Ames-Dryden Flight Research Facility Edwards, CA 93523	11. Contract or Grant No.
	13. Type of Report and Period Covered
12 Sponsoring Agency Name and Address	Technical Memorandum
National Aeronautics and Space Administration Washington, DC 20546	14. Sponsoring Agency Code 506-53-51

15 Supplementary Notes

Point of Contact: Robert Quinn, Ames-Dryden Flight Research Facility, M/S D-OFS, Edwards, CA 93523.

16 Abstract

Structural temperatures were measured on a hypersonic wing test structure during a heating test that simulated a Mach 8 thermal environment. Measured data are compared to design calculations and temperature predictions obtained from a finite-difference thermal analysis.

17 Key Words (Suggested by Author(s))	18 Distribution Statement
Hypersonic structure Radiant heating Thermal analysis	Unlimited Subject category - 05

19 Security Classif. (of this report)	20. Security Classif (of this page)	21 No. of Pages	22 Price*
Unclassified	Unclassified	140	A07

*For sale by the National Technical Information Service, Springfield, Virginia 22161